GA–A26361

STABILIZATION OF THE EXTERNAL KINK AND THE RESISTIVE WALL MODE

by

M.S. CHU and M. OKABAYASHI

JUNE 2009

GENERAL ATOMICS

DISCLAIMER

GA–A26361

STABILIZATION OF THE EXTERNAL KINK AND THE RESISTIVE WALL MODE

by
M.S. CHU and M. OKABAYASHI*

This is a preprint of a paper to be submitted for publication in *Plasma Phys. and Control. Fusion.*

*Princeton Plasma Physics Laboratory, Princeton, New Jersey.

Work supported in part by
the U.S. Department of Energy
under DE-FG03-95ER54309 and DE-AC02-76CH03073

GENERAL ATOMICS PROJECT 03726
JUNE 2009

GENERAL ATOMICS

General Atomics Report GA-A26361 M.S. Chu, et al.

M. S. Chu[a] **and M. Okabayashi**[b]

[a]General Atomics, P.O. Box 85608, San Diego, California 92186-5608 USA
[b]Princeton Plasma Physics Laboratory, P.O. Box 451, Princeton, New Jersey 08543 USA

Abstract.

The pursuit of steady state economic production of thermonuclear fusion energy has led to research on the stabilization of the external kink and the resistive wall mode. Advances in both experiment and theory, together with improvements in diagnostics, heating and feedback methods have led to substantial and steady progress in the understanding and stabilization of these instabilities. Many of the theory and experimental techniques and results that have been developed are useful not only for the stabilization of the resistive wall mode. They can also be used to improve the general performance of fusion confinement devices. The conceptual foundations and experimental results on the stabilization of the external kink and the resistive wall mode are reviewed.

PACs Nos.: 52.35.-g, 52-35.Bj, 52.55.-s, 52.55.Tn, 52.65.Kj

Contents

1. Background

1.1. Introduction

One of the major goals in thermonuclear fusion research is to produce a stable high pressure plasma, preferably at steady state, for the economic production of fusion energy. Substantial effort has been focused on optimizing the plasma configuration in experiments to increase the projected fusion power density and achieve a compact power source at steady state. With the maximum magnetic field limited by practical engineering constraints, high power density implies high β_T, ($\beta_T = 2\mu_0\langle p\rangle/B_T^2$, [In this review, we use a consistent set of symbols for useful physical quantities such as β_T. However, in some original figures, different authors could have adopted different symbols.] $\langle p\rangle$ is the average plasma pressure, μ_0 the vacuum permeability and B_T the strength of the toroidal magnetic field), since fusion power density increases roughly as $\langle p\rangle^2$ [1]. The research at maximizing the plasma β_T for steady state operations has culminated on the adoption of elongated tokamak with moderate aspect ratio ($2 < A < 4$, $A = R/a$, with a being the minor radius and R the major radius of the toroidal configuration) for all the principal next step devices [1]. At the same time, active research is being carried out in major laboratories world-wide on the pursuit of even more compact configurations.

Plasmas with high pressure are likely to operate near one or more stability limits, so control of magnetohydrodynamic (MHD) stability in such plasmas is crucial. The external kink (XK) has often been considered as a major obstacle to achieving higher β_T. A good review of the various observed instabilities up to 1994 has been given by Strait [2]. (This work did not include post 1994 data from the very low aspect ratio $A \sim 1$ tokamaks.) A more recent review of these instabilities relevant for ITER is given by Hender *et al.* [3]. Shown in figure 1 is the summary of β_T achieved by tokamaks worldwide at the end of 1994 given in reference [2].

One notable feature of figure 1 is that the value of β_T is bounded by a straight line with the value of

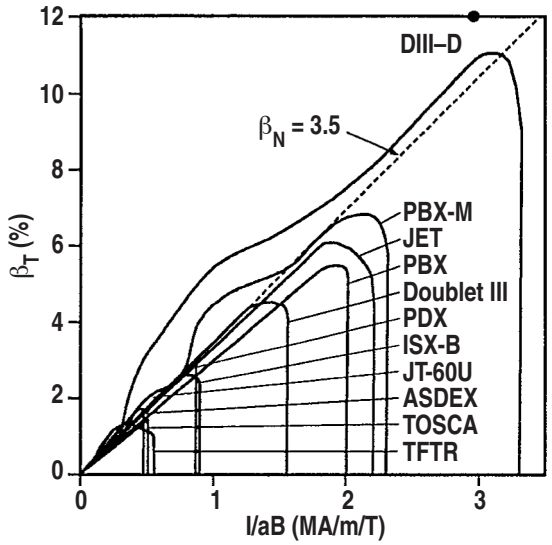

FIG. 1. Comparison of experimental achieved β_T versus normalized current I/aB_T for major tokamaks in 1994. The operational envelope is bounded by a straight line with slope given by the parameter $\beta_N = 3.5$ (reference [2]). [Reprinted courtesy of AIP, Phys. Plasmas **1**, 1415 (1994).]

$\beta_N = 3.5$. β_N therefore characterizes the achievable β_T normalized with respect to the plasma current. It is defined explicitly as

$$\beta_N = \beta_T(aB_T/I) \quad , \qquad (1)$$

and I is the toroidal plasma current. The units of the quantities in equation (1) are β_T in %, a in meters, B_T in Tesla, I in MA, and β_N being in units of % m T MA^{-1}.

The XK has long been thought of as "the instability" that ultimately limits the pressure of the plasma. In the beginning of tokamak research, the plasma was heated by ohmic current only. Ohmic heating was not sufficient to increase plasma β_T up to the pressure limit. In this early period, the cause of the XK was due to the current limit — trying to force the discharge to carry too large a current. In general, this limit is reached when the safety factor q at the plasma edge has reached the value below 2. (The safety factor q is a measure of the twistedness of the magnetic field. For a circular plasma with minor radius a, toroidal magnetic field B_T, aspect ratio A and current I, $q \sim [(2\pi aB_T)/(\mu_0 AI)]$.)

The major advance in heating the plasma is brought about by the development of powerful neutral beam injectors. With the injection of multi-mega-watt neutral beams into the tokamak, the plasma β_T was increased and instabilities specifically resulted from this increase were reported. Magnetic loop measurements indicated catastrophic events could be related to the XK [4].

To avoid confusion with transient equilibrium variations, research initially focused on instabilities with fast growth rates. This growth rate was implicitly assumed to be on the Alfvén time scale [$\tau_A = R/(B_T/\sqrt{\mu_0\rho})$, with ρ being the plasma density] for the Alfvén wave to transit the torus. Although a lot of discharges ended with unstable modes with growth rates much slower than $1/\tau_A$, there did not exist strong experimental evidence to relate such phenomena to the XK. Initial research considered the XK to be uncontrollable. The only way of reducing the impact of this global MHD phenomenon was simply to stay away from "bad" parameter regimes even if the achievable plasma pressure was less attractive.

One of the important advances in the gradual changing of this attitude came from the theoretical developments in understanding the stability properties of ideal MHD modes.

1.2. Theory of the XK mode

The basic theoretical foundation for the systematic investigation of the stability of ideal MHD plasma was the development of the energy principle by Bernstein *et al.* [5]. In this principle, the plasma is treated as an ideal conducting fluid. The plasma stability is related to the availability of the free energy given by the energy functional δW. For a given plasma equilibrium specified by magnetic field $\vec{B}_0$, current $\vec{J}_0$, and pressure p_0, the energy functional δW is given by

$$\delta W = \delta W_p + \delta W_v \quad , \tag{2}$$

$$\delta W_p = \frac{1}{2}\int_{plasma} \times \left[\frac{\delta\vec{B}^2}{\mu_0} - \vec{J}_0\cdot(\delta\vec{B}\times\vec{\xi}) + \Gamma p_0(\vec{\nabla}\cdot\vec{\xi})^2 + (\vec{\xi}\cdot\vec{\nabla}p_0)\vec{\nabla}\cdot\vec{\xi}\right] d\tau \quad , \tag{3}$$

$$\delta W_v = \int_{vacuum}\frac{\delta\vec{B}^2}{2\mu_0}d\tau \quad . \tag{4}$$

In equation (2), (δW_p, δW_v) is the perturbed potential energy in the (plasma, vacuum). In equation (3), $\vec{\xi}$ is the plasma displacement, $\delta\vec{B}$ is the perturbed magnetic field, Γ is the ratio of specific heats. Inside the plasma $\delta\vec{B} = \vec{\nabla}\times(\vec{\xi}\times\vec{B}_0)$. In its original formulation, the plasma is surrounded by an external wall with perfect conductivity. Therefore, the vacuum region in equation (4) is enclosed by a perfect conducting wall. The plasma is stable with respect to ideal MHD instabilities if $\delta W > 0$ with respect to all plasma displacements and unstable if $\delta W < 0$ for any displacement $\vec{\xi}$. The growth rate γ of the unstable mode is given by

$$\gamma^2 = -\frac{\delta W}{\delta K} \quad , \tag{5}$$

where

$$\delta K = \frac{1}{2}\int_{plasma}(\rho\vec{\xi}^2 d\tau) \quad . \tag{6}$$

Here ρ is the mass density and $\gamma^2\delta K$ is the kinetic energy of the plasma. The meaning of equation (5) is that the available free energy δW is expended in the plasma kinetic energy. The growth rate is usually at a fraction of inverse Alfvén transit time $1/\tau_A$. If the plasma remains unstable even if the perfect conducting wall encloses the plasma completely, therefore the component of $\vec{\xi}$ normal to the plasma boundary vanishes ($\xi_n = 0$), then the plasma is unstable to an internal plasma mode. This is an interesting area with an extensive literature. However, the internal kink is not the main topic of this review. We refer the reader to the work by Strait [2] for an introduction to this subject.

A useful and interesting viewpoint to adopt for the study of MHD instability is that the perturbed plasma state can be viewed as consisting mainly of a set of mutually interacting currents (Appendix A). The perturbed currents in the plasma are given by $\mu_0 \delta\vec{J}_p = \vec{\nabla} \times \vec{\nabla} \times (\vec{\xi} \times \vec{B}_0)$. The perturbed current on the ideal wall is then given by a skin current of magnitude $\delta\vec{J}_w = \hat{n} \times \vec{\delta}B$. Equation (5) then describes the growth in time of an unstable system of currents. The interacting current system $(\delta\vec{J}_p, \delta\vec{J}_w)$ and the plasma displacement $\vec{\xi}$ are equivalent concepts. In many situations in which we also have to describe the interaction of an unstable plasma with the external systems of currents, the concept of a system of interacting currents is especially appealing. We may symbolically represent the system of perturbed plasma currents as I_p and the perturbed currents on the wall as $I_w = \hat{n} \times \delta\vec{B}$.

The analytic property of the ideal stability of the tokamak plasma was first investigated by Shafranov [6] in 1970. He mapped out the basic stability of the plasma in terms of the safety factor q, the current profile, and the radius of the external conducting wall. There are many subsequent analytic refinements of the theory by Shafranov, such as the work by Frieman *et al.* [7] that provided great insights into the stability property of the XK mode at large aspect ratio. Others pointed out the effects of moderate plasma elongation, triangularity, small aspect ratio and analytic current profiles. However, these works were not comprehensive or quantitative enough for the experiments operated at finite aspect ratio, with a general elongated plasma cross section with finite triangularity and general current and pressure profiles. The definitive advance for the systematic study was brought about by the construction of the large ideal MHD stability codes. Notable amongst these are the ERATO [8], PEST [9], GATO [10] and KINKX [11].

One of the most important results from the systematic application of the large scale ideal MHD codes to the study of stability of the XK in tokamaks in the 1980's was the discovery of the Troyon scaling law [12]. In this work, a group at Lausanne found that the maximum achievable β_T in a tokamak, when studied over a wide class of current and pressure profiles, scales as the total current carried by the plasma. Specifically, the maximum achievable value of β_N defined in equation (1) is predicted to be a constant for all tokamaks. This maximum value of β_N, symbolically represented as β_N^{Troyon}, was determined through computation to be 2.8. Or more explicitly

$$\beta_N^{Troyon} = 2.8 \quad . \tag{7}$$

The boundary condition chosen was that there is no external conducting wall. The reason being that as a reactor, the tokamak needs to operate at near steady state, i.e. being stable over a very long time scale. Since it is not possible to enclose the plasma by a super-conducting first wall, the perturbed flux from the unstable XK mode would

inevitably diffuse through the external resistive wall. Any reasonable estimate shows that the flux diffusion time scale, τ_w, is much shorter than the discharge time scale of the reactor. (Here, τ_w is given by $\mu_0 \sigma b \delta$; with σ being the conductivity of the resistive wall; b the minor radius; and δ its thickness.) Thus, any external conducting wall would not be effective in stabilizing the XK mode throughout the discharge lifetime in a reactor. The eigenfunction of the most unstable displacements in this study [12] revealed a global structure with non-negligible displacement at the plasma surface. These instabilities are appropriately called the XK mode.

We note that prior to Troyon's investigation, the effect of an external resistive wall on the XK mode has been studied by Pfirsch and Tasso [13]. They proved a theorem: A MHD-unstable configuration with a dissipationless plasma surrounded by vacuum and possibly superconducting walls cannot be stabilized by introducing walls of finite electrical conductivity. (Note that the theorem was proved for a plasma with no rotation and also without dissipation. Therefore even if the plasma were rotating, it implies that they were considering a plasma with resonant layers that do not produce an imaginary energy or toroidal angular momentum flux). Their conclusion was that the resistivity in the external wall only reduces the growth rate of the XK to $1/\tau_w$ and does not stabilize it. The resultant instability with its growth rate significantly reduced ($\tau_w >> \tau_A$ in general) is appropriately called the resistive wall mode (RWM). Viewed in this way, the RWM is a special form of the XK mode. A text book example of the RWM is given by Freidberg [14]. In terms of the alternative concept of interacting currents introduced previously, we note that in this case the skin currents on the resistive wall I_w will spread out and become distributed currents and reduce in magnitude. The theorem by Pfirsch and Tasso then states that this system of currents will be unstable and grow at a rate approximately equal to the rate at which flux can diffuse through the resistive wall.

The above picture of the interaction of the XK with the external resistive wall was recognized in the important class of current driven devices of reversed field pinches (RFPs). In comparison to the tokamak, the ratio of toroidal current to the toroidal magnetic field in RFP is larger by a factor of $A = R/a$. XK in RFP is never stable without an ideal external wall. It was recognized early that the XK in RFP was stabilized over its discharge lifetime by the external conducting wall. And the RWM needs to be stabilized for the RFP reactor. The stabilization of the RWM was first studied by Gimblett in 1986 [15] in the context of RFP. It is interesting to note that in this first study, many of the concepts that remain useful up to date were also introduced, such as the dissipation in the plasma, the stabilizing effect of the relative rotation between the plasma and the resistive wall. The RWM in RFP was first positively identified in 1989 by Alper *et al.* [16]. An interesting scheme, utilizing a rotating secondary wall was explicitly proposed by Gimblett [17] in 1989 to stabilize the RWM.

However, before early 1990's, there was no systematic study of the RWMs for the tokamak. Nor were there computer codes that could take into account the effects of the resistive wall on the XK mode to allow such a systematic study.

1.3. Experimental verification of the high β_T XK mode

1.3.1. Verification of the Troyon scaling law. The first important verification of the Troyon scaling law was the systematic exploration of the β_T limits in tokamaks with low toroidal field and high power neutral beam injection. These experiments were carried out in the DIII-D [18] and the PBX [19] tokamaks. The major results from the DIII-D tokamak are summarized in figure 2(a). It is seen that in the DIII-D tokamak, the plasma stability was bounded by a triangular region in the $I/aB_T - \beta_T$ plane. The vertical I/aB_T lines are the $q = 2$ lines which come from the current limit predicted by Shafranov [6]. The vertical extent of the triangular region, or the β_T limit is bounded by a straight line proportional to the normalized total plasma current I/aB_T. It was noted that this straight line corresponds to the value of

$$\beta_N^{exp} = 3.5 \quad , \tag{8}$$

instead of 2.8. Although the maximum achieved value of β_N is different, the scaling of the stability limit pointed out by Troyon [12] is unambiguous. Investigation of this discrepancy has led to the conclusion that during the development of these instabilities, the external conducting wall does provide a stabilizing effect. The value of 3.5 given in equation (8) is consistent with the assumption that the external conducting wall was effective in stabilizing the XK when β_N reached its maximum value. However, it has not been found possible to keep the plasma at the maximum achieved β_T value throughout the subsequent discharge history. It is also noted that there were a lot of discharges which terminated before reaching the β_T limit. These can be attributed to the unoptimized current and pressure profiles and the presence of other instabilities [2].

The β_T well above the no-wall limit was also achieved in the bean shaped PBX configurations (indentation=$10\% - 20\%$). The observed β_T values are summarized vs. $\beta_c^* = \mu_0 I(A)/[a(m)B_T(T)]$ in comparison with the β_T limit of the ideal MHD calculated by PEST shown in figure 2(b) [19]. Since the bean configurations are stable to the internal kink modes even with $q(0) < 1 = (0.8)$ [$q(0)$ is the value of the safety factor q at the magnetic axis] with the advantage of strong averaged minimum B (i.e. the averaged value of B at the plasma center is lower than that at the plasma boundary), the possibility of β_T limit due to instabilities other than the XK (the internal kink) was greatly reduced. The achieved values of $\beta_T \geq 5.2\%$ at $\beta_c^* \sim 2.5$ is below the predicted ballooning mode (reference [2]) β_T limit $\sim 9\%$ and is well above the β_T limit of 3.5% of the $n = 1$ XK without wall. Similar to the conclusion reached in DIII-D [18], the achieved β_T is consistent with $n = 1$ XK limit with the ideal wall located at $b/a \sim 1.5 - 2$. We note that results in PBX also showed that the β_T limit scales as predicted by Troyon, but experimental data definitely extended beyond the no external wall value predicted by Troyon.

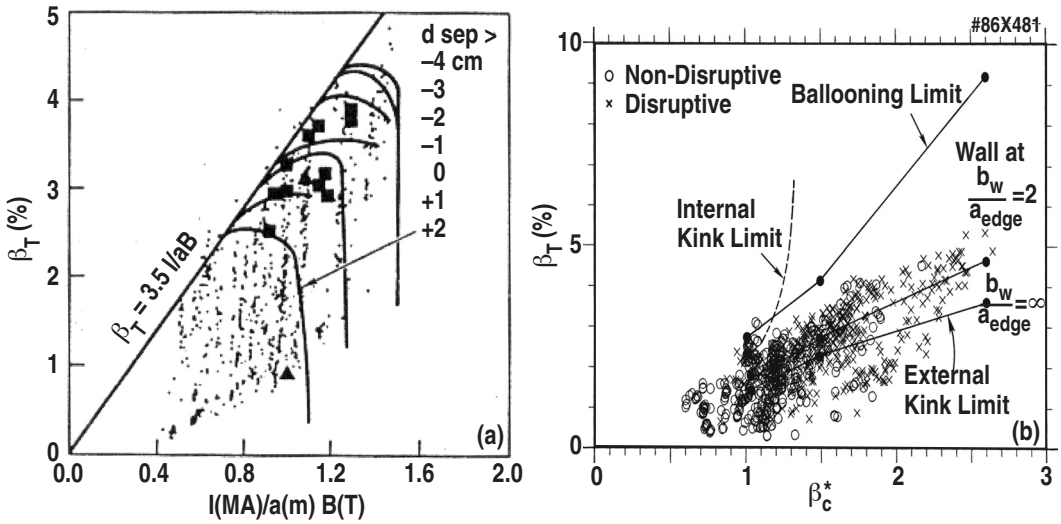

FIG. 2. (a) β_T versus I/aB for DIII-D tokamak with strong neutral beam injection heating. Curves show the operating space limit for β_T and I for various distances between the plasma and the external limiter d_{sep}. The wall is a few centimeters beyond the limiter. Solid triangles identify $m = 2, n = 1$ external kink disruptions. Solid squares identified modes with $3 \leq n \leq 5$ (reference [18]). [Reprinted courtesy of IAEA, Plasma Phys. and Control. Fusion Research 1984, Vol. I (IAEA, Vienna, 1985) p. 217.] (b) The experimentally achieved β_T values in PBX versus $\beta_c^* = \mu_0 I(A)/[a(m)B_T(T)]$. Note the inclusion of the factor μ_0 in the definition of β_c^*. Shown are also stability limits computed by the PEST code with external conducting wall at different locations. External wall at ∞ corresponds to limits predicted by Troyon. It is seen that the experimental data extends beyond the Troyon limit (reference [19]). [Reprinted courtesy of IAEA, Plasma Phys. and Control. Fusion Research 1987, Vol. I (IAEA, Vienna, 1985) p. 275.]

It was also noted in the above experiments [18, 19], after reaching the β_T limit, the subsequent development of the plasma instability did not occur on a fraction of Alfvén transit time, but on a much longer time scale. Some times the plasma can be kept at the high β_T phase longer than τ_w. These observations can not be easily explained in terms of the assumptions of the non-dissipative and non-rotating plasma state and the conclusions derived from the theory by Pfirsch and Tasso [13].

1.3.2. Verification of the stability threshold and mode structure of the XK mode. Subsequent experiments started to reveal more details of these global MHD phenomena. Experimental diagnostics have revealed no observable magnetic island verifying the ideal MHD nature of the displacement. More detailed verification of the XK as the plasma instability, which limited the plasma performance was obtained by following the discharge trajectory in the stability space determined by the ideal MHD codes [20]. One example of this is provided by the teams working on the JET tokamak in the high Q_{DT}.

[Here Q_{DT} is the fusion gain, the ratio of fusion power to the input power required to raise the plasma temperature.] operation shown in figure 3(a). It is observed that the higher β_N was achieved by carefully adjusting the plasma pressure profile to stay very close to the no-wall β_T limit. In this case the plasma finally developed an "outer mode" that limited the fusion performance of the enhanced confinement mode discharges in JET. Prior to its identification, it was previously proposed that the outer mode is a nonlinearly saturated XK. This was based on the localization of the perturbation close to the edge as observed in soft x-ray (SXR), electron temperature and electron density measurements. In the present case, MHD stability calculations showed that the plasma edge was close to the ideal XK stability boundary at the time when the outer mode was observed. The SXR data of the outer mode (Note that the SXR data does not actually show perturbation at the plasma boundary. This is inferred from comparison with numerical computation and experimental consequences after the development of the mode.) shown in figure 3(b) were compared with predictions based on the mode structure of the computed ideal $n = 1$ XK mode shown in figure 3(c). Excellent agreement was found, confirming the identification of the outer mode as an XK mode [21].

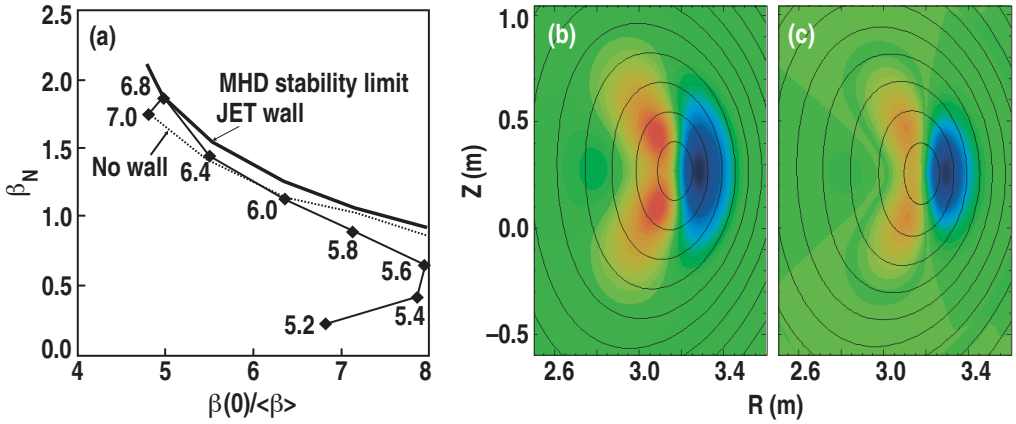

FIG. 3. Experiments in JET that identified the structure of the XK mode through detailed mapping of the stability phase space and comparison of the soft x-ray signals. (a) The details of plasma discharge trajectory in $\beta(0)/\langle\beta\rangle$ - β_N, showing the flattening of the pressure profile and increase of β_N above the no wall limit towards the ideal wall limit. (b) Tomographic reconstruction of the SXR emission profile for the $n = 1$ perturbation and (c) expected emission profile constructed based on ideal perturbation from ideal MHD calculation (reference [20]). [Reprinted courtesy of IOP, Nucl. Fusion **39**, 1489 (1999).]

In JT-60U, the internal and XK activity limited the achievement of high fusion triple product, $n_D(0)\tau_E(0)T_i(0)$, to equivalent $Q_{DT} \sim 1.05$ [22]. Fluctuation profiles determined by electron cyclotron emission (ECE) are shown in figure 4 and compared with the mode pattern calculated with ERATO-J [23]. Apart from the growth time, the observed fluctuation profile appears to be consistent with the ideal $n = 1$ kink ballooning mode, with indication of possible coupling to the internal kink at the plasma center.

Extensive results on the verification of the stability boundaries of DIII-D plasmas, including the identification of stability boundaries formed by the XK, is summarized in the work of Turnbull *et al.* [24].

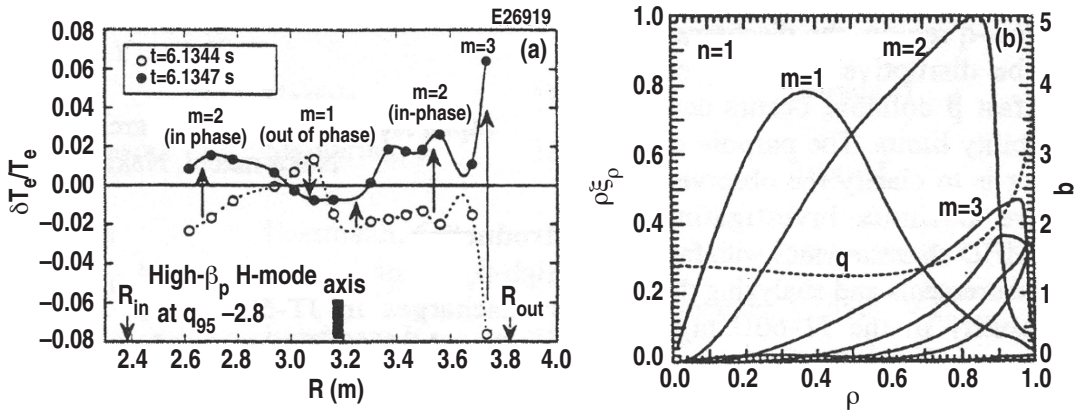

FIG. 4. The measured fluctuation in electron temperature vs. major radius in JT-60U for a high performance high β_p discharge that is limited by MHD activity. Shown in the left panel are the amplitudes of different poloidal harmonics of $\delta T_e/T_e$ (not normalized to ∇T) which are to be compared with the computed amplitudes from the ERATO-J code shown in the right panel (reference [22]). [Reprinted courtesy of IOP, Nucl. Fusion **39**, 1489 (1999).]

1.3.3. Verification of the growth rate of the XKs. Even in the very early experiments that established the Troyon scaling law [18, 19], it was noted that the growth rates of the limiting instabilities could be much different from that predicted by ideal MHD theory.

Therefore, although much of the characteristics of the β_T limit in tokamak discharges can be attributed to the XK, it seems that quite a lot of these discharges cannot be described completely by the ideal MHD plasma model, neglecting the effect of the external conducting wall. It was clear that the characteristics of the external wall would have an important effect on the plasma stability. An example of the discrepancy between the experimental time scale with the time scale of XK is given in experiment

in TFTR [25] and shown in figure 5. The external mode, which was locked to the wall (not rotating), grew on a time scale much slower than the expected Alfvén transit time. A few hypotheses were proposed, including the possibility of a hybrid time scale of the instability introduced by the evolving equilibrium [26, 27]. (Note that for these experiments, the Alfvén time scale was of the order of sub μs, the equilibrium evolution time of the order of tens of ms, whereas the resistive wall time was of the order of a few ms. Therefore a hybrid time scale between the Alfvén and equilibrium evolution time could be of the same time scale as the resistive wall time.)

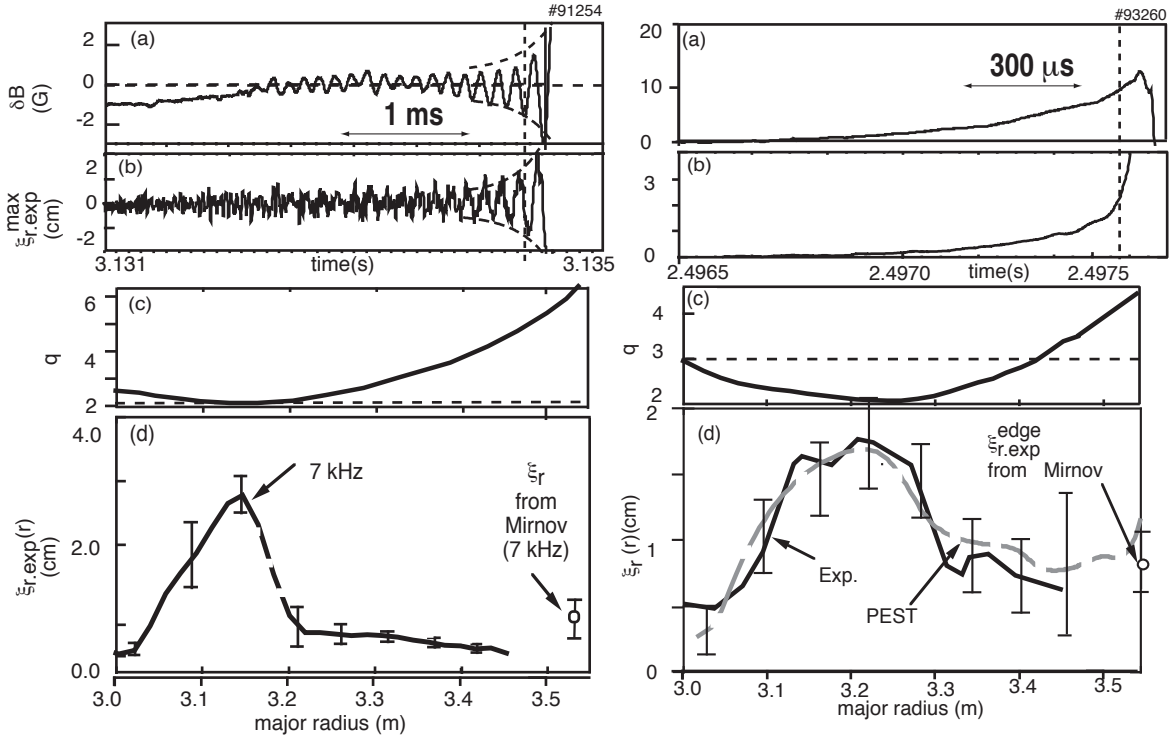

FIG. 5. Experiments in TFTR showing the slow development in time of the instability which limited the plasma discharge. Shown are (a) time evolution of perturbed magnetic field amplitudes (in Gauss), (b) time evolution of maximum measured plasma displacement, (c) safety factor q, and (d) comparison of computed displacement from PEST to the experimentally measured displacement for two discharges with different $r_{q_{min}}$'s in TFTR. The discharge on the right has a larger radial region of shear reversal. The growth times of the instabilities are inferred to be 1 ms (left) and 300 μs (right) and much longer than the Alfvén time around 1 μs (reference [25]). [Reprinted courtesy of IAEA, adapted from Nucl. Fuson **38**, 1149 (1998).]

1.4. Development of the advanced tokamak

One of the main drawbacks of the tokamak as a reactor has been that its configuration is formed by the presence of substantial plasma current. Due to plasma resistivity, the plasma current will invariably decay, limiting the discharge lifetime and prevent the development of the tokamak into a truly steady state reactor. Various schemes have been proposed to maintain the plasma current. The verification of the presence of bootstrap current has completely changed this picture [28]. This self-generated plasma bootstrap current has been verified to be proportional to plasma poloidal beta, $\beta_p = \langle p \rangle 2\mu_0/\langle B_p^2 \rangle$. ($B_p$ is the strength of the poloidal magnetic field.) In principle, the tokamak can be optimized to fully utilize this bootstrap current with additional external current drive to produce steady state regimes. Steady-state operation with low recirculation power for current drive implies operation at high poloidal beta, maximizing the fraction of self-generated bootstrap current. Further, the values of β_T, β_p, and β_N obey the following relationship

$$\beta_p \beta_T \sim 25[(1+E^2)/2](\beta_N/100)^2 \quad , \tag{9}$$

where E is the elongation of the plasma surface. According to this relationship (9), shown in figure 6(a), high β_p together with the requirement of high toroidal β_T led to the requirement of operation at high normalized beta (β_N). The advanced

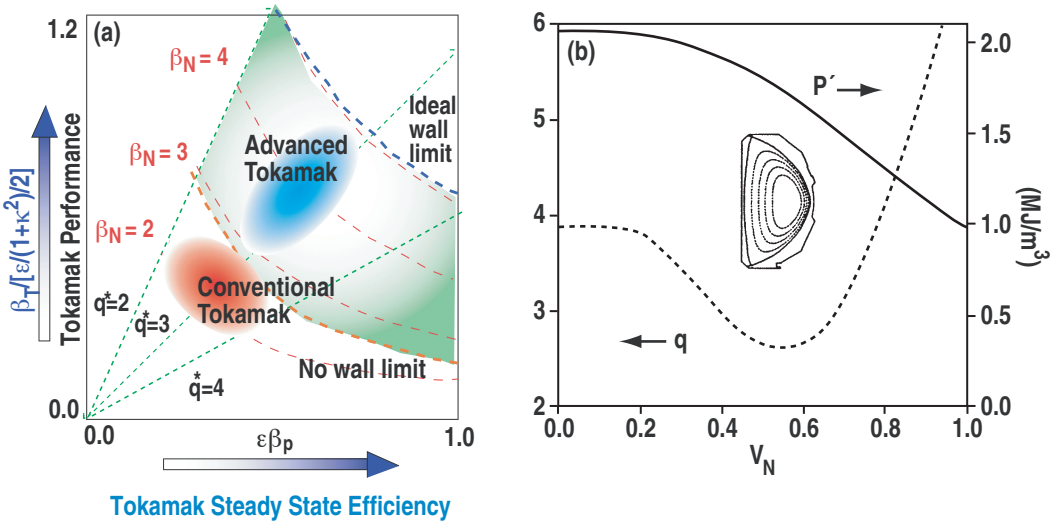

FIG. 6. (a) The schematic operation space of the tokamak in the β_T vs β_p plane showing that raising β_N will allow the simultaneous achievement of high β_p for high bootstrap current fraction and high β_T for high fusion power density. (b) The cross-section of the plasma and shape of the external wall of a typical advanced tokamak together with profiles of the safety factor q and pressure gradient p' vs. the normalized volume V_n (reference [30]). [(b) Reprinted courtesy of APS, Phys. Rev. Lett. **74**, 718 (1995).]

tokamak [29, 30] was proposed which promises a high bootstrap current fraction, yet still with high enough β_T for sustained fusion reaction. This advanced tokamak regime lies in the upper right quadrant of the parameter space of figure 6(a). In this figure, $q^* = \pi B_T a^2(1+E^2)/(\mu_0 RI)$. According to equations (8) and (9), the full advantage of the advanced tokamak relied on stabilization of the XK with an ideal wall close to the plasma edge beyond what was achieved so far. The typical shapes of the plasma and resistive wall, and profiles of the safety factor q and pressure gradient p' for an advanced tokamak is shown in figure 6(b) [30].

1.5. Challenges posed by the early theory and experiments

At the end of the early 1990's, there was broad agreement between theory and experiments recognizing that the XK limited plasma β_T in tokamaks. The experimentally achieved β_T values were beyond the ideal MHD no-wall limit. Sometimes, the time scale of the development of the instability has been found to be slower than the Alfvén transit time scale or even the flux diffusion time scale through the external resistive wall. A number of hypotheses were proposed as the cause of these discrepancies, including the presence of a plasma mantle — a pressureless plasma which surrounded the confined plasma, the halo current, two fluid effects, the presence of stochastic regions surrounding the confined plasma. The contribution of the resistive wall was definitely proposed, but no clear theoretical elucidation has been forwarded. It was recognized that, a potentially large advantage can also be realized for the advanced tokamak if the external resistive wall could be turned into a perfect conducting wall.

1.6. Response to the challenges

The most definite response to the challenges posed by the initial experiments and the theory regarding the XK was provided by Bondeson and Ward [31]. They noted that in the high β_T discharges up to that time, the plasma was invariably heated by neutral beam injection, which injected not only energy but also toroidal angular momentum to the plasma. Plasma dissipation, when coupled with rotation would cause the otherwise "slowly" unstable RWM predicted by Pfirsch *et al.* [13] to rotate with respect to the external wall and stabilize it. They proposed that low n (n being the toroidal mode number), pressure-driven, XK modes in tokamaks could be fully stabilized by the resistive walls when the plasma rotated at some fraction of the sound speed. The nature of this stabilization was shown in the figure 7(a) [31]. In this figure, the limiting location for stability with an ideal wall is $d/a = 1.7$, here d and a are the radii of the wall

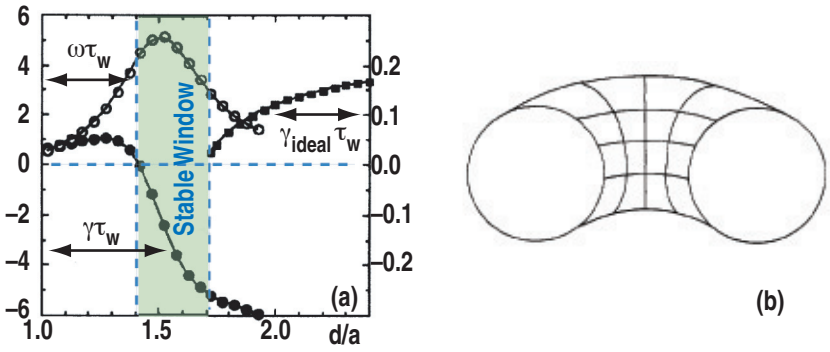

FIG. 7. (a) Bondeson and Ward's proposal for stabilization. Growth rate γ and slip frequency ω of RWM w.r.t. the resistive wall and growth rate of plasma mode γ_{ideal} are plotted versus the wall radius for the $n = 1$ modes. The plasma pressure is about 30% above the no wall limit and the plasma is rotating at $\Omega/\omega_A = 0.06$ w.r.t. the resistive wall. Note the shaded region of $1.4 < d/a < 1.7$ in which both γ and the extended γ_{ideal} are expected to be negative. This is the stability window in which the plasma is stable to both the ideal branch and the resistive wall branch of the XK (reference [31]). [Reprinted courtesy of APS, Phys. Rev. Lett. **72**, 2709 (1994).] (b) Bishop's intelligent shell concept. The lines are a network of coils which cover the surface of the resistive wall to compensate for the dissipated flux on the resistive wall (reference [32]). [Reprinted courtesy of IOP, Plasma Phys. Control. Fusion **31**, 1179 (1989).]

and plasma respectively. The ideal mode is stable with $d/a < 1.7$. When the resistivity of the wall is taken into account, we observe the resistive branch of the XK, i.e. the RWM. When the slip frequency of RWM with respect to the wall (due to the momentum input from the plasma to the unstable mode) is large, the growth of the RWM is stabilized. In their calculation, the physical mechanism for momentum transfer from the plasma to RWM is toroidal coupling to sound waves and was effected by ion Landau damping. They demonstrated this stabilization effect through extensive two-dimensional stability calculations. With the RWM stabilized, they showed there is substantial gain in the steady state β_T limit. Bondeson's proposal was that in a rotating plasma, the perturbed plasma current I_p would force the perturbed current in the wall to rotate with respect to the resistive wall. In this case, the I_w will not be able to grow in phase with I_p, leading to stabilization.

As mentioned earlier, the similar proposal for the RFP in this context was forwarded by Gimblett in 1989 [17]. This proposal later developed into the concept of rotating real or virtual walls.

An alternative proposal was first presented by Bishop [32] [figure 7(b)] to use a network of external currents outside the resistive wall to replenish the flux leakage though the resistive wall. The lines shown are Bishop's conceptualization of a network of coils. He pointed out that due to the good conductivity of the external resistive wall, a very small amount of power supplied to the external coils is sufficient to replenish the flux leakage and mimic the presence of an ideal wall for the discharge. This is the basis of the feedback stabilization of the XK or RWM. In terms of the unstable current systems introduced previously, Bishop's proposal is to introduce yet another current, the feedback current I_f. The purpose of this current is to compensate for the diffusion of flux through the dissipation of I_w.

The stability of the XK in a non-rotating plasma is schematically shown in figure 8. With no external wall ($\tau_w = 0$), the plasma is unstable if $\beta_N > \beta_N^{no-wall}$. Whereas for an ideal-wall ($\tau_w = \infty$), the plasma is stable up to the ideal wall β_T limit [figure 8(a)]. The growth rate of the XK is large and usually of the order of the Alfvén frequency. When the finite conductivity of the resistive wall is taken into account, a new branch, the RWM branch appears in the range of β_N ($\beta_N^{no-wall} < \beta_N < \beta_N^{ideal-wall}$) that was destabilized by a resistive wall. However although the RWM is unstable, the growth rate is only of the order of the flux diffusion rate of the wall ($\gamma\tau_w \sim 1$), and it is much slower than the characteristic Alfvén frequency of the XK (as shown by the dotted line). With plasma rotation and dissipation included, first the stability criteria of the RWM is modified. At a critical plasma rotation frequency, a stability window first appears if the β_N value is close to the $\beta_N^{ideal-wall}$. The size of the stability window increases with plasma rotation and dissipation. This dependence is shown in figure 8(b). It is interesting to

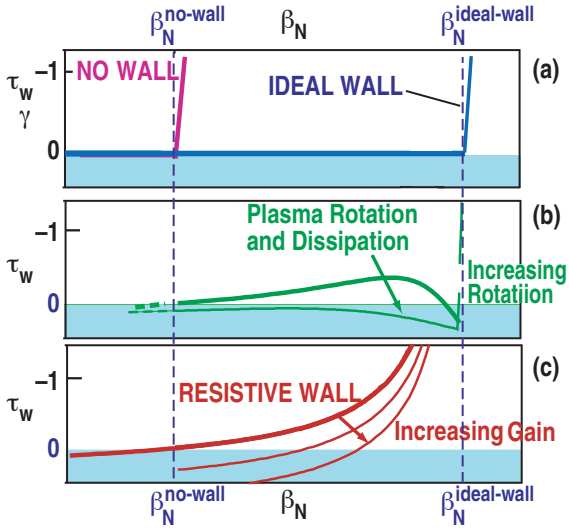

FIG. 8. Schematic diagram of growth rates of the XK mode and RWM as a function of the normalized plasma pressure β_N. Shown are (a) stabilization of the XK mode by an ideal wall and the RWM branch (dotted line) by a wall with a finite conductivity, (b) stabilization of the RWM by an increased amount of plasma rotation and dissipation, and (c) magnetic feedback stabilization of the RWM with an increasing amount of feedback gain. This schematic is based on the extended lumped parameter model described in Appendix A.

note that increasing Ω_ϕ (the toroidal rotation frequency of the plasma relatively to the resistive wall) extends the stability window towards a lower value of β_N. Above a critical value of Ω_ϕ, a complete stable path from low β_N to the ideal-wall beta limit $\beta_N^{ideal-wall}$ appears. The magnetic feedback stabilization approach is suggested by Bishop, taking advantage of the greatly reduced growth rate of the RWM. For slowly growing modes, it can be feedback stabilized by a system with a modest power supply, since the feedback merely has to replace the flux loss through the vacuum vessel, which is taking place over the skin time τ_w. With a low feedback gain, a stable domain starts to appear first at the $\beta_N^{no-wall}$ limit. The stable region is extended to higher β_N by increasing the feedback gain figure 8(c).

1.7. Brief description of the sections

Following the proposal of Bondeson and Ward [31] and that of Gimblett [17] and Bishop [32], a host of experiments were dedicated to the study of the stabilization of the RWM. These studies led to the identification of the global structure of the RWM and its improved stability by plasma rotation. However, the effort of trying to determine the rotation threshold resulted in varied predictions in both theory and experiment. It is found the rotation threshold could depend on the experimental approach in which the minimum rotation was arrived at. One approach is to introduce a large external non-axisymmetric field to slow down a fast rotating plasma (magnetic braking) and the other is to control the angular momentum input (low torque input) to the plasma while minimizing the non-axisymmetric field which slows the plasma rotation and also interferes with the development of the RWM.

Results from detailed experiments (in 1995 to 2005 in DIII-D) utilizing the magnetic braking method pretty much follow the prediction of the Bondeson theory, i.e. the plasma stability is observed when the rotation frequency is high. Because of the effect of the large imposed non-axisymmetric ($n = 1$) field, the plasma rotation always keeps on decreasing accompanied an increase of the extrnal perturbed signal at a very slow rate, until a fast growth (on the resistive wall time scale) of the RWM is observed. The threshold rotation frequency for the fast growth to occur was measured to be a small percent of the Alfvén frequency.

This apparent two-phase-grwoth phenomena from DIII-D were at vairance with some of the other experiments, for instance from JT-60 or NSTX. Although the values of the rotation threshold were reported to be similar. In particular, experiments in NSTX (reported in 2006) using $n = 3$ magnetic braking found only one growth phase.

Results from experiments from JT60-U and DIII-D (reported in 2007) utilizing the method of low torque input with minimum external non-axisymmetric field were measured to be less than 1% of the Alfvén frequency, i.e. much less than the prediction of the Bondeson theory.

These varied results posed a puzzle to the true nature of rotation stabilization of the RWM. Independent of the effort in the research on RWM, the theory of plasma rotational equilibrium in the presence of an external non-axisymmetric field was developed. It resulted in the bifurcation theory of the plasma rotation speed. After examination of the experimental data on rotational stabilization of the RWM, it was recognized that the true RWM rotation threshold should correspond to the smaller value obtained in the low torque input method. Whereas the threshold value observed in the large non-axisymmetric field regime corresponds to the loss of rotational equilibrium when the rotation speed falls below a threshold value. The prediction of threshold value using fluid theory with phenomenological dissipation coefficient as shown in Bondeson's is also not appropriate. In the low rotation regime, the plasma dynamics can only be described by the full kinetic models. The details of this development will be reviewed in section 2. Therefore, the research into the stabilization of the RWM has firmly established that for very low frequency MHD instabilities, the ideal MHD model for the plasma dynamics is not valid any more. Rather, we need to take into account the full kinetic dynamic response of the plasma. We also learned that in this regime, it is important to consider the details of the plasma rotational equilibrium through torque balance in determining the stability of the plasma.

By observing that the RWM can slow down the plasma, the research in RWM has conclusively demonstrated the importance of non-axisymmetric fields in determining the stability of the discharge in the very low frequency regime. This slowing down effect is especially large when the plasma is close to marginal stability of the RWM. By compensating for the non-axisymmetric field, the discharge can usually be maintained stably for a long duration. The interaction of the plasma with the external non-axisymmetric field was intensely studied both theoretically and experimentally. It is found that the plasma viscosity is affected by the particle drifts in the non-axisymmetric field, giving rise to the neoclassical toroidal viscosity. This drift also prescribes a definite rotation speed to the plasma and it is proposed that this rotation can be utilized to stabilize the RWM. The progress in this area is reviewed in section 3.

In addition to rotation stabilization, the plasma instability can be actively stabilized by utilizing magnetic feedback as proposed by Gimblett and Bishop. The progress in this area relevant for the stabilization for the RWM is reviewed in section 4. The techniques developed up to now can be utilized not only to stabilize the RWM, it can also be used to stabilize various other instabilities.

Most of the research activities reported in sections 2, 3, and 4 are for present day tokamaks. In section 5, the application to ITER is discussed. We also briefly review the related work for other confinement systems such as reversed field pinch (RFP) and stellerators. The RWM is an important and active research topic for the RFP. Much important progress has been achieved. In the RFP, Bishop's [32] original idea has truly come to fruition. Whereas it is conceivable that in the future the stabilization of the RWM could also become a potentially important topic for compact high beta stellerators.

Finally a brief summary and discussion is given in section 6.

It is the purpose of this review to present the necessary theoretical foundations for each topic within each separate section. Because the ITER class devices are being recognized as the major next step devices, the emphasis of this review is on results that can more readily be extrapolated to ITER.

2. Rotational Stabilization of RWM

As mentioned in section 1.5, rotational stabilization of the RWM is probably the major reason for the discrepancy between the experimentally observed β_T limit and the theoretically computed value ignoring the stabilizing effect of the resistive wall. However, how this stabilization comes about in conjunction with the MHD theory needed a convincing demonstration. The necessary modification of ideal MHD theory given in section 1 was proposed and demonstrated first by Bondeson and Ward [31].

2.1. Bondeson and Ward's proposal of rotation-dissipation stabilization of RWM

In 1994, through extensive computation (with a rotating wall surrounding a stationary plasma), Bondeson and Ward proposed that the pressure-driven, ideal XK modes in tokamaks can be fully stabilized by resistive walls with plasma rotation. For plasmas with a resistive wall, there are two types of potentially unstable modes: (1) the "RWMs" that penetrate, and are nearly locked to the wall, and (2) modes that rotate with the plasma and for which the wall acts as a near perfect conductor. For modes rotating with the plasma (quickly relative to the wall), the stabilizing effect of the wall increases when the wall is brought closer to the plasma, while for the RWMs, the stabilization improves with increasing wall distance. When the plasma rotates at some fraction of the sound speed, there is a window of stability to both the wall-locked and the rotating mode. This is the main result of the work by Bondeson and Ward [31] and was shown in figure 7(a).

Bondeson and Ward [31] provided the following explanation for the stabilization of the RWM. As shown in reference [6] for the tokamak, during an instability, the energy flux through the plasma boundary to the vacuum region is given by the equation

$$\delta W_p = \frac{1}{2}\int_{plasma-surface} \xi \frac{\partial \xi}{\partial x} dS \quad . \tag{10}$$

For a plasma with rotation, the energy flux becomes complex. It means that the perturbed magnetic field at the plasma boundary becomes a rotating field. In other words, the radial and poloidal components of the perturbed field acquired a phase shift with respect to each other. Because the perturbed flux is proportional to the perturbed displacement, we may also express Bondeson's idea in terms of the perturbed magnetic flux function ψ. For linear stability, the amplitudes of the perturbed quantities are arbitrary, the stability information is contained in the logarithmic derivatives of the perturbed quantities. Therefore Bondeson's hypothesis is equivalent to demanding the logarithmic derivative of ψ at the plasma edge $r = a$ be written as

$$\left.\frac{\psi'}{\psi}\right|_{a-} = -\frac{m}{a}(1 + x + iy) \quad . \tag{11}$$

Here, m is the poloidal mode number. The real part of equation (11), $\sim (1+x)$ means that the perturbed magnetic field transfers energy through the plasma boundary (1 is the amount for marginal stability, and x determines whether there is an excess or deficit for instability or stability) and the imaginary part iy means that "angular momentum" is also carried by the perturbed magnetic field through the plasma boundary. One remarkable feature of figure 7(a) is that when the RWM is stabilized by rotation (with $d/a > 1.4$), it becomes increasingly more stable with increasing wall distance. This counter intuitive behavior was explained by the following observation. In cylindrical geometry, the perturbed magnetic flux function satisfies $\nabla_\perp^2 \psi = 0$ in the vacuum region and the poloidal harmonic m is a linear combination of r^{-m} and r^m. The growth rate of the RWM is $\gamma = d\Delta'_w/\tau_w$, where $\Delta'_w = [\psi'(d_+) - \psi'(d_-)]/\psi(d)$. A simple calculation gives

$$\frac{d\Delta'_w}{2m}\left[1-\left(\frac{a}{d}\right)^{2m}\right] = -\frac{(x+iy)}{(w-x-iy)} \quad , \tag{12}$$

where $w = 2/[(d/a)^{2m} - 1]$. For the case without rotation, $y = 0$, and the equilibrium is unstable without an external wall, $x > 0$. Equation (12) then predicts that the RWM is unstable for $d < d_{ideal} = a(1 + 2/x)^{1/2m}$. With increasing wall radius, $\Delta'_w \to +\infty$ when $d \to d_{ideal}$. When the rotation frequency is finite, y is non-zero. This eliminates the zero in the denominator of equation (12) so that Δ'_w remains finite and complex for all wall distances. Thus, rotation effectively separates the resistive wall mode from the plasma mode. As d increases, γ will behave as shown in figure 7(a) and the RWM is stabilized when d exceeds the threshold distance of $a[1 + 2x/(x^2 + y^2)]^{1/2m}$.

Bondeson and Ward [31] used both extensive computation and a simple mathematical model to support the proposition that the RWM can be stabilized by plasma rotation when the inherent plasma dissipation is taken into account.

We may summarize the salient features of this mode as predicted by the theoretical investigations of reference [13, 31]:

- The mode is unstable only if the plasma β_T is above the no-wall limit yet below the ideal-wall limit,
- The growth rate of the mode is comparable to the rate of flux diffusion through the resistive wall,
- The frequency of the mode is comparable to its growth rate yet the plasma could be rotating very fast relative to the wall,
- The mode has a global structure,
- The mode can be stabilized by plasma rotation.

These properties can all be tested by appropriately designed experiments. Since the mode is unstable only if the plasma β_T is above the no-wall limit yet below the ideal-wall limit, it is useful to define a parameter C_β to indicate how much the plasma is above the no-wall limit.

$$C_\beta = \frac{\beta_N - \beta_N^{no-wall}}{\beta_N^{ideal-wall} - \beta_N^{no-wall}} \quad . \tag{13}$$

2.2. Theoretical development of rotational stabilization of the RWM

2.2.1. Essentially ideal plasma response — robustness of the rotation-dissipation stabilization mechanism. The publication of the theory by Bondeson and Ward [31] has aroused much theoretical interest. Because their original results were obtained numerically, there were theoretical efforts aimed at clarifying the analytic properties of this stabilization. Amongst these are: (1) the mechanism of stabilization of the RWM, (2) the predicted critical rotation speed, (3) the size of the stability window. Notable among the theories are those of Betti and Freidberg [33] and that of Fitzpatrick and Aydemir [34] in their efforts to clarify the analytic relationships between the stability properties of the plasma and the assumed dissipation mechanisms.

In the analytical theory developed by Betti and Freidberg, a stability analysis of the XK mode is carried out for a cylindrical plasma in the presence of a resistive wall, plasma flow, and coupling to the sound wave continuum. It is confirmed that the resonance of the mode with the sound wave continuum produced an effective dissipation. The combined effect of dissipation and plasma flow opened up a window of stability for the RWM and provided an explanation of the numerical results of Bondeson and Ward. They also noted that toroidal effects increase the dissipation expected from the cylindrical model and the basic dispersion relation is cubic in the growth rate γ.

Fitzpatrick and Aydemir developed a simplified cylindrical model of this rather complicated stabilization mechanism in which the required plasma dissipation is provided by edge plasma viscosity. Due to its simplicity in capturing the key physics of the RWM, it has been useful in comparison with experiments or for further developments of theoretical insights. The details of this model are presented in Appendix B. In this model, the dispersion relation of the RWM also reduces to a simple cubic equation, which results from the coupling between the quadratic equation of the ideal mode and the linear equation of the flux diffusion on the resistive wall (section 2.3.2). Although the plasma models are very different, the predictions of the Fitzpatrick-Aydemir model agree surprisingly well with the more sophisticated model of Betti and Freidberg. According to both models, the critical toroidal plasma velocity required to stabilize the RWM

is of the order $k_{\|}aV_A$, where $k_{\|}$ is the parallel (to the magnetic field) wave number of the RWM at the edge of the plasma, a the plasma minor radius, and V_A is the typical Alfvén velocity. XK modes are only unstable in cylindrical tokamak plasmas when $k_{\|}a << 1$ for low n (toroidal mode number) kink modes. Hence the critical rotation velocity is only a few percent (5%, say) of the Alfvén velocity. Such rotation velocities are regularly generated in present day tokamaks when they are heated via neutral beam injection (NBI). Although plasma dissipation is needed for the stabilization of the RWM, the width of the stability window (in β_T) becomes independent of the dissipation once it exceeds a (small) critical magnitude. This fact helps to explain why the Fitzpatrick-Aydemir and Betti-Freidberg models agree fairly well, despite their quite different dissipation mechanisms. Thus, both of these works confirm the physical picture advanced by Bondeson and Ward. Both plasma dissipation and rotation have been shown to be necessary for stabilization of the RWM. The plasma rotation required for stabilization has been estimated to be a few percent of the Alfvén speed. However, the ion sound speed scales well with the Alfvén speed and the plasma rotation is thus typically of the order of the sound speed. Further, the ion species scaling is the same, making the experimental determination of critical rotation between scaling with respect to sound speed (C_s) or Alfvén wave speed (V_A) intractable [35].

2.2.2. Influence of plasma resistivity. A different stabilization mechanism was proposed by Finn [36]. He also studied the stability of the RWM in the context of a cylindrical plasma (with infinite aspect ratio) surrounded by a resistive wall and with rigid plasma rotation. He showed that modes with mode rational surfaces in the plasma, for example, β_T driven XKs in a torus, are stabilized just below the ideal threshold by becoming resistive (tearing-like) modes, which can be stabilized in the presence of a resistive wall and rotation. One consequence of the plasma becoming resistive is the possibility of the development of magnetic islands, which are very effective in transferring momentum to the RWM and it is predicted that only very small plasma rotation frequency ($\leq$1% of Alfvén transit frequency) is sufficient for the stabilization of the RWM. This branch of the RWM is subsequently called the resistive plasma RWM (RP-RWM).

The stability of a plasma with the inclusion of resistivity was further analyzed by Betti [37] for a circular plasma with a large aspect ratio $A = 1/\epsilon$. He found that, as proposed by Finn, the resistive plasma RWM (RP-RWM) occurred at a lower β_T value than the ideal plasma RWM (IP-RWM).

Finn's model and the RP-RWM mode was subsequently analyzed by Bondeson *et al.* [38]. These authors analyzed the situation of a single mode rational surface $q = m/n$ in a finitely conducting plasma by the resistive kink dispersion relation of Coppi [39]. The possibilities for stabilization of both the ideal and the resistive instabilities are explored systematically in different regions of parameter space. The study confirms that an ideal instability can be stabilized by a close fitting wall and a bulk plasma rotation frequency in the order of the resistive growth rates [36]. However, the region in parameter space where such stabilization occurs is very small and appears to be difficult to exploit in experiments. The overall conclusion from the cylindrical plasma model is that resistive modes can readily be wall stabilized, whereas complete wall stabilization is hard to achieve for plasmas that are ideally unstable with the wall at infinity.

2.2.3. Torque balance in a rotating plasma. In an axisymmetric confinement device such as the tokamak or the RFP, the plasma rotation and rotation profile are determined by the combination of several factors. First, even without any external torque input, the plasma has been found to have a natural tendency to rotate [40, 41]. The source of this rotation is most likely due to the ambipolar transport processes that maintain the macroscopic charge neutrality of the plasma. It is an area of active research and beyond the scope of the present review to discuss its detail. But this rotation speed is fairly small, of the order of the plasma diamagnetic frequency. Second, the plasma may be subject to an external torque input, such as through the injection of neutral beams and/or through the electromagnetic interaction with the external resistive wall and also the possible interaction with the external error field. Third, the plasma flux surfaces have an anomalous viscosity with respect to each other. These various factors combine together to determine the rotation profile.

The torque induced by a plasma resistive instability and the external resistive wall was first studied in detail by Nave and Wesson [42]. Rotation of MHD modes and torque balance between the plasma and the external resistive wall has also been pointed out as being important in determining the stability of MHD modes by Hender [43]. In 1993, two pioneering studies on the bifurcation of plasma equilibria with flow appeared. In the paper by Jensen *et al.* [44], the authors considered the problem of determining the equilibrium rotation velocity of a magnetic island in a plasma heated by neutral beam injection and surrounded by a resistive wall, by considering the torque balance relation for the magnetic island. The plasma, which is assumed to be trapped by the magnetic island, is imparted with angular momentum by neutral beam injection and moves through the ambient plasma, which provides viscous drag, to slow down the island. This was the situation of the tearing mode generated island interacting with

an external resistive wall. They found that, depending on the plasma viscosity, the equilibrium rotation velocity of the island can have two different values as shown in figure 9. For the case of a "large" viscosity, only one (slipping) solution exists; for a "small" viscosity, only a locking solution exists. For a "medium" viscosity, both a stable slipping and a locking solution exist as well as an unstable solution. This "bifurcation phenomenon" can be viewed in different ways. For the situation where the viscosity is fixed, then the size of the magnetic island could be used as the control parameter. In this case, a small island would be in the slipping branch, a large island would be in the locked branch and an island with an intermediate size could be either in the slipping or the locked branch. This same bifurcation was also discovered by Fitzpatrick in 1993 [45] with the same conclusion. Of course, the torque balance and bifurcation relation is quite general and could be applied either to a tokamak or an RFP. For an RFP, the transition between these branches has been studied quite extensively by Guo *et al.* [46, 47, 48].

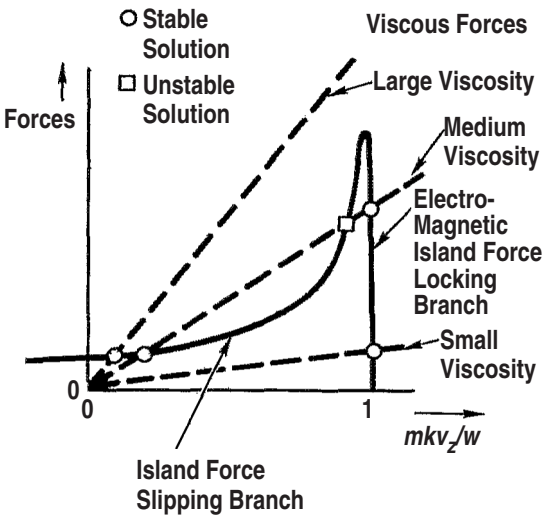

FIG. 9. Viscous and electromagnetic forces acting on a magnetic island versus normalized flow velocity in the z (toroidal) direction (assumed to dominate). An intersection represents a solution of force balance. For the case of a "large" viscosity, only one (slipping) solution exists; for a "small"" viscosity, only a (locked) solution exists. For a "medium" viscosity, both a stable slipping and a locking solution exist as well as an unstable solution (reference [44]). [Reprinted courtesy of AIP, Phys. Fluids **B5**, 1239 (1993).]

Plasma with a magnetic island and in equilibrium with an external resistive wall has been observed to be in either a high or a low rotation frequency and a forbidden frequency band was observed by Gates and Hender [49] in COMPASS-D.

The connection of this bifurcation phenomenon with the RWM is clarified quite elegantly by Fitzpatrick [50]. He showed that the bifurcated states of a rotating tokamak plasma in the presence of a static, resonant, error-field (external field) are strongly analogous to the bifurcated states of a conventional induction motor. The two bifurcated plasma states are the unreconnected state, in which the plasma rotates and error field

driven magnetic reconnection is suppressed, and the fully reconnected state, in which the plasma rotation at the rational surface is arrested and driven magnetic reconnection proceeds without hindrance. Therefore, the two bifurcated states of the plasma do not have to have islands rotating through the plasma. In his investigation, the problem was viewed as the response of the plasma to an external error field. He found that the response regimes of the rotating plasma depends critically on the state of the plasma in the vicinity of the rational surface. This response is characterized by three dimensionless parameters: the normalized plasma viscosity, P, normalized plasma rotation Q, and the normalized plasma resistivity, R.

$$P = \frac{\tau_R}{\tau_v} \quad ,$$

$$Q = \tau_H^{2/3} \tau_R^{1/3} \omega \quad ,$$

$$R = \kappa_p^{1/5} \frac{\tau_H^{1/5}}{\tau_R^{1/30} \tau_v^{1/30}} \quad . \tag{14}$$

In equations (14), the resistive diffusion time τ_R is given by $\tau_R = \mu_0 r_s^2 \sigma(r_s)$, μ_0 being the vacuum permeability, r_s the radius of the singular surface, and σ the conductivity; the viscous diffusion time τ_v given by $\tau_v = [r_s^2 \rho(r_s)]/[\mu(r_s)]$, ρ being the density and μ the fluid viscosity; and the hydrodynamic time τ_H given by $\tau_H = (R/B_T)\left(\left[\sqrt{\mu_0 \rho(r_s)}\right]/(ns)\right)$, with R the major radius, B_T the toroidal magnetic field, n the toroidal mode number; and s is the magnetic shear given by $s = (r/q)(dq/dr)$, with q being the safety factor. ω is the rotation frequency of the plasma and κ_p is here a profile parameter of the viscosity. The appropriate response regime for low density, ohmically heated tokamak plasmas is found to be the nonlinear constant ψ regime for small tokamaks, and the linear constant ψ regime for large tokamaks. The details of these regimes are explained in reference [50]. For a plasma rotating at a frequency ω_0 in the absence of the external error field, the transition between the high rotation state to the low rotation state occurs at approximately $\omega_0/2$, quite independent of the details of the different regimes. One of the conclusions of this study is that the critical error-field amplitude required to trigger error-field driven magnetic reconnection in such plasmas is a rapidly decreasing function of machine size, indicating that particular care may need to be taken to reduce resonant error fields in a reactor-sized tokamak [50].

2.2.4. RWM in the presence of error fields. Around the late 1990's, the prevailing opinion was that Bondeson's hypothesis of rotation-dissipation stabilization of the RWM was correct and the threshold rotation speed for stabilization was around a few

percent of the Alfvén speed. The experimental evidence indicated that reducing the error field in rotating plasmas and thus raising the rotation by removing drag led to longer duration of the plasma discharges. Gimblett and Hastie [51] realized that the torque balance relation in section 2.2.3 could provide insight into the dynamics of the plasma and should be included in the analysis. They first employed Finn's model [36] and showed that development of the magnetic island provided momentum exchange between the plasma and the resistive wall. A nonlinear mechanism is then available to determine plasma rotation self-consistently by an equation of torque balance. Using this RWM development model, the small stability window found in the linear studies of references [36, 37, 38] can be considerably extended at the expense of the growth of a magnetic island. On the other hand, depending on the initial rotation, the system can reduce the plasma rotation rate asymptotically to zero while the island continues to grow.

In 2002, Fitzpatrick [52] generalized the Fitzpatrick-Aydemir model (Appendix B) to include the effect of an external error field and with the torque balance relation to determine the rotation velocity of the plasma. One important element of this model is that rotation together with edge dissipation can stabilize the RWM in the range of the observed rotation speed. Numerical methods were applied to solve the resultant equation that determines the rotation speed and amplitude of the RWM. The results indicated that the development of the amplitude and rotation speed agree qualitatively with observation [53].

In a subsequent analysis by Gimblett and Hastie [54], they classify the stability of the RWM as three types: (a) with a stability window ($\Omega_1 \leq \Omega \leq \Omega_2$), such as the theory of Bondeson and Ward [31]. (b) never stable, $\Omega \neq 0$ merely reduces linear growth rate and never stabilizes the plasma, such as Finn's model [36] (c) with only a Ω_{crit}, $\Omega \geq \Omega_{cirt}$ for stability, such as Fitzpatrick-Aydemir's model [34] and Boozer's assumption [55] to be discussed in detail in sections 3.1, 3.2.1. It is noted that during the plasma evolution, the error field current is fixed, and not the error field flux, which is essentially an eigenvalue of the plasma-external error field system during the evolution. They used Finn's model to show theoretically that reducing error field amplitude in this type of models actually lengthens the duration of a "stable" discharge, but the mode actually was never stable. This shows features in accord with experimental observations from the DIII-D device. They then went on to suggest that if models of type (b) or (c) were valid for the RWM in ITER, it would require either active (section 4) or passive feedback stabilization of the RWM. They suggested detailed comparison of experimental data from large tokamak devices, with the predictions from alternative plasma models in future experiments to resolve this issue.

2.2.5. Further development of the theory of a secondary rotating wall The very attractive concept of a secondary rotating wall for stabilizing the RWM in RFP originally proposed by Gimblett in 1989 [17] was further investigated by many theorists. In 2000, this concept was studied for its suitability for a tokamak [56]. It was concluded that provided the second wall is suitably positioned, RWM stabilization of a tokamak is possible even in the absence of plasma rotation. In 2001, it was concluded by Freidberg and Betti [57] that the required rotation speed of the wall was too large to be practical. On the other hand, the equivalent concept of a virtual rotating shell (which is discussed in section 4.3.1) was studied by Fitzpatrick and Jensen [58] in 1996 and concluded to be quite feasible. The secondary rotating wall concept was analyzed by Taylor *et al.* [59] instead for a wall with non-uniformly rotation to avoid the locking of the RWM to the wall. Their conclusion was that in the case of toroidal rotation, the RWM is readily stabilized at large rotation velocity. In case of poloidal rotation, RWMs do not lock to the wall and have a complicated behavior at intermediate velocities. The RWMs are again stabilized by large poloidal wall velocity. The rotating wall concept was later analyzed by Hegna [60] for the case of a linear screw pinch with line-tying at the end walls. He found that the screw pinch can be stabilized if the edge q value is small. For a given equilibrium, there exists an optimal spacing between the stationary and the rotating wall that minimizes the critical rotation frequency of the wall for stabilization.

2.2.6. Challenge imposed by slow plasma rotation — kinetic plasma models. By 2004, there was experimental evidence of a reduced plasma rotation threshold for the stabilization of the RWM below the range of 1% of the Alfvén transit frequency (section 2.2.2). A numerical study was presented by Hu and Betti [61] considering the potential energy δW_k induced by MHD displacements on plasma particles in a high temperature plasma. This represents a major deviation from previous analytic models in which the plasma was considered to essentially obey the fluid equations. Their kinetic approach also went beyond the models used by MARS [31, 62] at that time in considering not only the bounce and transit resonances, but also the diamagnetic and magnetic drift resonances of the particles. This is more appropriate for plasmas with rotation frequency comparable to the magnetic (curvature and gradient) drift frequencies of the plasmas. They pointed out that the diamagnetic drifts and the magnetic drifts (which were neglected in previous studies), can provide substantial additional stabilization through δW_k. The trapped particle compressibility and the resonance between the mode and the precession drift frequency leads to a significant improvement of the β_T stability limits. It

was suggested that, within the framework of their simplified model, the RWM could be fully suppressed and the plasma could be stable up to the ideal wall β_T limit with slow plasma rotation. In short, they pointed out that the more relevant dispersion relation for the RWM is

$$\gamma\tau_w = -\frac{\delta W_\infty + \delta W_k}{\delta W_b + \delta W_k} \quad . \tag{15}$$

Here δW_∞ is the fluid potential energy without the external conducting wall and δW_b is the fluid potential energy with the inclusion of an ideal external wall at b, δW_k is the kinetic contribution to the potential energy evaluated using the fluid RWM eigenfunction (section 2.3.5). Their suggestion stimulated much interest and improved understanding of the plasma dynamics during the development of the RWM. Note that in equation (15) it was assumed that the bulk of the plasma behaves ideally at the singular layers at which $q = m/n$. Therefore, it was implicitly assumed that there were no islands present at these singular layers.

2.3. Models and codes for analysis of experimental data

The analytic theories developed in the previous section 2.2 provided important insights into the stabilization of the RWM. In analyzing experiments, it has been found useful to resort to the equivalent circuit models for the plasma. This provides a simple first type of model for the RWM. The second type of model is a comprehensive model for simulation of the RWM experiments. It was pointed out the precise dissipation mechanism could be quite immaterial according to Betti and Friedberg's [33], and Fitzpatrick and Aydemir's theory [34, 52] and Bondeson and Ward [31] (section 2.2.1). On the other hand, other class of theories, such as Finn's [36, 37, 38] theory or the more recent theory by Hu and Betti [61] predict very optimistic low rotation requirements for stabilization. Therefore alternative lines of approach were adopted for the systematic investigation of the stabilization mechanism and comparison with experiment.

2.3.1. The lumped parameter model. The lumped parameter model provides a simplified description of the plasma in terms of the perturbed plasma current I_p and the wall current I_w for comparison with experiment. It was introduced in the paper by Okabayashi *et al.* [63] for a cylindrical plasma without flow, with the perturbed plasma current concentrated at the plasma surface. It was further generalized to plasmas with flow in reference [64]. The details of this model are given in Appendix A. We note that

in principle, this model, when generalized to account for the actual spatial distribution of the current in the plasma and the wall, should be able to provide a complete description of the plasma dynamics in the fluid regime [64]. From the discussion in the previous section, to describe the interaction of plasma current with the external wall using surface current could be sufficient to account for the energy and momentum exchange. Including plasma flow, the basic equation is:

$$L_{eff} I_p + M_{pw} I_w = 0 \quad . \tag{16}$$

In equation (16), the I_i's with $i = (p, w)$ are the currents in the (plasma, wall). L_{eff} is the effective self-inductance of the plasma. The M_{pw} is the effective mutual inductances between the plasma and wall currents. The time scale is set by the resistive wall, therefore the current on the resistive wall satisfies

$$\frac{\partial}{\partial t}(M_{wp} I_p + L_w I_w) + R_w I_w = 0 \quad . \tag{17}$$

This model provides a description of the plasma and wall in terms of direct measurable quantities The major advantage of the lumped parameter model is the extreme simplicity of the model, the full dynamics of the system is encapsulated in the effective self- and mutual-inductances. Yet the major draw back is that many different more detailed plasma models that include the full dynamics of the plasma can result in the same lumped parameter model. Therefore, the suitability of one specific lumped parameter modeling for the description of a particular experiment may not guarantee its suitability for another experiment. For the purpose of extrapolation to future experiments, we have to be sure that the key parameters for the two experiments are compatible with each other. A discussion on the sufficiency of simplified models from a more theoretical point of view was provided by Pustovitov [65].

2.3.2. The MARS code and its generalization. The goal of the continued development of the MARS code is to validate the stabilization mechanism for the RWMs. MARS [62, 66, 67, 68], is a linear stability code using the eigenvalue approach to find the plasma stability with the complex growth rate being the unknown eigenvalue. Detailed formulation of this model with improved physical models of the plasma or the external vacuum regions are given in references [62, 66, 67, 68]. A brief summary of the formulation in MARS is given in Appendix C.

The first study of the RWM by Bondeson and Ward [31] was carried out with MARS, using analytic equilibrium profiles, assuming the plasma to be stationary and the wall to be rotating. It is natural in the ensuing research on the RWM to employ and extend MARS for detailed comparisons with experiments. For instance in the study by

Bondeson and Ward, they assumed the wall is rotating, therefore implying a uniform plasma rotation frequency with respect to the resistive wall. It was reasoned that the stabilization of RWMs derives from the relative rotation of the plasma with respect to the wall and should be relatively independent of whether the wall or the plasma is rotating. However, this study did not address the role of sheared plasma rotation and would not be able to determine whether rotation at the plasma center or edge is more effective in providing the dissipation and stabilization. The generalization of the MARS code to include sheared plasma rotation was reported in the work of Chu *et al.* [62]. In this work, it was also pointed out that the dispersion relation for the XK given in equation (5) is generalized from a quadratic to the following cubic equation.

$$(\gamma + in\Omega)^2 \delta K + (\gamma + in\Omega) D + \delta W_p + \frac{\delta W_v^b \gamma \tau_w + \delta W_v^\infty}{\gamma \tau_w + 1} = 0 \quad . \tag{18}$$

In equation (18), Ω is the rotation frequency of the plasma, $(\gamma + in\Omega)D$ is the energy dissipated in the plasma and δW_v^b and δW_v^∞ are the perturbed energy in vacuum with the wall at b and ∞ respectively. The general characteristics of its solution are given in reference [62].

Without rotation, and with a perfectly conducting external wall, there are two modes present in the plasma. One is the unstable XK when b is larger than b_c and the other is a stable plasma mode. Resistive diffusion of flux on the resistive wall introduces a third branch into the stability diagram and destabilizes the XK when b is less than b_c and appears as the RWM. As Ω increases, the RWM is stabilized by coupling to XK mode. This mode coupling is indicated in figure 10 by the curve $\Omega = \Omega_c$. At Ω_c, the two branches coalesce and exchange character (note this is not the rotation frequency at which the stability window first appears). A further increase in Ω leads to further opening up of the stability window.

A further extension of the MARS code was the implementation of magnetic feedback and the kinetic damping model into MARS-F [67]. The damping model

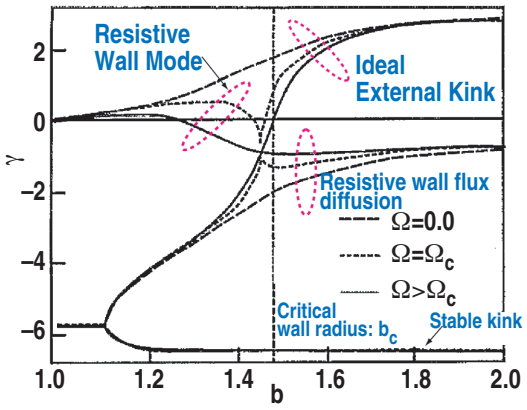

FIG. 10. Generic stability diagram for the cubic dispersion relation for RWM. Growth rate γ as a function of the external wall location b for coupled XK and diffusion through the resistive wall. The critical wall distance is at b_c. Three branches of the solution are shown. At Ω=0 (no plasma rotation, long dashed curves), one of the branches is unstable at all b. The other two branches are stable. As Ω increases, induced coupling between the stable and unstable branches causes the stability window to appear. Here Ω^c is the critical frequency for mode coupling. It is also close to the frequency at which the stability window first appears. The three branches of solutions at Ω^c are shown as dotted curves. For $\Omega \gg \Omega^c$, the stability windows become substantial in size. These three branches are shown as solid curves (reference [62]). [Reprinted courtesy of AIP, Phys. Plasmas **2**, 2236 (1995).]

was based on the work of Bondeson and Chu [69]. In this work, the plasma rotation speed was assumed to be higher than the diamagnetic and magnetic drifts of the particles but comparable to their bounce frequencies. Although this provides an improved justification to the dissipation model than the sound wave damping model employed previously, it was still not valid when the rotation frequency drops further to the range of the particle diamagnetic or magnetic drift frequencies. Included in the MARS-F is also the capability of magnetic feedback with details of the poloidal structure of the external feedback coils.

Yet a further extension of the code was undertaken in 2008 [68]. In this new version (MARS-K), the particle diamagnetic and magnetic drift frequencies are included. Therefore, it can evaluate the kinetic stabilization effect pointed out by Hu and Betti [61]. Depending on the mode frequency and growth rate, these drifts afect the kinetic δW_k differently from that prescribed by Hu and Betti. In principle, the final value of the growth rate and frequency would depend on the complete eigenfunction (and not just the eigenfunction based on the ideal MHD theories), which should be evaluated self-consistently including these drifts. These non-perturbative effects of the real frequency on the δW_k are included self-consistently in MARS-K.

2.3.3. AEGIS and AEGIS-K. Adaptive Eigenfunction Independent Solution shooting (AEGIS) [70] code and AEGIS-K [71] represent a different numerical approach (from using finite element) in the development of multi-time and multi-spatial scale codes for the study of linear stability problems (including the RWM) in plasma. AEGIS-K generalizes AEGIS [70] which is an ideal 2D-MHD code. The salient feature of AEGIS is that it employs the adaptive shooting method in the radial direction and Fourier decomposition in the poloidal direction. It therefore uses a numerical method similar to that of DCON(Direct Criterion of Newcomb) linear ideal stability code [72]. The general solution is a linear combination of the independent solutions of the Euler-Lagrangian equations solved by the adaptive shooting. A multiple-region matching technique is used to overcome the numerical difficulty associated with the stiff nature of the independent solutions. Because it is adaptive, the AEGIS code has very good resolution near the singular surfaces of MHD modes. It has the additional advantage of allowing the investigation of low, intermediate and high mode numbers. In AEGIS-K [71], the plasma is assumed to obey the gyrokinetic equations. The gyrokinetic theory employed in AEGIS-K, which was developed mainly for the application to the RWM, has been shown to: (1) recover the MHD limit in both perpendicular and parallel dynamics, and (2) recover the full finite Larmor radius effects. The AEGIS-K code has been applied to study the low rotation stabilization of the RWMs in ITER AT scenarios. The particle wave resonances, the coupling of the shear Alfvén continuum damping, the trapped particle effects, and the parallel electric field are all taken into account.

The effect of finite wall thickness on the stability of $n = 1$ RWMs in toroidal plasmas is investigated by Zheng *et al.* [73] using AEGIS. The finite thickness of the resistive wall has been found to reduce the growth rate of the RWM. No contribution to stabilization is found to be made by the portion of the wall that is located beyond the critical position for a perfectly conducting wall to stabilize the RWM.

2.3.4. MARG2D. MARG2D [74] adopts the view point that for tokamak plasmas, the important nonideal MHD effects are concentrated near the mode rational surfaces. Across these surfaces, the plasma eigenfunctions are connected by the stability index — Δ' (the jump in logarithmic derivative of the resonant component of the eigenfunction). Therefore, the strategy of MARG2D for studying the RWM, in which kinetic and nonideal MHD effects are important, is to propose a tractable implementation of a numerical scheme for the computation of Δ'. The scheme divides the plasma region into inner layers and outer regions as in the conventional asymptotic matching method. The essential difference is that each inner layer in the new scheme has a finite width (including the rational surface). Thus, the outer regions, which are governed by the Newcomb equation will have no singularity at their terminal points. The matching condition in this scheme is that the normal component of the plasma displacement vector is connected smoothly among outer regions and inner layers. It has been demonstrated that the new scheme can be applied to the initial value problem of the Frieman-Rotenberg [75] equation to analyze the effects of rotation on MHD modes.

2.3.5. MISK The MISK code is based on equation (15). It adopts the perturbative approach and uses the eigenfunction from the MHD code PEST as input to evaluate δW_k (section 2.2.6). It was first used by Hu *et al.* [61] to study the stabilizing kinetic effect of bounce and magnetic drifts of trapped particles. Using this code, qualitative stability diagram is obtained for the stability of RWM in NSTX [76, 77]. It shows that NSTX is expected to be stable at low rotation, with reduced stability over the range of rotation frequency at which the RWM was observed in experiments. Thus indicating that either some other destabilization mechanism is present or perturbative approach is too optimistic.

It should be mentioned that for the models in sections 2.3.2, 2.3.3, 2.3.4, 2.3.5 to more accurately model the plasma in the frequency regime relevant for the RWM, the collisions of the particles, especially the ions are expected to be in the same frequency range. Therefore it needs to be modeled accurately. This is one of the aspects yet lacking in all models mentioned above.

2.4. Experimental identification of the RWM

Soon after the publication of the rotational stabilization theory of the RWM by Bondeson and Ward [31] and the confirmation by various analytical theories described previously in section (2.2), experiments were started to test these predictions. First amongst these experiments is to identify the existence of the RWM in a rotating plasma by looking for the signature of the predicted MHD perturbation.

By early 2004, the RWM in a rotating plasma had been identified in most of the major high β_T tokamaks. The cross-sections of these devices are shown (together with the location of the external perturbation or feedback coils) in figure 11. The parameters of the tokamak plasma and external wall in which unstable RWMs were studied are summarized in Table I. In those early experiments, the plasma rotation at the onset of RWM is 1%–2% of Alfvénic velocity at $q = 2, 3$ surfaces. The unexpected consequences were that growth of the RWMs is sometimes followed by a major or minor β collapse or disruption. These results also suggest that a toroidal rotation frequency below 1%–2% is insufficient for stabilization of the RWMs by the resistive wall (c.f. section 2.6).

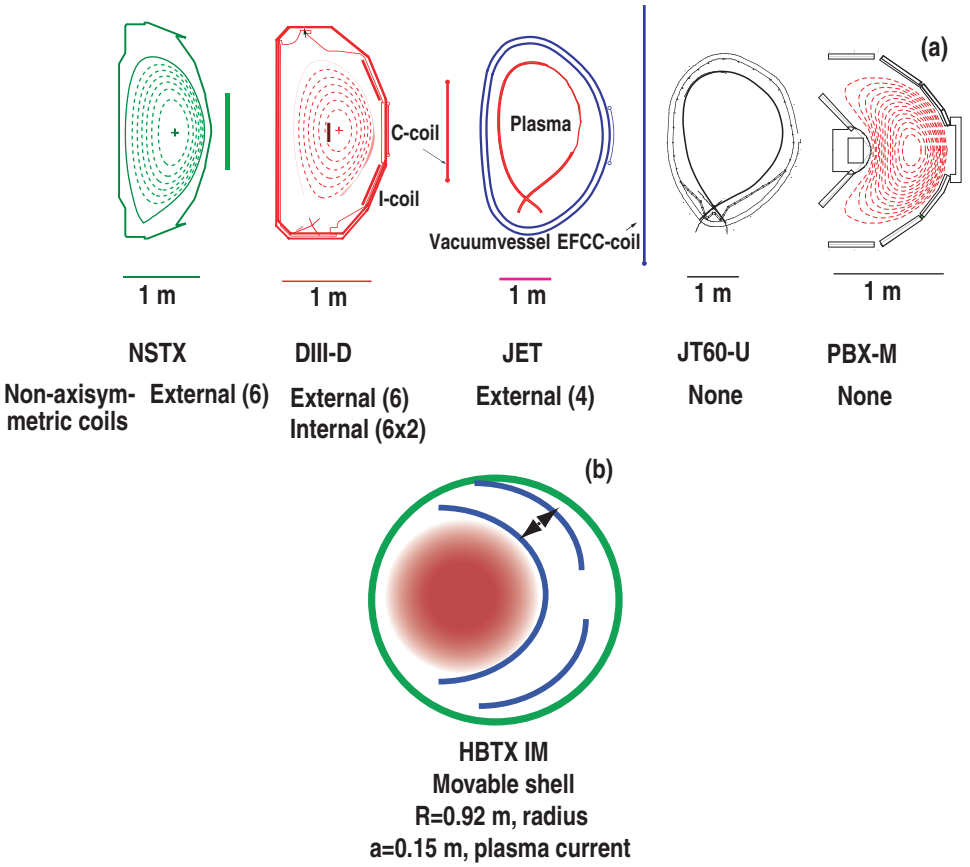

FIG. 11. Configuration of the tokamaks and external walls in which the RWM has been observed. Shown in (a) are the NSTX, DIII-D, JET, JT60-U, and PBX-M tokamaks with their typical plasma shape and the external walls. The relative sizes of the tokamaks can be discerned by the meter bar shown below. PBX-M is surrounded by stabilizing plates and does not have a closed external wall. Shown in (b) is the HBT-1B device with its surrounding wall and movable stabilizing shell.

Table I. Parameters of tokamaks in which experiments on RWM were carried out

	R/a	b/a	τ_w
DIII-D	2.5	1.15	Vessel ∼5 ms
JET	3	1.3	Vessel ∼3 ms
JT-60U	3.2	1.3	Vessel ∼5 ms
NSTX	1.2	1.2	Shell ∼16 ms
PBXM	5.5	1.2	Shell ∼30 ms
HBT-EX	10	Variable	Shell variable

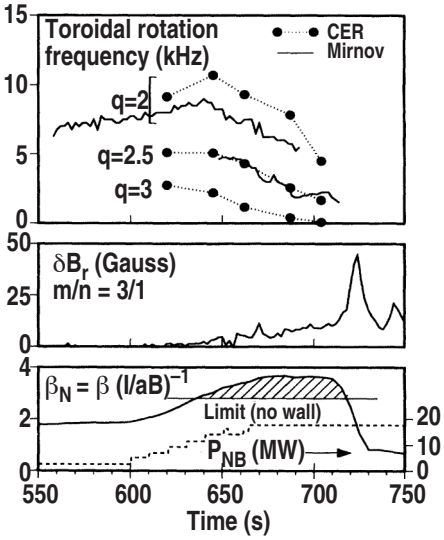

FIG. 12. Identification of the RWM in DIII-D. Top panel shows time evolution of rotation frequencies at several rational surfaces determined from magnetic (Mirnov) oscillations and CER spectroscopy in this discharge (80111). The second panel shows δB_r of the nonrotating $m/n = 3/1$ mode from saddle loops at the midplane. The third panel shows normalized β_N, and neutral beam power P_{NB}. A disruption followed the RWM; the β_N kept on decreasing and never recovered (references [78, 79]). [Reprinted courtesy of APS, Phys. Rev. Lett. **74**, 2483 (1995).]

2.4.1. RWM can lead to disruption. A 1995 experiment [78, 79] in DIII-D can serve as an example of a discharge identifying the RWM as the cause of plasma β collapse as shown in figure 12. Shown in this figure is the time evolution of a high β_T discharge. The first panel shows the reduction in time of the plasma rotation frequencies at several rational surfaces determined from magnetic oscillations and charge exchange recombination (CER) spectroscopy. The second panel shows growth in time of δB_r of the very slowly rotating $m/n = 3/1$ mode from saddle loops at the midplane. The third panel shows the trace of normalized β_N and that the growth of the mode occurred in the phase when the plasma β_N was above the no-wall limit $\beta_N^{no-wall}$. It is important to note that although the level of the magnetic perturbation has been increasing since the plasma entered into the phase of $\beta_N > \beta_N^{no-wall}$ around 645 ms, the rate of "growth" was very slow, presumably due to the fact that the toroidal rotation frequency was still sufficient to suppress the mode. Therefore, the beginning of the rapid growth of the RWM was identified at around 720 ms when the rotation had slowed down substantially across the plasma. The rotation profile at that instant was identified as the critical rotation profile. The fast growth phase of the RWM was followed by a disruption. It was noted that the onset of the RWM which led to disruption was not predictable.

In addition, we note that in a later 2007 experiment, in a discharge in DIII-D, β_N was ramped up by increasing the neutral beam injection (NBI) heating power while keeping the NBI torque very low. Measurements of the poloidal magnetic field B_p show that the high β phase is terminated by a nonrotating $n = 1$ mode with a characteristic growth time $\tau_g = 20\,\text{ms}$, which is several times the value of the resistive wall time. This is consistent with an RWM for $\beta_N > \beta_N^{no-wall}$. Thus, verifying that the RWM in a very-slowly-rotating plasma does agree with the expectation according to the ideal MHD theory surrounded by a resistive wall [80].

2.4.2. The slowly rotating RWM in a fast rotating plasma. In all the rotation stabilized experiments, despite the fast rotation ($\gtrsim$kHz) of the plasma, the mode was rotating very slowly with respect to the resistive wall ($\sim$Hz) or locked to the wall. This is shown for example, in figure 13(a) and 13(b) in the JT-60 experiment by Takeji [81]. In this case, it is interesting to note that the growth of the RWM did not slow down the plasma in JT-60 [83], whereas the slowing down of the plasma was very evident in DIII-D [figure 12(a)]. This poses an interesting question as to how the magnetic perturbation exchanges angular momentum with the plasma.

To clarify the effect of plasma-wall separation on the stability of the RWM, the current-driven RWM was studied by systematically changing the position of the plasma relative to the resistive wall shown in figure 13(c). It is found that the growth rates became smaller with decreasing separation. In addition, the growth rates were compared with the AEOLUS-FT code [84], which is based on the resistive MHD equations with a resistive wall. The dependence of the observed growth rate on the wall position is in qualitative agreement with the numerical results and shown in figure 13(d) [82].

2.4.3. The evolving RWM can lead to thermal collapse. The consequence of the excitation of the RWM has not been found to be predictable. It could lead to a disruption or to a thermal collapse, which acts as a precursor to a disruption. This is shown, for example in an experiment on PBX-M.

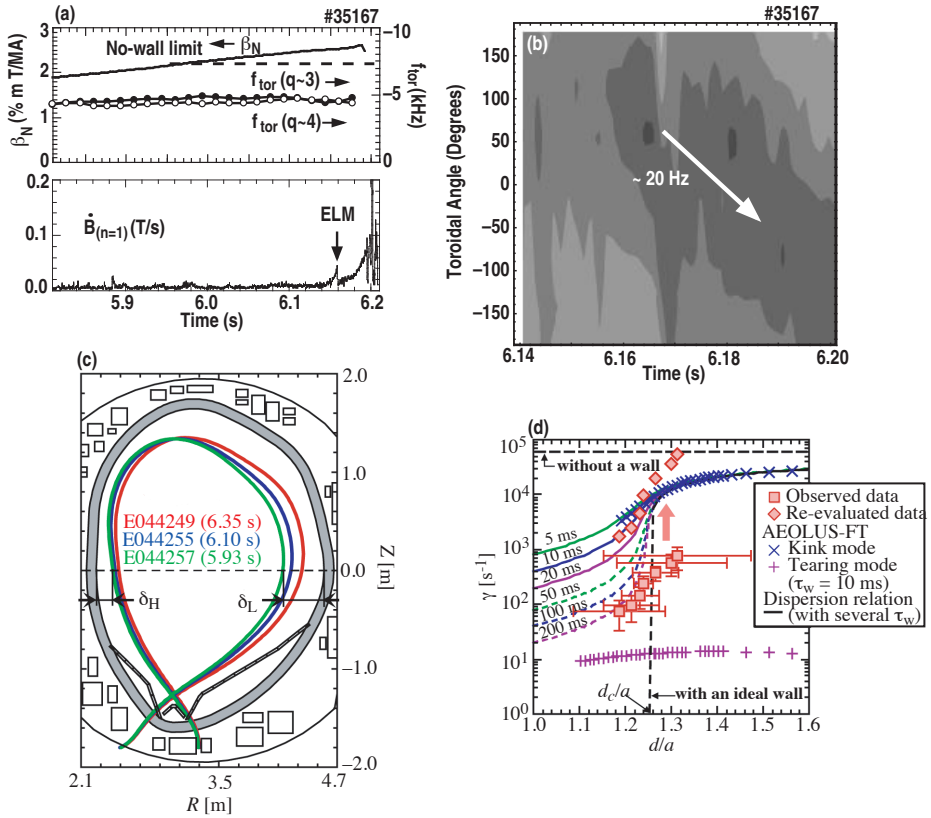

FIG. 13. Observation of a slowly rotating (∼20 Hz) RWM with fast plasma (∼5 kHz) rotation in JT-60U. On the left are waveforms of (a) β_N and plasma rotation frequency in the toroidal direction, f_{tor}, near the $q = 3$ and $q = 4$ rational surfaces; (b) time derivative of $n = 1$ radial magnetic perturbations. On the right (c) is the contour plot of the time derivative of the perturbed radial magnetic field measured by a toroidal array of eight saddle loop sensors inside the vessel (reference [81]). Shown in (c) are separatrices of plasma-wall separation scan experiments. δ_H and δ_L are the separation at the high- and low- field side, respectively. Shown in (d) is the dependence of growth rates on wall position. Thick lines show a dispersion relation with τ_w of $5, 10, 20, 100$ and 200 ms. Growth rates with an ideal wall and without a wall are also shown. Crosses and pluses are the growth rates of kink and tearing branches calculated by the AEOLUS-FT code. Squares and diamonds indicate the experimentally obtained and evaluated growth rates (reference [82]). [Reprinted courtesy of IOP, Nucl. Fusion **42**, 5 (2002).]

The RWM was identified in PBX-M using the eddy currents induced on the passive stabilizing shell. Figure 14(a) shows the time dependence of the eddy current in one of the connection jumpers on the upper/lower stabilizer shell during a disruption precursors, while figure 14(b,c) shows the amplitude and phase of the $n = 1$ component of the eddy current distribution obtained from all midplane jumpers distributed in

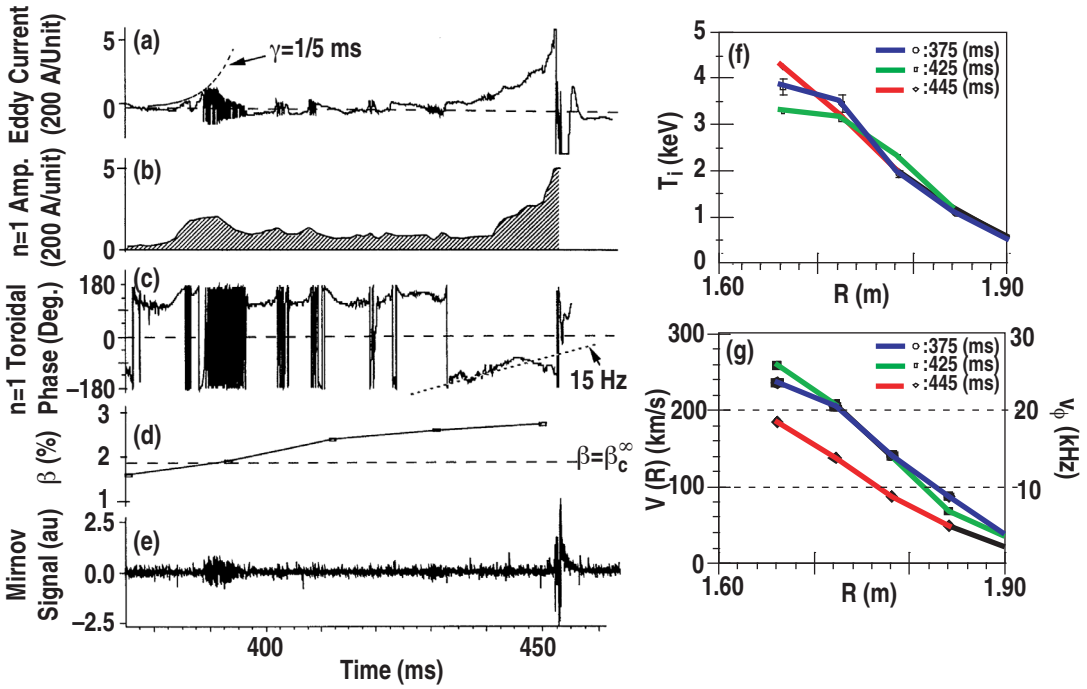

FIG. 14. Development of the RWM can lead to thermal collapse which acts as a precursor to disruption for the bean-shaped PBX-M discharge 273849. (a–c) Evolution of the eddy current on the passive shell; (d) evolution of plasma β_T, and its relation to the β_T no-wall limit, the β_T for the $n = 1$ kink mode computed by PEST with a conducting wall at infinity; (e) Mirnov signals; (f) velocity profile, obtained at $t = 375$, 425 and 445 ms; and (g) ion temperature profile measured at $t = 375$, 425 and 445 ms (reference [85]). [Reprinted courtesy of IAEA, Nucl. Fusion **36**, 1167 (1996).]

the toroidal direction. Figure 14(d) shows the time evolution of plasma β_T, calculated by equilibrium reconstruction, and its relationship to the critical β_T for marginal stability of $n = 1$ ideal XK mode calculated by using the PEST code with a perfectly conducting wall at infinity. The initial growth of the precursor around $t = 380$ ms is correlated with the time at which β_T is close to the $n = 1$ no-wall limit. At $t = 385$ ms a non-rotating precursor grows with $\gamma = 1/5(ms)^{-1}$. After a short period of growth, the mode begins to rotate rapidly at 3 to 5 kHz. During the transition to a rotating state, no discontinuities in the time derivative of the eddy current pattern are observed, indicating that the rotating mode is a continuation of the existing non-rotating mode, rather than some other newly triggered mode (such as a tearing mode). Coincident with the mode rotation is a substantial decrease in mode amplitude. Finally, when the mode amplitude is small, the mode ceases to rotate. The cycle of mode growth, followed by mode rotation and mode amplitude decrease, occurred several times before the final phase of mode growth which began at $t = 430$ ms. The mode is essentially non-rotating (with extremely slow rotation), and has a growth rate of $\gamma = 1/5(ms)^{-1}$.

In spite of the excitation of the $n = 1$ mode, the change in the ion temperature profile, $T_i(r)$ is modest and the toroidal rotation velocity remains finite. The observation of an MHD perturbation with near zero mode frequency in a plasma with finite rotation is similar to the observations of the RWM on other devices.

2.4.4. Verification of the global structure of the RWM. The global nature of the RWM is identified through the correlation of measurements from different diagnostics and through comparison with numerical computations based on ideal MHD codes. An example of this is shown in figure 15 [85, 86], for a representative discharge with dynamic error field correction (section 3.7) in DIII-D. It is accomplished by using two soft x-ray array systems 150 degrees apart in the toroidal direction together with the flux loops located outside of the resistive vessel. The amplitude of the RWM started to grow slowly at 1380 ms, reached $2 - 3$ G at 1410 ms, and saturated later at an amplitude of 10 G. At 1475 ms, a major disruption took place. Note that the dynamic error field correction was being applied from 1300 ms onward. The close correlation in the behavior of

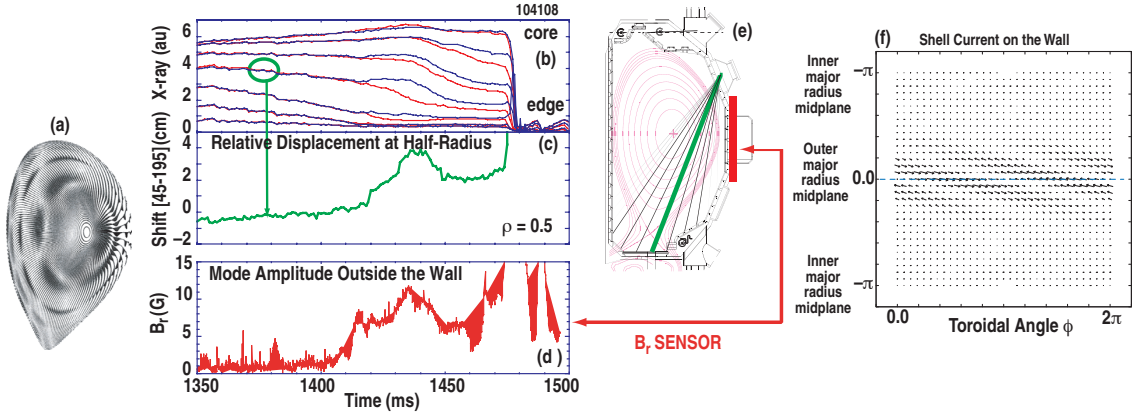

FIG. 15. Identification of the global structure of the RWM in DIII-D. Shown are $n = 1$ displacements computed from PEST and mode amplitudes measured inside the plasma and that observed in the vacuum region. (a) A typical mode structure of the RWM displacement computed by PEST, (b) signals from the array of soft x-ray detectors observed at two different toroidal locations separated by 150 degrees in the toroidal direction which allowed identification of the $n = 1$ character of the mode, (c) the magnitude of the displacements at $\rho = 0.5$, (d) integrated fluctuating magnetic signal of the mode amplitude measured outside the vacuum vessel, and (e) schematic of SXR channels and location of external B_r sensor (reference [86]). [(a-e) Reprinted courtesy of AIP, Phys. Plasmas **8**, 2071 (2001).] (f) The distribution of skin current on the resistive wall. Vertical axis is in the poloidal direction starting from the inboard side counter clockwise to the outboard midplane and then back to the inboard midplane. The central band of large skin current located on the outboard midplane is typical of MHD ballooning modes. The horizontal axis is in the toroidal direction (reference [87]). [(e) Reprinted courtesy of AIP, Phys. Plasmas **4**, 2161 (1997).]

the mode amplitudes outside of the vacuum vessel and that of the internal perturbations indicates that the RWM is a global mode with structure extending from the plasma core to the vacuum. This characteristic agrees with the predictions from ideal MHD theory. Furthermore, the global mode pattern did not change significantly during the feedback process. Note that the mode pattern shown in figure 15(a) computed by PEST agrees with an independent computation using GATO. The derived external signals from PEST and GATO compared well with the magnetic measurement by the external probes. Both of these calculations show that the plasma displacement on the same flux surface on the toroidal midplane is larger on the outboard side than the inboard side. This is also confirmed by the computed pattern of the skin current on the resistive wall. Shown in figure 15(f) is the eddy current computed by using the VACUUM [87] code for this discharge in the (toroidal angle-poloidal angle) plane. The poloidal angle starts from the inboard midplane ($-\pi$) counter clockwise along the vessel to the outboard midplane 0 *deg* and then back to the inboard midplane (π). It is seen that the eddy current is concentrated on the outboard midplane which is typical of the eddy current for a plasma mode structure that balloons towards the outboard side.

2.4.5. RWM with higher toroidal mode numbers. The $n = 1$ RWM as well as modes with higher ($n \geq 2$) toroidal mode numbers can be excited simultaneously. Unstable RWMs with $n = 1 - 3$ have been observed in high β_T NSTX plasmas [88]. The mode spectrum and mode growth for discharges showing no mode rotation, and with mode rotation are shown in figure 16. Mode growth and associated β_T collapse occur in a few τ_w (about 5 ms). The B_p sensor array shows nearly simultaneous growth of $n = 1 - 3$ modes in figure 16(a) at a peak $\beta_T = 35\%$ and the measured toroidal phases ($n = 1$ phase is shown) do not show mode rotation. RWM dynamics from the Fitzpatrick-Aydemir theory [34] indicates that the mode may rotate as the plasma becomes unstable. This is observed in the plasma shown in figure 16(b). As expected by theory, the measured mode rotation frequency of 120 Hz is of the order of $(1/\tau_w)$ and the phase propagation is in the direction of plasma rotation. At this rate, the mode significantly slips behind the measured plasma rotation frequency of 2 kHz. The phase velocity changes in time as the mode rotates through the toroidal location of maximum error field. The $n = 1$ locked mode detector external to the vacuum vessel begins to measure the RWM about τ_w after it is observed on the B_p sensors due to the mode penetration of the vessel. It measured a factor of five less signal, and is not capable of detecting the detailed phase shift during RWM growth. A rapidly rotating (20 kHz) $n = 2$ mode exists throughout the high β_T phase, which is easily distinguished from the RWM. Time-evolved ideal MHD stability,

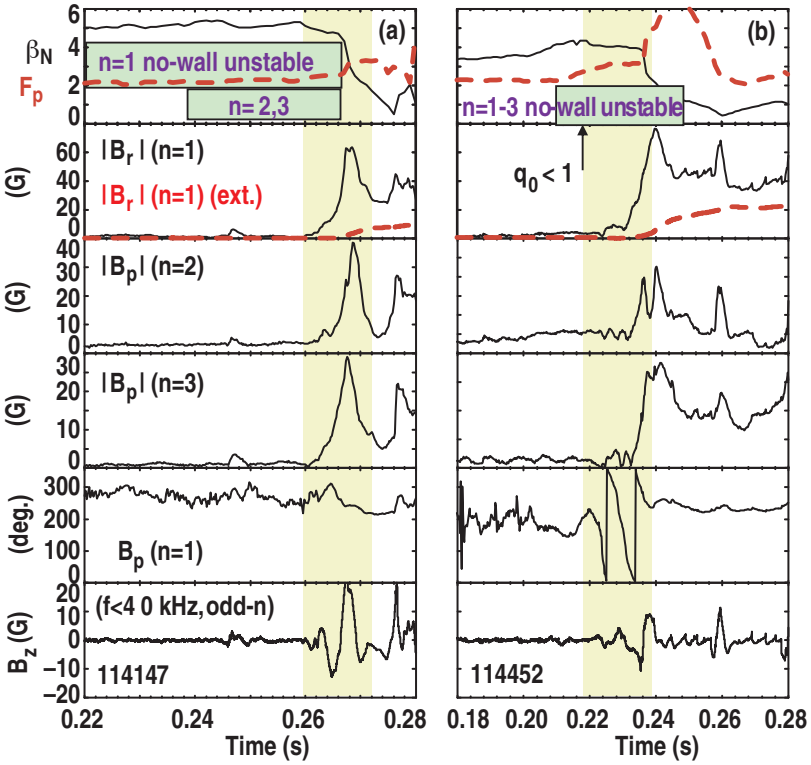

FIG. 16. Spectrum of toroidal mode numbers and mode dynamics of RWMs observed in NSTX. The figures show (a) mode amplitudes and (b) toroidal phase evolution due to mode rotation during growth. Signals measured by sensors inside(outside) the vacuum vessel are shown in black (red). The green bands cover time periods during which reconstructed plasma equilibria unstable to the XK predicted by DCON. The vertical yellow bands cover periods during which unstable RWMs are observed (reference [88]). [Reprinted courtesy of IAEA, Proceedings of 20th IAEA Fusion Energy Conference, Vilamoura, Portugal (IAEA, Vienna, 2004) Paper EX/3-2, available on CD.]

assuming no stabilizing wall for $n = 1 - 3$ modes, was computed for these plasmas with DCON [72] using time-evolved EFIT [89] equilibrium reconstructions. Figure 16(a,b) shows that before RWM mode growth, both plasmas exceed the computed $n = 1 - 3$ ideal no-wall β_T limit. In the final stage of the RWM in NSTX, the mode amplitudes grow to $B_n \geq 30 - 50$ gauss for all $n = 1, 2, 3$ and indicates that the mode growth might have entered into the nonlinear regime.

We note that plasma in NSTX is heated by NBI injection and inherently has a large rotation velocity relative to the Alfvén velocity. The RWM is usually induced by magnetic braking using resonant field amplification. The critical state with lower rotation velocity can be connected with the higher velocity state without going through rotation bifurcation. [76, 90, 91, 92](c.f. 2.6), indicating a situation in which the plasma is approaching the marginal stable state faster than the rate of increase of the applied error field [54].

2.5. The critical rotation speed and critical rotation profile

2.5.1. Initial investigation of the damping mechanism with MARS. The MARS code was used to study the critical rotation and damping mechanism for the RWM. The critical rotation velocity is defined as the rotation velocity below which, the RWM is observed. Since in general, the plasma rotation profile is not a constant, we should study the rotation profile of the whole plasma to obtain an understanding of the role of the rotation and its shear. Previous studies assumed that this critical rotation speed is independent of the way in which the plasma was prepared, such as whether external (non-axisymmetric) fields were used, whether the plasma β_T is increasing or decreasing at the time when the mode was first observed. Some of these assumptions turned out to be incorrect for reasons associated with the torque balance of the plasma rotation with the error field drag.

In the early works, the simplest assumptions are made. It is assumed that the plasma rotation profile alone determines the critical rotation speed. The damping mechanism used was the ion Landau damping which was appropriate for high temperature collisionless plasmas.

To include ion Landau damping as a mechanism in the fluid MARS code, two models were adopted. The first model assumes that Landau damping can be simulated as a parallel viscosity. This has been proven to be accurate for electro-static modes [93]. For the electro-magnetic RWM mode, it was assumed that the analytic form of this process is still valid, but that the damping coefficient is adjustable. This is called the ion sound wave damping model, because it can be shown that the damping enters directly into the ion-sound wave dispersion relation. The second model is the "more accurate" semi-kinetic model without free parameters. In the semi-kinetic model, it is recognized that the damping can be viewed as a drag on the ions. This drag is introduced as a local force, derived from the imaginary part of the kinetic potential energy δW_k acting on the displacement perpendicular to the field lines. For this dissipative part of the δW_k, a further assumption of the large aspect ratio cylindrical plasma equilibrium was made [69]. We note that this was a simplification from the original and exact formulation by Antonsen and Lee [94]. The semi-kinetic damping model was incorporated into the MARS-F [67] code in 2003. An important consequence of the semi-kinetic model is that when the rotation is subsonic, the ion Landau damping comes predominantly from regions where the parallel phase velocity is near sonic, i.e., close to the resonant surface where $(m/q - n)v_{th,i}/R \sim \Omega$ [95]. Implicitly, effects due to gradient B and toroidal curvature drifts [69, 96] are assumed insignificant. The parallel motion involves the toroidal sidebands; e.g., an $m = 2$, $n = 1$ magnetic perturbation couples to parallel flows with $m + 1$ or $m - 1$, i.e. to $m = 1, 3$, $n = 1$, and for small rotation speeds, these sidebands produce damping around the rational surfaces $q = 1$ and 3. For larger rotation speeds, when the rotation speed is a few percent of v_A, the kinetic damping is spread out across the entire cross section.

The first direct comparison of experiment with theory was using the ion-sound wave damping model on DIII-D data. The data was taken at the time when the amplitude of the RWM started a phase of fast growth at $t = 720\,\text{ms}$ (figure 12). The results of the computation are shown in figure 17. These curves with different plasma rotations at fractions of the observed rotation speed, resemble and are the more general behavior of the growth rate curves given in figure 7(a). It is seen that the experimentally observed and calculated stabilization occurred within the computed range of the rotation speeds. The best fit to the computed stabilization is obtained by setting the damping coefficient $\kappa_{\|} = 0.5$. It is therefore concluded that the observed RWM stability threshold can be described by the ion-sound wave damping model with a damping coefficient of $\kappa_{\|} = 0.5$.

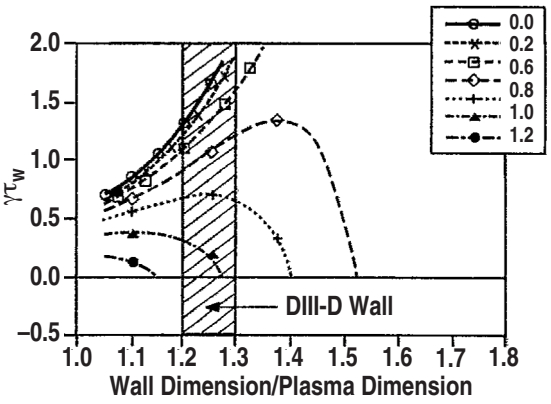

FIG. 17. Using the sound wave damping model, the growth rates at different fractions of plasma rotation frequency are shown as a function of the position of the external wall. When the rotation multiplier is low, the RWM is always predicted to be unstable. With increasing rotation (multiplier >0.6), stabilization becomes possible. The equivalent DIII-D wall is between 1.2 to 1.3 plasma radius. It is seen that the experimentally observed stabilization of RWM is within the computed range of frequencies (curves labeled 1.0 and 1.2) (reference [62]). [Reprinted courtesy of AIP, Phys. Plasmas **2**, 2236 (1995).]

Subsequent computational studies by Gregoratto [97], using several different rotation profiles, have been used to explore the interaction of plasma rotation profile with the q profile to determine the stability threshold of the RWM. One of the conclusions of this paper was that the Alfvén continuum damping, combined with the rotation profile effect, gave the major contribution for the RWM stabilization. The result of this study indicated that for typical advanced tokamak profiles, the plasma rotation at $q \sim 2$ was an important factor for determining stability. The rotation speed at $q = 2$ was used as a guide for determining the key parameters for experiments while recognizing the effect of damping really originates from the whole rotation profile.

It was then found that the dissipation also depended substantially on the plasma current profile (l_i, here l_i is the internal inductance) [35, 98]. A more extensive comparison was made for plasmas with both low and moderate l_i. In this study, the experimental pressure profile was scaled from the no-wall to the ideal-wall limit. At each pressure the measured rotation profile was scaled until marginal stability was found.

The critical rotation frequency at $q = 2$ calculated using the sound wave damping model with $\kappa_{\|} = 0.1$, 0.25 and 0.5 and the kinetic damping model were compared with the measurements. It was found that sound wave damping using values of 0.25 and 0.5 for $\kappa_{\|}$ underestimated Ω_{crit} for C_β in the range from 0.0 to 0.2 and over estimated Ω_{crit} for C_β greater than 0.4. Kinetic damping predicted a weak dependence of Ω_{crit} on C_β but underestimated the magnitude of Ω_{crit} by approximately 40%.

These comparisons showed in 2004 we still needed more work to improve the predictive capability of the models.

2.5.2. Comparison of the damping mechanisms vs. experimentally observed threshold. Although the various codes, including the ideal MHD codes PEST, GATO and DCON, and the RWM code MARS were able to simulate the global structure of the RWM, the damping mechanisms included in the MARS code were based on approximations to the kinetic response of the plasma. It was not clear whether an improved kinetic model or a more extensive phenomenological model for the dissipation could give us a more useful guide to the damping mechanism. A systematic comparison of the two damping models: sound wave damping vs. semi-kinetic damping were undertaken in 2004 [99]. Shown in figure 18 is the comparison of the stability boundary computed using MARS-F with two different plasma dissipation models with the critical rotation speed determined from the DIII-D RWM experiments. We note that the semi-kinetic damping model gives stronger damping. But it is the ion sound wave model (with $\kappa_{\|} = 0.5$, a (smaller,larger) value of $\kappa_{\|}$ will give a (larger,smaller) Ω/ω_A) that provided a better qualitative agreement with the experimental results. The computed results from

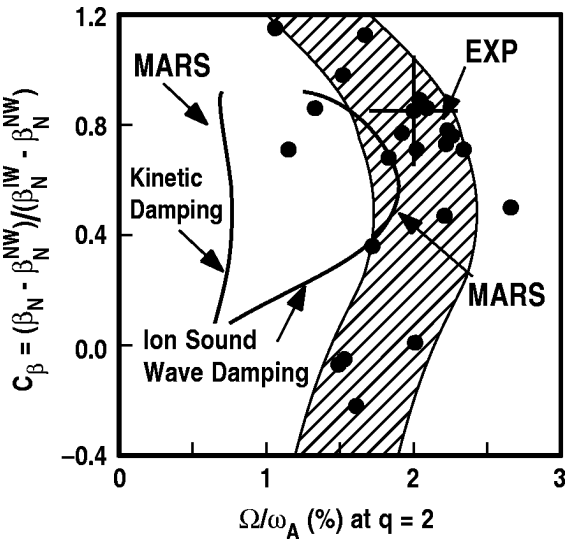

FIG. 18. Comparison of the stability boundary computed for a model set of equilibria using MARS with the ion sound wave damping and semi-kinetic damping dissipation models with the experimentally determined thresholds from DIII-D data taken before 2004. Results from MARS with the ion sound wave damping model agrees more with the experimental results qualitatively. The computed thresholds given by the semi-kinetic damping model were deemed too low. However, experiments in 2006 and later revealed even lower stability thresholds (reference [99]). [Reprinted courtesy of AIP, Phys. Plasmas **11**, 2497 (2004).]

the semi-kinetic models were regarded as being too low. Because the sound wave damping model is more of a phenomenological model, whereas the semi-kinetic model is based more on the kinetic response of the plasma, we would expect that if the damping of the RWM can be obtained from linear kinetic theory, the semi-kinetic model should provide a better qualitative description to the experimental results. Therefore, based on theoretical grounds, we should draw the puzzling conclusion that the damping of the RWM is dominated by anomalous processes. (In section 2.7, an explanation is given to this puzzle.)

2.6. Stabilization of RWM in tokamaks with slow rotation

Around 2007, first experiments on the stabilization of the RWM in tokamaks with slow rotations were reported both by the DIII-D [100] and JT-60U [101] research groups.

Experiments on DIII-D showed that the RWM can be stabilized by smaller values of plasma rotation than previously reported. Stable discharges have been observed with β_T up to 1.4 times the no-wall kink stability limit and ion rotation velocity (measured with Carbon-VI emission) less than 0.3% of the Alfvén speed at all integer rational surfaces, in contrast with previous DIII-D experiments that indicated critical values of 0.7%–2.5% [53, 78, 86] of the local Alfvén speed. Shown in figure 19(a) are trajectories of several discharges with different β_T and toroidal rotation, parameterized by time. The abscissa is the rotation frequency at radius $\rho = 0.6$, normalized by the local Alfvén time, and the ordinate is C_β. The square at the end of each trajectory represents the onset of a RWM. A key feature of these experiments is that slow plasma rotation was achieved by reducing the neutral beam torque. It was conjectured that earlier experiments with strong neutral beam torque and "magnetic braking" by applied magnetic perturbations to slow the rotation, and resonant effects of these perturbations may have led to a larger effective rotation threshold. In addition, the edge rotation profile may have a critical role in determining the RWM stability in these low-torque plasmas [100].

Similarly, in JT-60U, the plasma rotation necessary for stabilization of RWMs was investigated by controlling the toroidal plasma rotation with external momentum input using injection of tangential neutral beams. The observed threshold is 0.3% of the Alfvén velocity and much smaller than the previous results obtained with magnetic braking [81, 83]. Shown in figure 19(b) are trajectories of the C_β versus toroidal rotation at the $q = 2$ surface. The crosses denote the onset points of RWM in JT-60. The critical rotation has a very weak β dependence as the ideal wall limit is approached (c.f. figure 18). These results indicate that for large plasmas such as in future fusion reactors with low rotation, the requirement of additional feedback control for stabilization may be much reduced [101].

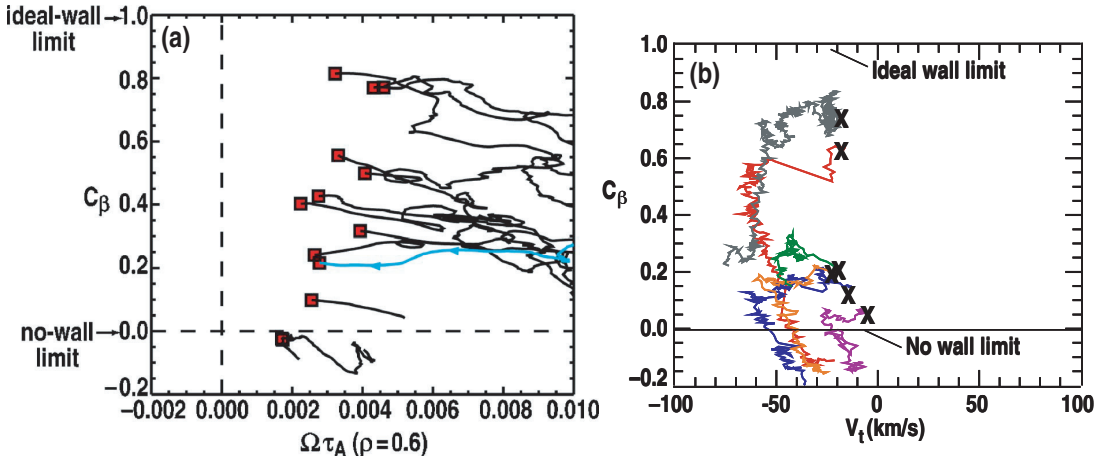

FIG. 19. (a) Trajectories of several discharges in beta and toroidal rotation in DIII-D, parameterized by time. The abscissa is the rotation frequency at radius $\rho = 0.6$, normalized by the local Alfvén time, and the ordinate is $C_\beta = [\beta - \beta(no - wall)]/[\beta(ideal - wall) - \beta(no - wall)]$. The square at the end of each trajectory represents the onset of a RWM (reference [100]). [Reprinted courtesy of AIP, Phys. Plasmas **14**, 056101 (2007).] (b) Trajectories of the C_β versus toroidal rotation at the $q = 2$ surface. The crosses denote the onset points of RWM in JT-60 (reference [101]). [Reprinted courtesy of APS, Phys. Rev. Lett. **98**, 055001 (2007).]

2.7. Reconciliation between the high(old) and low(new) torque input experimental data in DIII-D and JT-60U.

An important step towards reconciling the new observation [100, 101] of a low rotation threshold with the higher threshold values obtained in DIII-D and JT-60U experiments with using high NBI torque [35, 53, 78], is to take into account the torque balance in the plasma equilibrium (section 2.2.3). In the magnetic braking experiments, an externally applied non-axisymmetric $n = 1$ field is amplified by the rotationally stabilized RWM, leading to a torque which decelerates the plasma. Eventually a threshold is reached where the growth of the RWM amplitude suddenly increases.

By examining the evolution of the rotation speed at the $q = 2$ surface during external braking, it was observed that the rotation shows a slow deceleration accompanied by an increase in the $n = 1$ magnetic field. After this slow phase, the rotation drops sharply when the magnetic perturbation transitions to a rapid growth phase. The rotation profile at this point is similar to that shown in figure 12. Previously, this discontinuity was interpreted as the crossing of the rotation threshold below which the RWM is unstable. The new conjecture is that it represents a bifurcation in the torque-balance equilibrium of the plasma, in which the rotation jumps from a high value to a low value. The actual threshold value for RWM stabilization may lie in the intervening band of rotation values.

Bifurcation of the equilibrium solution for plasma rotation can be understood in terms of the "induction motor" model of error field-driven reconnection [44, 45], and a conceptually similar process has been proposed involving the RWM [52]. A bifurcation can arise when the rotational drag caused by the applied field has a non-monotonic dependence on the rotation. In the induction motor model, the non-monotonic dependence results from electromagnetic shielding of the error field at the singular surface as rotation increases. In the RWM model it results in greater RWM stabilization (and hence a smaller resonant response to the error field) as rotation increases. In high β tokamak experiments, one or both of these mechanisms may be at work. Such models predict that the plasma rotation at the critical point is on the order of half of the unperturbed rotation. Higher neutral beam torque gives higher unperturbed (or "natural") rotation frequency of the plasma, therefore a higher critical rotation at the entrance to the forbidden band of rotations.

A new analysis [102] of the experimental results is illustrated in figure 20(a), interpreted with the help of the "induction motor" model of error-field driven reconnection. In the new analysis, the critical rotation, V_{crit} at the the $q = 2$ surface

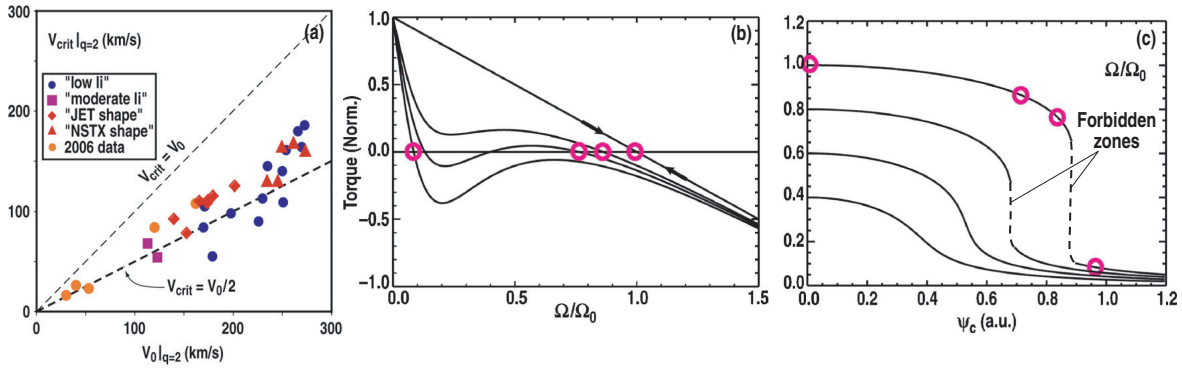

FIG. 20. (a) Critical plasma rotation in DIII-D measured just before the rotation bifurcation following the application of resonant magnetic braking, plotted as a function of the unperturbed rotation (before the braking). Discharges with lower unperturbed rotation also have lower critical rotation (about half), consistent with entrance into a "forbidden band of rotation" (reference [102]). [Reprinted courtesy of IAEA, Nucl. Fusion **47**, 1121 (2007).] (b) Torque balance calculated with the model of reference [52]. The net torque versus normalized plasma rotation Ω for several values of magnetic perturbation Ψ_c. Circles indicate torque-balance equilibrium for each condition (reference [100]). (c) Steady state rotation Ω versus increasing Ψ_c, for several values of neutral beam torque. Circles indicate the same torque balance equilibria as in (b). Some curves have a break where the rotation jumps to a lower branch. Portions of the curves that are inaccessible with increasing Ψ_c are shown as dotted lines (reference [100]). [(b,c) Reprinted courtesy of AIP, Phys. Plasmas **14**, 056101 (2007).]

just before bifurcation and the unperturbed rotation V_0 just before the braking are re-analyzed. The behavior of the rotation at the $q = 2$ surface in all experiments (spanning over an order of magnitude in the rotation values) is consistent with a 50% reduction between the estimate of the unperturbed rotation and the value of the critical rotation, as in the induction motor model of resonant braking.

Note that at the point of bifurcation in the induction motor model, the eddy currents on the resonant surface no longer effectively shield the plasma from the static non-axisymmetric field. This is the entrance into the forbidden band of rotation, and a transition occurs from shielded to fully penetrated braking field, during which the plasma rotation quickly collapses to a nearly locked state. For example, it is worthwhile to re-examine the time-traces of the error field and plasma rotation at the $q = 2$ surface for the discharge shown in figure 12. At the time of bifurcation, around 720 ms, a vanishing of the shielding currents as the rotation decreases could explain the increasing magnitude of the $n = 1$ magnetic field measured by the sensors. The following ∼20 ms are a phase of fully penetrated non-axisymmetric field.

The Fitzpatrick model ([52]) for time dependent development of the rotation and RWM amplitudes is analyzed for its steady state solutions. This version of the model describes the torque balance equilibrium when the plasma is rotating at a constant rate and the RWM is stabilized by rotation. The model yields an equation for the steady-state rotation frequency Ω in terms of the perturbed flux Ψ_c from the external coils or error field:

$$\nu_*(\Omega_0 - \Omega) - \nu_*\Big(\frac{1 - md}{1 + md}\Big)\Big(\frac{(2md)^2\Omega}{[\Omega^2 + \kappa(1 - md)]^2 + (\nu_*\Omega)^2}\Big)|\Psi_c|^2 = 0 \quad .(19)$$

The left-hand side of the equation is proportional to the total torque on the plasma, which equals zero in a stationary state. The first term (the viscous torque) on the left includes the driving torque from neutral beams or other source, and angular momentum transport processes other than the drag due to the applied magnetic perturbation Ψ_c. When $\Psi_c = 0$ these contributions return the rotation to the unperturbed value Ω_0. The second term (the electromagnetic torque) results from the drag due to Ψ_c. Both torque terms depend on the dissipation ν_* in the inertial layer. The RWM stability index κ runs from 0 at the no-wall limit to 1 at the ideal-wall limit, where m is the poloidal mode number and d is the coupling coefficient related to the radius of the wall. The equation is evaluated with parameters representative of DIII-D plasmas. The left-hand side, proportional to the net torque is plotted in figure 20(b) for several values of the applied perturbation. Torque balance equilibrium occurs where a curve crosses zero. With $\Psi_c = 0$, a stable equilibrium exists at the unperturbed rotation $\Omega = \Omega_0$. At small but non-zero Ψ_c, the drag shifts the equilibrium point to smaller Ω. As Ψ_c increases, the torque curve becomes nonmonotonic and crosses zero in three places. These correspond

to two stable equilibrium points at high and low rotation and an intermediate unstable equilibrium. As Ψ_c increases further, the two equilibria at larger rotation vanish, and the system must make a discontinuous jump to the low-rotation state in order to restore torque balance. If this new state has a rotation below the critical rotation Ω_{crit} for RWM stability, then the full dynamic solution would yield not a low-rotation torque balance equilibrium, but rather a low rotation state with an unstable growing RWM. The equilibrium rotation frequency is plotted in figure 20(c) as a function of the applied perturbation Ψ_c, for several values of the initial, unperturbed rotation. Cases with a large initial rotation undergo the bifurcation, but evolve smoothly from higher to lower rotation as Ψ_c increases. It is suggested similar behavior may occur in DIII-D experiments: in cases with strong neutral beam torque and a large unperturbed rotation, where strong magnetic braking is used to reduce the rotation, the bifurcation of the torque balance could lead to a sudden decrease in rotation and increase in RWM amplitude that begins when the rotation is well above Ω_{crit}. On the other hand, cases with small neutral beam torque and little or no magnetic braking should be able to reach the expected MHD stability boundary at Ω_{crit}.

The modeling of this low rotation regime has been undertaken using the MARS-K code. Shown in figure 21 is the comparison of the stability diagram computed using the MARS-K code with the DIII-D low rotation data [103]. On the left hand side of this figure shows the result of assuming the eigenfunction is determined mainly by free

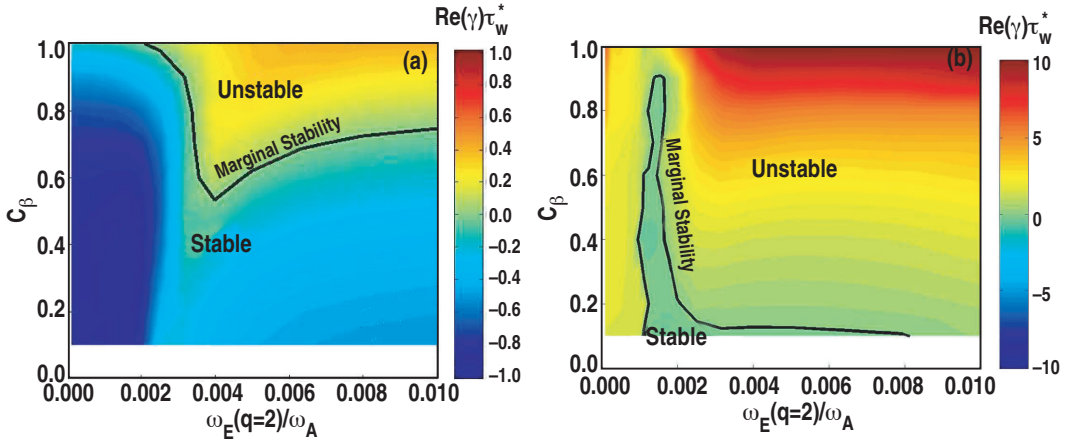

FIG. 21. Comparison of the growth rates of the RWM computed by MARS-F with the experimentally determined stability point in DIII-D. The left is the stability boundary obtained by using a perturbative approach, ignoring the effect of trapped particles on the eigen-function. On the right is that obtained by using a self-consistent eigenfunction. The self-consistent approach predicts less stability than observed in experiments, pointing to the possibility of some missed stabilization mechanism (reference [103, 104]). [Reprinted courtesy of AIP, Phys. Plasmas **16**, 056113 (2009).]

energy from the background plasma (perturbation approach of Hu and Betti [61]). A strong stabilization is obtained. On the right is the result from the self-consistent kinetic approach. The strong stabilization predicted by the perturbative approach is severely reduced. The stability boundary has shrunken to a very small region. This points out the possibility of some additional damping physics, which is not considered so far, could be operative in the experiments in DIII-D.

2.8. Status of RWM stabilization by plasma rotation

In summary, following the pioneering work of Bondeson and Ward [31], the RWM has been observed in many devices. Its predicted global structure has been verified. In a rotating plasma enclosed by a stationary external wall, this mode is separated from the ideal MHD XK mode, which is rotating with the average (fast) speed to the plasma relative to the wall, by its characteristic slow rotation (almost locked to the resistive wall). Rotation of the plasma can lead to stabilization of the RWM. The RWM can also be excited by external resonant ($n = 1$) non-axisymmetric field which causes a drag that slows the plasma and makes the maintenance of rotational stabilization difficult. In this case, the plasma loses its toroidal torque balance and enters into the "forbidden band" in rotation velocity. On the other hand, a non-resonant ($n = 3$) external non-axisymmetric field can be utilized to slow down the plasma to its critical rotation state and excite the RWM without invoking a rotation bifurcation. When the resonant error field is minimized, it becomes possible in present day tokamaks to be rotationally stabilized against the RWM close to the ideal-wall β limit or $C_\beta = 1$ of the XK. The critical rotation required to stabilize the RWM has been observed in experiments to be around 0.3% of the Alfvén speed. This critical rotation speed (profile) appears to be relatively independent of the value of C_β. It is even possible that such a level of rotation can be maintained by NTV through the natural offset rotation velocity of the plasma in an external non-resonant field (section 3.9).

Broad advances are also achieved in the theoretical understanding of the dynamics in the development of the RWM. Within fluid theories, Bondeson's thesis of dissipation-rotation stabilization of the RWM has been established analytically. The presence of error fields has been shown to be important in providing the torque balance in determining the rotational state of the plasma. In particular, this rotational equilibrium in the presence of an external resonant ($n = 1$) perturbation shows a bifurcation in the rotation speed, which complicates the determination of the critical rotation value for the stabilization of the RWM. The evolution of the plasma equilibrium from high to low rotation regime has not yet been modeled in detail. Most of the modeling effort up to now relied in fluid models with various simplifying assumptions on plasma dissipation.

It was not clear whether these models were sufficient for the description of the full dynamical behavior of the plasma during the high to low rotation transition. In the very low rotation regime, in which the rotation speed was comparable to the plasma diamagnetic drift and magnetic drifts, it was important to take these drifts into account. These kinetic effects provided substantial stabilization to the RWM.

Substantial advancement has also been achieved in the numerical modeling of the rotational stabilization of the RWM. The MARS-K code has extension which takes into account the diamagnetic and magnetic drifts of the particles self-consistently in the computation of the plasma stability. These calculations show that the experimentally reported very low rotational threshold is in very close range of accord with the results of computation. However, we cannot claim that the kinetic models are complete. One of the kinetic effects that has not been modeled correctly is collision of the plasma particles. Plasma collision frequency, especially the collision frequency of the ions, could be in the same frequency range as the RWM and will affect the kinetic response very significantly. Also, it is possible that some additional damping physics, such as the effect of energetic particles, which is not considered in detail so far, could be operative in the experiments in DIII-D and could be important in future devices.

Thus, we note that we do not yet have a self-consistent, experimentally validated theoretical model for predicting the stability threshold of the RWM together with the prediction of the bifurcated rotational equilibrium state. On the one hand, the bifurcated rotational equilibrium is predicted based on the fluid model with limited validity of its assumed dissipation; on the other, the main stabilization of the RWM at low rotation has been attributed to the kinetic effects. It would be more satisfactory if we have a uniform validated formulation with reliable dissipation mechanism which allows us to cover the whole range of rotation and C_β. Because of the difficulty in establishing the actual model of the plasma dynamics, although there are reasons to think the stability of the RWM could still fall into the category of type (a) in the scheme of classification of Gimblett and Hastie [54], we cannot claim that this is unambiguously proved. Further detailed validation of the experimentally found slow rotation threshold and the development of the more advanced numerical models is needed to allow predictions of the stability of the RWM in the full range of rotation velocities for future fusion devices.

3. Error Field, Resonant Field Amplification and Dynamic Error Field Correction

3.1. Introduction

From the discussions in section 2, it is clear that the stability of the RWM depends on how did the plasma equilibrium arrive at its critical rotation Ω_{crit}. If Ω_{crit} is arrived at through electromagnetic braking using resonant external ($n = 1$) error field, a loss of the rotation equilibrium at a high rotation value could be mistaken for the value of Ω_{crit} for the stability of the RWM. Therefore, the nature of the interaction of the external magnetic field with the RWM, the damping of the plasma rotation by the external field, and the possible natural rotation induced by the external magnetic perturbation are important topics for the RWM. It is the purpose of this section to review the recent progress in this area.

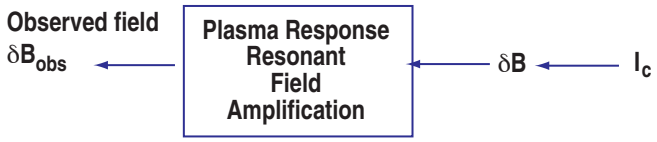

FIG. 22. Under kinetically and rotationally stabilized conditions, the plasma response is dominated by the resonant component of the inherent error field or the applied field produced by the external coils.

An axisymmetric magnetic configuration such as the tokamak (or RFP) without spurious non-axisymmetric magnetic components is an idealization. Usually, the non-axisymmetric components produced by external coil current I_c can interact and be amplified by the plasma. This external field thus spoils the axi-symmetry and is called the error field. It usually deteriorates the confinement and needs to be minimized. The situation is shown schematically in figure 22. Error fields are produced by the imperfections of the magnetic system (the misalignment and distortions of the toroidal field coils and the poloidal field coils that maintain the equilibrium). When the plasma equilibrium evolves, these external maintaining fields have to evolve with it in time. Thus, the magnetic error also evolves "dynamically" and needs to be compensated for "dynamically".

The degree to which the error field needs to be compensated depends on its effect on the plasma equilibrium. Normally, the "changing" error field will diffuse into the rotating plasma via plasma resistivity, whereas plasma rotation will shield the resonant component on the rational surfaces where $q = m/n$. For a high temperature plasma, the shielding is usually quite effective. However, if the external error field has components and frequency that can resonate with a natural mode of the plasma, the plasma response can become very large. This is called resonant field amplification (RFA). RFA enhances the effect of error fields on the plasma. Therefore it is specifically necessary to compensate this particular component of the error field to make sure it is minimized

and reduced to a level at which the plasma response is kept below the noise level. The consequence of uncompensated RFA in the context of its relation to the stability of RWM was first noted by Garofalo [53], pointing out that it could easily become so large as to become the dominant source for damping to plasma rotation and determines the limits of the β_N. The relationship of this response to the 'marginal stability' of the plasma was proposed by Boozer [55].

Due to its resonant nature, the RFA phenomenon can be utilized to understand the plasma properties. If the response of the plasma is particularly large for a special frequency and with a specific mode structure, it indicates that this mode structure is an eigenmode of the system. The frequency and band width of the resonance and the mode structure are an eigen-property of the plasma. The utilization of this effect to understand the plasma is termed MHD spectroscopy [105, 106].

In addition, plasmas with low collisionality in an external error field are found to have a natural rotation frequency. It is proposed that this rotation imparted by a non-resonant external field can be used to provide the rotation speed for stabilization of the RWM [107].

In many ways the actual experimental set up for dynamic error field correction (DEFC) is similar to feedback. This is the main topic of section 4 and will be discussed in detail there. We note that the difference between DEFC and feedback stabilization is that DEFC aims to reduce the distortion of a stable plasma which was excited by the external error field in the dynamically evolving discharge environment; whereas the goal of feedback is to stabilize an inherently unstable plasma.

3.1.1. A puzzle on the behavior of plasma rotation at $\beta_N \sim \beta_N^{no-wall}$.

In 1999, Garofalo [53] studied the change in plasma rotation during the experiments on RWM and related it to the plasma β_N. He found the curious correlation shown in figure 23, namely, whenever the plasma β_N exceeds the no-wall limit, it's rotation is observed to slow down, whereas the rotation starts to recover (or increase due to neutral beam momentum input) after the plasma β_N drops below the no-wall limit. The slowing-down was not correlated with any "externally detectable" MHD activity. He suspected that there were new physical phenomenon involved in this unexpected slowing down. Several explanations were forwarded. One of these was the existence (excitation) of a small amplitude (undetected) RWM always present whenever $\beta > \beta_N$. This conjecture was later formulated by Boozer [55]. Therefore the experimental result shown in figure 23 was the main motivation of the RFA phenomenon. One of the prime candidates of the resulting drag was through the neoclassical viscous damping predicted by Shaing [108] and observed in NSTX by Zhu and Sabbagh [109] and discussed in section 3.6.

3.2. Theoretical investigation on the effect of electromagnetic perturbations

3.2.1. Boozer's formulation of resonant field amplification. Toroidal rotation is normally weakly damped in plasmas that are magnetically confined in the nominally toroidally symmetric tokamak. However, a strong damping of toroidal rotation is observed as such plasmas approach "marginal stability" for perturbations that produce a kink-like distortion of the plasma [53]. Boozer [55] stipulated that the damping of toroidal rotation by very small departures of the magnetic field from toroidal symmetry is greatly enhanced as "marginal stability" is approached. The response of a plasma to perturbations is studied using a set of electric circuit elements, which provides an equation for the rotational damping that requires minimal information about the plasma.

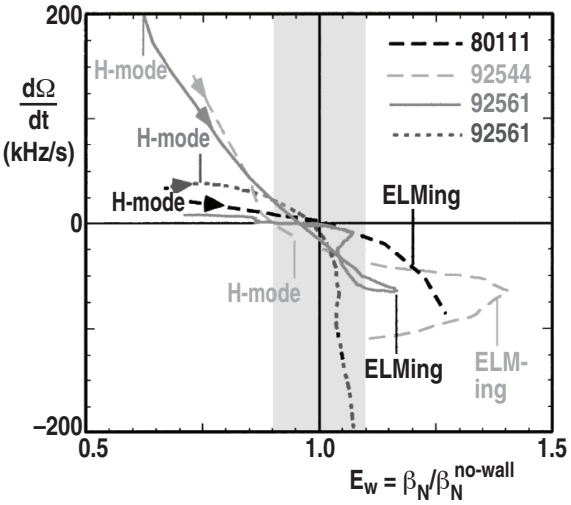

FIG. 23. Correlation of the rotation slowing rate $d\Omega/dt$ at a normalized radius of $\rho = 0.55$ for several wall stabilization discharges versus enhancement factor E_w in DIII-D. The H-mode transitions and onset of ELMs are also indicated (reference [53]). [Reprinted courtesy of APS, Phys. Rev. Lett. **82**, 3811 (1999).]

Boozer's [55] proposal of the "marginal stability" condition which the plasma approaches was first identified as the no-wall β_T limit against the XK. At this limit, the amplitude of the plasma helical distortion to a residual external perturbation (such as error field) increases inversely proportional to a torque parameter — hence the plasma toroidal rotation. The "marginal stability" condition at the no wall limit was subsequently "generalized" to arbitrary "marginal stability" of the plasma (with the inclusion of both rotation and dissipation in the plasma and also the effect of external resistive wall and feedback coils [110]). The amplitude is larger near the onset condition and this helical distortion is balanced by the intrinsic field generated by the plasma. Thus, this distortion has a linear dependence on the external field like "amplification". This phenomenon can also be summarized by the simple equation proposed by Boozer:

$$\Phi = -\frac{\Phi_e^{(p)}}{(s - i\alpha)} \quad , \tag{20}$$

where Φ is the total perturbed flux at the plasma surface, $\Phi_e^{(p)}$ is the externally imposed perturbation error field flux on the plasma, s is the stability parameter ($s = 0$ at marginal stability), and α is related to the magnetic torque on the plasma. It is important to note that equation (20) is inherently a linear response of the plasma (at the stationary state). It assumes that the plasma is stable. The s and α are an integral property of the plasma at steady state. It is implied that s and α do not depend on the amplitudes of Φ. This formulation and conjecture led to many subsequent attempts in the interpretation of s and α. But, it is far from clear which interpretation is more appropriate.

Boozer's conjecture should be understood in conjunction with the low rotation threshold experiments discussed in section 2.7. The different identification of the stability parameter s in [55] and [110] hints at the possibility of an alternative interpretation of the formula equation (20). To be consistent with the discussion in section 2.7, it might be more appropriate to interpret equation (20) as the response of the plasma as it reaches a new equilibrium state with the external field. α is an integral parameter related to the dissipation involved in this adjustment. This interpretation agrees with the notion that, in principle, a marginal stability cannot be perturbatively probed. In addition the concept of evolution to a new neighboring equilibrium state could be more consistent with the experiments (section 3.5.1). Although the resistive wall has slowed down the time scale of the process to the scale to that of τ_w, it is relatively difficult to interpret all plasma states in this situation as being "marginally stable".

3.2.2. Neoclassical toroidal viscosity (NTV) in plasmas with low collisionality In the presence of MHD perturbations, such as the RWM or external error fields, the toroidal symmetry of the tokamak magnetic configuration is broken. This results from the modification of $|B|$, and the variation of $|B|$ on the distorted magnetic surfaces. In this situation, the plasma viscosity is greatly enhanced by the presence of the symmetry breaking field. In a plasma with low collisionality, particle orbits in the non-axisymmetric field is quite different from the orbits in an axisymmetric field, especially for the trapped particles. Their banana orbits are not closed in the non-axis-symmetric field. This naturally leads them to have much larger excursion from their averaged flux surfaces. This results in greatly enhanced transport through their collisions and relaxation interactions with other particles. It appears as a damping to the toroidal plasma rotation and is appropriately named neoclassical toroidal viscosity or NTV. Thus the nature of this viscosity is very different in its dependence on plasma parameters that were usually used for the plasma viscosity in fluid theories such as in reference [52].

When the perturbation has a non-negligible component which can be resonant with a plasma surface, i.e. $m - nq \sim 0$, (here m is the poloidal mode number, n the toroidal mode number and q the safety factor of the resonant surface), and a magnetic island is formed, the plasma viscosity scales as $\delta B/B$, and is dominated by this "island viscosity" in the region close to the resonant surface [111, 112]. In this case, the symmetry breaking is mainly due to the variation of $|B|$ on the distorted magnetic surface.

For non-resonant modes, i.e. $m - nq \neq 0$, the viscosity in a more collisional plasma due to the magnetic perturbations were discussed in references [113, 114]. For the conventional neoclassical banana regime where $\nu^* \leq 1$ ($\nu^* = \epsilon^{-3/2}\nu\sqrt{2}qR/v_{th}$ is the effective ion collision frequency, $\epsilon = a/R = 1/A$ is the inverse aspect ratio, ν the ion-ion collision frequency and v_{th} is the ion thermal speed) the behavior of the viscosity depends further on whether the trapped-particles are collisionless or collisional in the helical field. For the collisional helical fields, i.e. $[(\delta B/B)/\epsilon]^{3/2} < \nu^*$, the viscosity scales like $(\delta B/B)^2$. For the case of even lower collisionality, i.e. $\nu^* < [(\delta B/B)/\epsilon]^{3/2}$, the viscosity scales like $\epsilon^2(\delta B/B)^{3/2}/\nu$. The details of these viscosities are given in reference [108]. An overview of the NTV for plasma in different collisionality regimes is recently summarized in reference [115].

Due to the external perturbation, the particle orbits are not closed as in the unperturbed axisymmetric configuration. In this case, the external perturbation also induces a natural "equilibrium (to the external perturbation) flow" to the plasma on the perturbed flux surfaces. This flow is given by

$$v_i^\zeta = v_i^\theta q + \left(\frac{cT_i}{e_i}\right)\left(\frac{\Lambda_{2i}}{\Lambda_{1i}\chi_i'}\right)\frac{T_i'}{T_i} \quad . \tag{21}$$

Here, $(\zeta,\ \theta)$ is the Hamada coordinate in the (toroidal, poloidal) direction, and the $\Lambda's$ are neoclassical transport coefficients [108]. The poloidal flow is usually very heavily damped. Therefore, we have a resultant toroidal flow induced by the magnetic perturbations.

3.2.3. Penetration of error field in plasma with low collisionality. The standard theory of the penetration of a resonant error field into the tokamak was given by Fitzpatrick [50, 116]. As discussed in section 2.2.3, the penetration of the magnetic field into the plasma causes the plasma rotation to slow down and bifurcate. The plasma with a fast rotation will bifurcate downward to a lower rotation state when the viscous torque induced by the magnetic island at the resonant surface becomes too large for the skin current in the island region to sustain.

In the torque balance, the resonant component of the error field provides one component of the drag on the plasma rotation. Another component is the viscosity of the axisymmetric tokamak. A third component is the torque provided by the NTV [113] given in section 3.2.2. In the absence of other torques, the NTV torque will lead the plasma to the rotation profile given in equation (21). In the presence of other torques, they combine to determine the rotation profile of the plasma. In the work by Cole *et al.* [117], it was emphasized that in a high temperature plasma, the development of the error field should take into account all of the relevant torques, especially the NTV torque. This new theory was used to examine resonant error-field penetration threshold scaling in ohmic tokamak plasmas. Compared to previous theoretical results, the plasma is found to be less susceptible to error-field penetration and locking, by a factor that depends on the amplitude of the non-resonant error-field. This same mechanism is expected to be operative in a high β plasma.

3.3. Codes and modeling for study of resonant field amplification

To quantitatively investigate the phenomenon of RFA, the modeling codes need to be generalized to properly model the presence of these externally imposed fields.

3.3.1. Description of resonant field amplification in lumped parameter model. When there is an external error field, the lumped parameter model introduced in section 2.3.1 has to be extended to include the circuit that produces the external error field. The simplest possible representation of this is the introduction of an external coil current I_c with mutual inductance M_{pc} with the plasma and M_{wc} with the skin current on the resistive wall. Thus the generalized equation with the inclusion of I_c should be

$$L_{eff} I_p + M_{pw} I_w + M_{pc} I_c = 0 \quad , \tag{22}$$

$$\frac{\partial}{\partial t}(M_{wp} I_p + L_w I_w + M_{wc} I_c) + R_w I_w = 0 \quad . \tag{23}$$

In equation (22), the I_i's with $i = p, w, c$ are the currents in the plasma, wall, error field circuit, respectively. The M_{ij}'s are the effective mutual inductances between the (i, j) currents. The time scale of the error field is assumed to be longer than the time scale of the RWM. At steady state $\partial/(\partial t) = 0$, $I_w = 0$, equation (22) indicates

$$I_p = -\frac{M_{pc} I_c}{L_{eff}} \quad . \tag{24}$$

It might be interesting to compare this equation with equation (20). The RFA hypothesis is, therefore, equivalent to the assertion that L_{eff} is proportional to $s - i\alpha$ near "marginal stability", which was expected [64]. But the generality of this relation was only recognized after Boozer's work.

3.3.2. Ideal perturbed equilibrium code (IPEC). Tokamak plasmas respond sensitively to externally driven 3D magnetic fields. An external field as small as $\delta B/B \sim 10^{-4}$ can greatly change the performance of plasmas by causing plasma mode locking (plasma locked to the external error field), or rotational damping by non-ambipolar transport. In order to understand such sensitive plasma responses, a precise description of plasma equilibria would be required as typical in 2D tokamak problems. The IPEC [118] has been developed for this purpose, based on DCON [72], and VACUUM [87] stability codes, since perturbed equilibria is essentially the same subject as plasma stability. Using IPEC, it has been shown that there are strong ideal plasma responses to imposed external perturbations — poloidal harmonic coupling, shielding and amplification of the external field (or the imposed displacement at the plasma boundary). These effects have been observed in experiments on DIII-D and NSTX. In particular, for each configuration, there is a distribution of the external perturbing field that will be most "effective" in producing the electromagnetic torque for mode locking. IPEC can be utilized to identify these perturbations. Shown in figure 24 is the most sensitive external field on the plasma boundary, $\delta B \cdot n_b = A(\theta)cos(\phi) + B(\theta)sin(\phi)$ in NSTX, where the red line is $A(\theta)$ and the blue line is $B(\theta)$. With the plasma response known, it is then possible to evaluate the effect of non-axisymmetry on the damping of toroidal rotation - the non-axisymmetry breaks the toroidal symmetry of the orbit of trapped particles and results in the NTV [108].

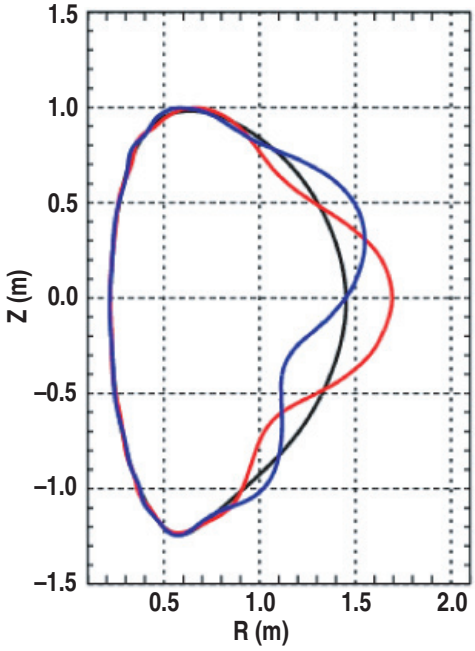

FIG. 24. The most sensitive external field on the plasma boundary, $\delta B \cdot n_b = A(\theta)cos(\phi) + B(\theta)sin(\phi)$, in NSTX, where red line is $A(\theta)$ and the blue line is $B(\theta)$ (reference [118]). [Reprinted courtesy of IAEA, Proceedings of 22nd IAEA Fusion Energy Conference, Geneva, Switzerland (IAEA, Vienna, 2008) Paper EX/5-3rb, http://www-pub.iara.org/MTCD/Meetings/fec2008pp.asp.]

3.3.3. Other codes and models. As mentioned previously, the main assumption in the physics of the resonant error field amplification is that the plasma has an amplified response close to the "marginal stability" or has a path to reach a "neighboring equilibrium" with respect to the external field. This is a universal relationship for a system close to such conditions. Note that "marginal stability" and "neighboring equilibrium"' satisfy the same equations. Therefore, in principle, all plasma models given in section II should exhibit this behavior. All models mentioned previously, appropriately extended to use the external error field as input will be able to study the phenomenon of RFA. This was actually the situation. However, there are important differences in the treatment of the effect of dissipation on the stable and/or quasi-stable RWM and the damping of the toroidally symmetric component of the toroidal angular momentum.

Fitzpatrick [52] generalized the Fitzpatrick-Aydemir model [34] to model the RFA in cylindrical tokamak and the damping of the toroidal angular momentum. For simplicity, he assumed the same edge fluid viscosity could be operative in both the helical RWM and the damping of axisymmetric toroidal angular momentum. The simplicity of this model to represent the integral plasma response both in the energy channel and the momentum channel is its salient feature. The result of this study is that it was able to model the triggering of the plasma deceleration by the error field and subsequently led to the destabilization of the RWM (section 2.7).

By the time of publication of Boozer's theory on RFA, the full feedback model with toroidal geometry for the coils had already been incorporated into the MARS-F code [67]. Therefore, it is natural to use the code to study RFA without further modification.

Chu *et al.* [119] generalized the relationship found from the normal mode approach (NMA) [120, 121] between the perturbed magnetic field on the wall B_w and the perturbed magnetic field on the plasma B_p to derive the following complex form,

$$A = \frac{\delta W_{Iw} + in\Omega D}{\delta W_{Nw} + in\Omega D} - 1 \quad , \tag{25}$$

for the amplification factor A. Note that the amplification factor defined here shows it depends explicitly on the dissipation factor $in\Omega D$. If the plasma were extremely stable, $\delta W_{Iw} \sim \delta W_{Nw} \to \infty$ and there is no amplification. If D is real, comparison to equation (20) shows that $\delta W_{Nw} \sim s$ and $n\Omega D \sim \alpha$, and the marginal stability point should occur at the no-wall limit. However, if D is complex, the marginal stability point shifts away from the no-wall limit.

We see that the resonant field amplification (RFA) is a universal relationship which is present in all theories and can be very useful in understanding the various aspects of plasma, including the proper dissipation models for the MHD perturbations. Up to now, these theories have largely been phenomenological in nature and is not detailed enough to allow us pin down the exact dynamic model for the plasma.

3.4. Experimental observations of resonant field amplification

After the recognition of the importance of RFA in affecting the plasma behavior in high β_N plasmas for RWM stability, extensive experimental activity ensued to use it as a guide both in understanding the plasma property and in improving its stability. The important concept introduced by Boozer was to describe the RFA in terms of simple measurable parameters, which can, in turn, be compared with more detailed plasma models.

To study the time-dependent error field, the capability of the active coil and the external resistive structure is very important. A list of these characteristics for different devices is given in Table II.

Table II. Active coil and power supply characteristics

	Coil Location	Number of Coils	Stabilizing Shell
DIII-D	External	6 coils	Vacuum vessel
	Internal	Upper 6, lower 6	Vacuum vessel
JET	External	Midplane 4	Vacuum vessel
NSTX	External	Midplane 6	Passive upper lower plates
HBT-EX	Variable	Variable	Variable

3.4.1. The versatile error field compensation coils in DIII-D. The coil geometry employed for studying static and dynamic error field amplification (and mitigation) in DIII-D is shown in figure 25 [122, 123]. It includes both the C-coils (external) and I-coils (internal to the vacuum vessel). The C-coils consist of six four-turn coils located on the outboard side and are symmetric with respect to the midplane. The I-coils consist of six single-turn coils, located above the outer midplane (but inside the vacuum vessel) and an identical set of six coils below the midplane. For the external C-coils, the amplitude of the harmonic components is at its maximum for $m = 1$ and monotonically decreases for higher m components. Due to its top-bottom symmetric

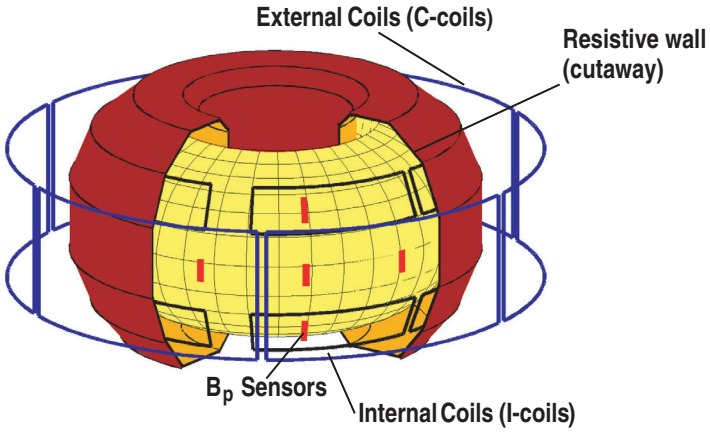

FIG. 25. The versatile external C- and internal I-coil geometry used for static and dynamic error field correction and also the magnetic feedback experiments in DIII-D. The locations of the B_p sensors are also indicated (reference [122, 123]). [Reprinted courtesy of AIP, Phys. Plasmas **11**, 2505 (2004).]

location on the outside midplane, the magnetic field produced by the C-coils has no net helicity content. For the internal I-coils, the helicity content in the external field produced by them can be varied depending upon the upper/lower connection. For most experiments, the connection with 240 degrees phase difference between the top and bottom I-coils was used, maximizing the $m/n = 3/1$ resonant component. The 3/1 component is expected to be the dominant component of the perturbed magnetic field produced by the RWM. However, the m-spectrum of I-coils is quite broad so that the magnitude of the resonance is determined by the plasma mode structure, not by the applied field. Although a non-resonant component of the external field can be as large as the resonant component, the plasma distortion due to the non-resonant component is usually rather modest.

3.4.2. RFA signal carries helicity of the plasma. The first experiments to demonstrate clearly the RFA phenomena were performed by applying pre-programmed square wave (dc) $n = 1$ magnetic field produced by the C-coils to the plasma [124]. In these experiments, A_{RFA} is defined as

$$A_{RFA} = [B_r - B_r(vac)]/B_r(vac) \quad . \tag{26}$$

It is measured using radial flux loops near the outboard midplane of the tokamak. Note that this experimental definition equation (26), based on the vacuum field, is expected to capture the resonant features of equations (20), and (25), but are different from them.

One important point to note is that the dc pulse was turned on for around 100 ms, which is definitely longer than any dynamic time scale in the plasma and the resistive wall. Therefore, the measured response represents a quasi-dc response of the plasma. The details of the experiment are shown in figure 26. Figure 26(a) shows the normalized beta and predicted no-wall limit, figure 26(b) shows the currents in the non-axisymmetric field coils. Figure 26(c) is the resonant left-handed $m/n = 2/1$ component of the magnetic field normal to the nominal $q = 2$ flux surface, and figure 26(d) is the plasma response to the $n = 1$ field pulse during investigation of RFA. Figure 26(e,f) shows the geometry of the RWM sensors. The correlation between the plasma β_N shown in figure 26(a) and the amplification measured in figure 26(e) shows that A_{RFA} increases with β_N above $\beta_N^{no-wall}$. The RFA can originate from plasma with such a wide range of β_N values, indicating it is hard to relate it to a "marginal stability" condition; rather more likely it is a condition of achieving different "neighboring equilibrium" states.

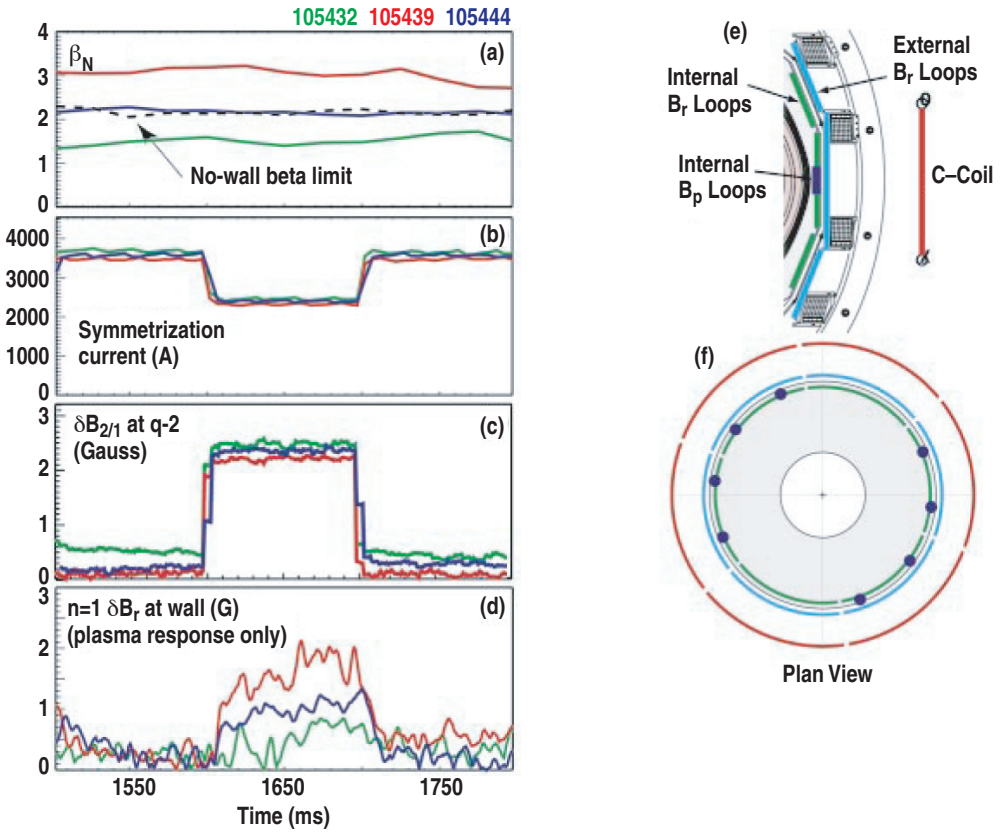

FIG. 26. The difference in the measured phases in the RFA experiment using the external C-coils in DIII-D. Shown in (a) is the toroidal phase of the $n = 1$ field measured by saddle loop arrays at different poloidal locations versus the toroidal phase of the C-coil current without plasma and (b) the same phases with plasma. Note the systematic shift in the phases induced by the plasma response (reference [124]). [Reprinted courtesy of AIP, Phys. Plasmas **9**, 1997 (2002).]

To show that the response of the plasma does possess the helicity of the equilibrium plasma field, the response at different poloidal angles are compared in figure 27. Shown in figure 27(a) is the toroidal phase of the $n = 1$ field measured by saddle loop arrays at different poloidal locations versus the toroidal phase of the C-coil current without a plasma and figure 27(b) is the toroidal phase of the plasma response measured by the three saddle loop arrays for the same C-coil current pulses. The systematic shift in phases of the plasma response vs. those from the vacuum response show that the source of the RFA signal comes directly from the plasma.

Experiments on JET [125] and NSTX [88] on RFA show similar dependence on $\beta_N/\beta_N^{no-wall}$.

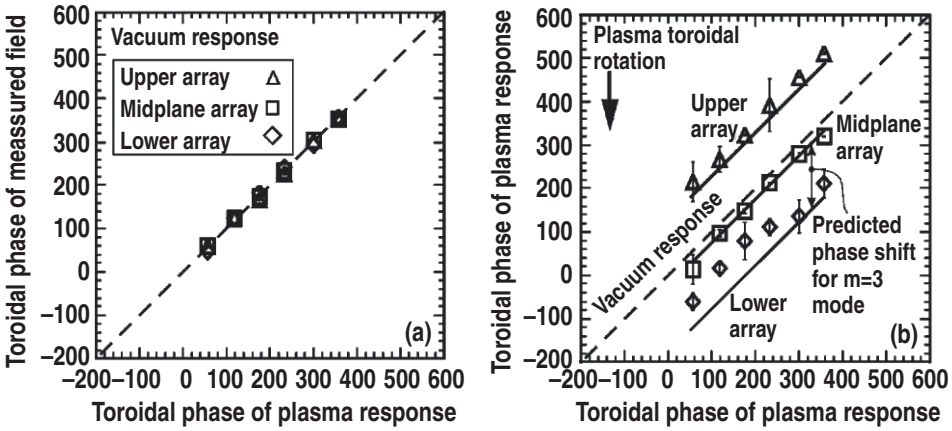

FIG. 27. The DIII-D C-coils notching experiment designed to verify the RFA phenomenon: (a) shows the time evolution of β_N, (b) the currents in the C-coils, (c) the resonant left-handed $m/n = 2/1$ component of the magnetic field normal to the nominal $q = 2$ flux surface, and (d) plasma response to the $n = 1$ field. (e) and (f) Show the geometry of sensors for the detection of RWM (reference [124]). [Reprinted courtesy of AIP, Phys. Plasmas **9**, 1997 (2002).]

3.4.3. Single mode modeling of RFA experiment in JET. On JET, saddle coil systems both internal and external to the vacuum vessel were used to study the RFA associated with driven stable RWMs.

The experimental measurements have been compared with calculations using the MARS-F MHD stability code [67] and shown in figure 28. Calculations with MARS-F using a fluid model with small parallel viscosity makes the RFA peak inconsistent with experiment near the no-wall limit, while models with stronger damping [fluid model and cylindrical parallel (ion sound) viscosity or the semi-kinetic model] reproduce the

experimental RFA for static error field rather well [95, 126]. One of the ansatz of RFA is that near "marginal stability", the external error field excites a particularly large plasma response [equations (20), (23), and (25)]. This also implies the response may be represented as an eigenmode of the system. The nature of the plasma response on JET is analyzed by use of the Pade approximation (Appendix D). It was found that the plasma response in the RFA process can indeed be reproduced with a single pole, indicating that a single mode dominated the RFA [127]. This indicates that the "neighboring equilibrium" state can be characterized as the distortion of the background plasma by a "single mode".

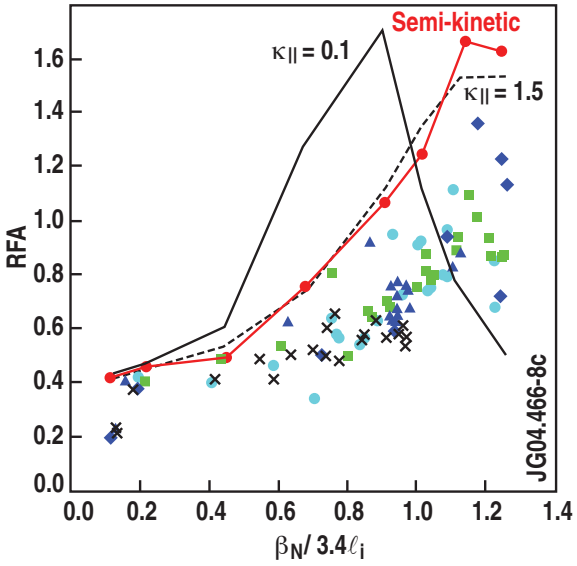

FIG. 28. RFA measured in JET with midplane B_r coils arising from fields applied using the internal error field coils. β_N is normalized with respect to the approximate no-wall limit, $3.4l_i$. Each symbol type represents a different pulse. The curves show the predictions of various damping models in MARS-F code — either the "semi-kinetic" model or strong parallel (ion sound wave) damping are in reasonable agreement with experimental measurements (reference [125]). [Reprinted courtesy of IASEA, Proceedings of 20th IAEA Fusion Energy Conference, Vilamoura, Portugal (IAEA, Vienna, 2004) Paper EX/P2-22, available on CD.]

3.4.4. Mode slipping near $\beta \simeq \beta^{no-wall}$ in HBT-EP compares well with Fitzpatrick-Aydemir model. The RWM was identified in the HBT-EP by Ivers *et al.* [128] and the control of the XK was demonstrated by Cates *et al.* [129, 130]. In a subsequent experiment, the dynamic plasma response is measured both before and following a phase flip of the external magnetic perturbation. The plasma response is compared with the Fitzpatrick-Aydemir model [34] and found to agree well. The dissipation [52] in the plasma was found to be high. The phase flip of the external perturbation was found to excite a transient mode, which damps away in time proportional to the inverse damping rate of the (stable) RWM as calculated by the Fitzpatrick-Aydemir dispersion relation.

For more stable plasma, the observed plasma response realigns with the applied field more quickly (0.2 ms). This is deduced from the rapid evolution of the relative phase between the mode and the external helical perturbation. For less stable plasmas, results show that the amplitude of the $m/n = 3/1$ resonant plasma response starts to oscillate immediately after the phase-flip. The relative phase between the perturbation and the plasma response also starts to oscillate. The overall phase realignment time increased to 0.5 ms. These characteristics are evident whenever the phase-flip was programmed to occur near marginal stability.

Numerical simulations of the phase-flip experiments using the Fitzpatrick-Aydemir equations reproduced the oscillations in the amplitude of the plasma response and its relative phase caused by the phase-flip of the applied resonant field (figure 29). Simulations show that the phase-flip excites a transient solution, responsible for the oscillations, whose $m/n = 3/1$ structure oscillates back and forth like a damped toroidal pendulum and ultimately realigns with the phase of the applied field. The simulation also shows that the phase-realignment time is proportional to the inverse damping rate of the stable RWMs, as calculated by the Fitzpatrick-Aydemir dispersion relationship [131, 132].

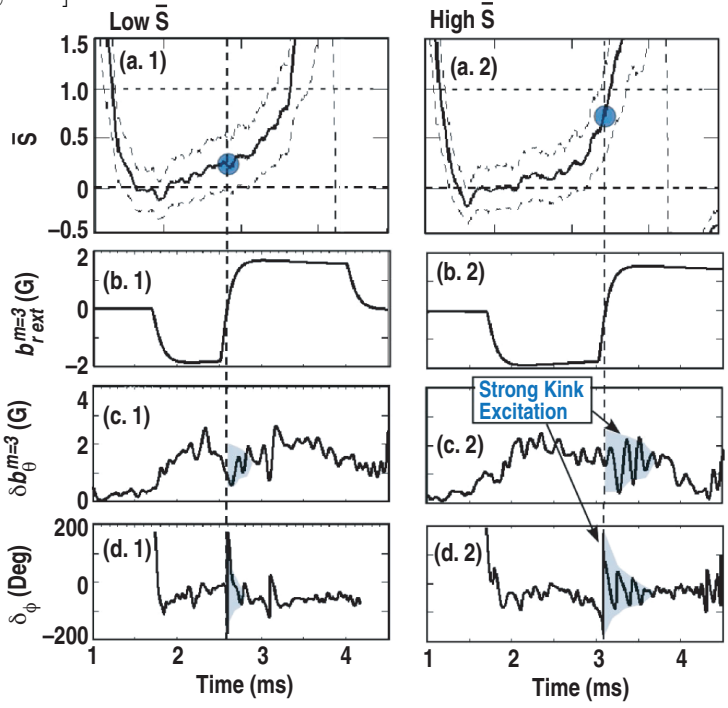

FIG. 29. Examples of "phase-flip" measurements in HBT-1B showing the plasma response to a step change in the applied external magnetic field. Here $\bar{s}$ is the stability index. $\bar{s} = 0$ corresponds to stability of the XK mode with no external wall; and $\bar{s} = 1$ corresponds to stability of the XK mode with an ideal wall. When the "phase-flip" is applied late in time ($t \sim 3$ ms when the plasma is less stable), temporal oscillations (near 5 kHz) in the plasma response indicate excitation of the wall-stabilized kink in a rotating plasma (reference [131]). [Reprinted courtesy of IAEA, Nucl. Fusion **45**, 285 (2005).]

3.5. Nature of the plasma damping with RFA

3.5.1. Implication of the complex D from experiments in DIII-D. A statistical analysis was performed for all the data in the resonant amplification experiments in DIII-D up to 2002 [133]. The goal of this study was to relate the observations to the dissipation characterized by the parameter equivalent to α [equation (20)] or D [equation (25)]. Experimentally it was demonstrated, as predicted by Boozer, that when β_N approaches the "marginal stable" condition, the applied pulsed error field can induce a large $n = 1$ helical response. But it was difficult to relate this to the "marginal stability" point of the no-wall limit of the XK. Shown in the upper right panels of figure 30 are the experimentally observed RFA amplitudes and phases of different discharges as a function of $\beta_N/\beta_N^{no-wall}$. Shown below are panels of the calculated amplitude if the results were to be described by introducing a complex dissipation parameter D in the lumped parameter model (rather than a single real parameter as originally proposed in reference [55]). It is found that D can be represented in the form $iD\Omega = \beta_0 + i\Omega\alpha$ in terms of the damping of the lumped parameter model. Shown in the left panel is

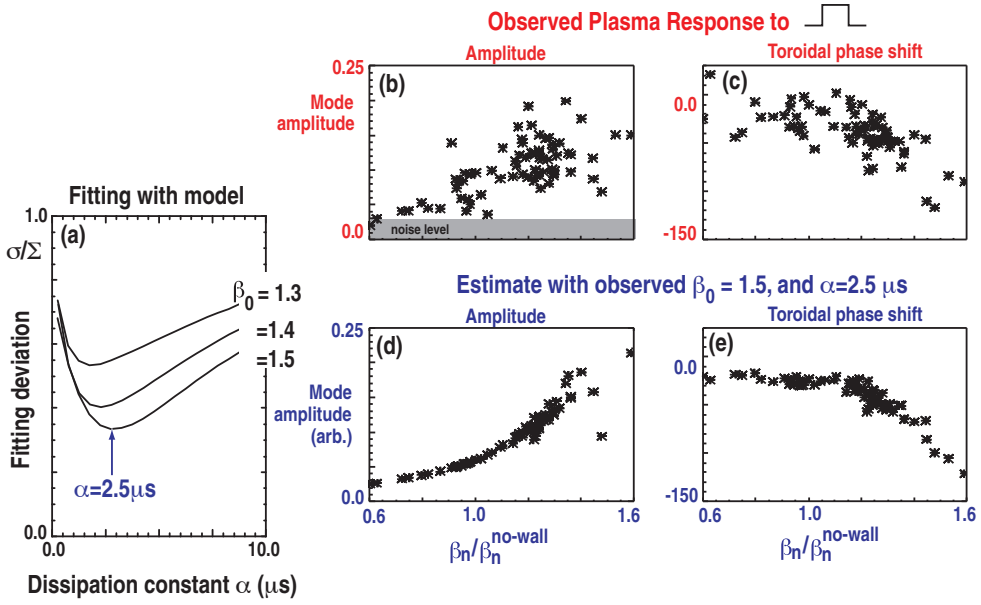

FIG. 30. Results from the complex D experiment in DIII-D. (a) Shows the best fitted parameters for this set of experiments for the value of α and β_0, note $iD\Omega = \beta_0 + i\Omega\alpha$. The other panels are the observed amplitudes (b) and phases (c) of the plasma response shown alongside the expected values (d) and (e) from the fitted model (reference [64, 124, 133]). [Reprinted courtesy of IOP, Plasma Phys. Control. Fusion **44**, B339 (2002).]

the variance of the fit versus α parameterized by $\beta_0 = (1.3, 1.4, 1.5)$. The fitted value of $\alpha \sim 2.5\,\mu$s for the dissipation coefficient, is found comparable to the Alfvén transit time for the experiment under study — indicating very strong intrinsic damping. The level of damping obtained in these experiments is high. It is comparable to the processes assumed in the equilibrium forming time. This indicates that the plasma adjusts to the external perturbing field more as the process during the establishment of a new equilibrium rather than a milder process that involves some small number of particles. This is in accord with the equilibrium evolution (include bifurcation) phenomena found in section 2.7. Other alternative interpretations could be: (1) existence of other strong stabilizing effects, as suggested by Hu and Betti [61]; or (2) existence of multiple resonant surfaces that may be important in providing the damping.

3.5.2. Development of the active MHD spectroscopy. It is natural to generalize the external quasi-dc pulse to sinusoidal pulses. It involved changing the standing wave used in the experiment in section 3.4.2 [124] to a traveling wave. This technique of probing the plasma for its response is appropriately called active MHD spectroscopy.

The frequency range employed in the active MHD spectroscopy were a few tens of Hertz [91, 105, 106]. The measured frequency spectrum of the plasma response to externally applied rotating magnetic fields is well-described by a single mode and provides an absolute measurement of the damping rate and the natural mode rotation frequency of the stable RWM.

In 2004, Reimerdes showed [105] that for an external field with angular frequency of ω_{ext}, after an initial transient phase all quantities oscillate with the externally imposed frequency and the RFA spectrum can be described by equation (27)

$$A_{RFA}(s, \omega_{ext}) = c_s \frac{1 + \gamma_0 \tau_w}{(i\omega_{ext} - \gamma_0)\tau_w} \quad . \tag{27}$$

According to equation (27) the RFA peaks when ω_{ext} matches $\Omega = \Im(\gamma_0)$, i.e. the natural rotation frequency of the mode. The maximum RFA amplitude is also predicted to increase as the plasma approaches "marginal stability". This is an excellent way to show that the perturbation that is in equilibrium with the plasma actually has a natural frequency, which is usually explicitly demanded by theories in these situations.

The evolution of various quantities during the experiment on MHD spectroscopy is shown on the left of figure 31. In figure 31(a) β_N is shown raised above the estimated no-wall limit; figure 31(b) shows the current in the upper I-coil, and the generation of a rotating $n = 1$ mode; figure 31(c) shows the B_r field at the midplane; figure 31(d) shows the deduced magnitude of the $n = 1$ plasma response; and figure 31(e) shows

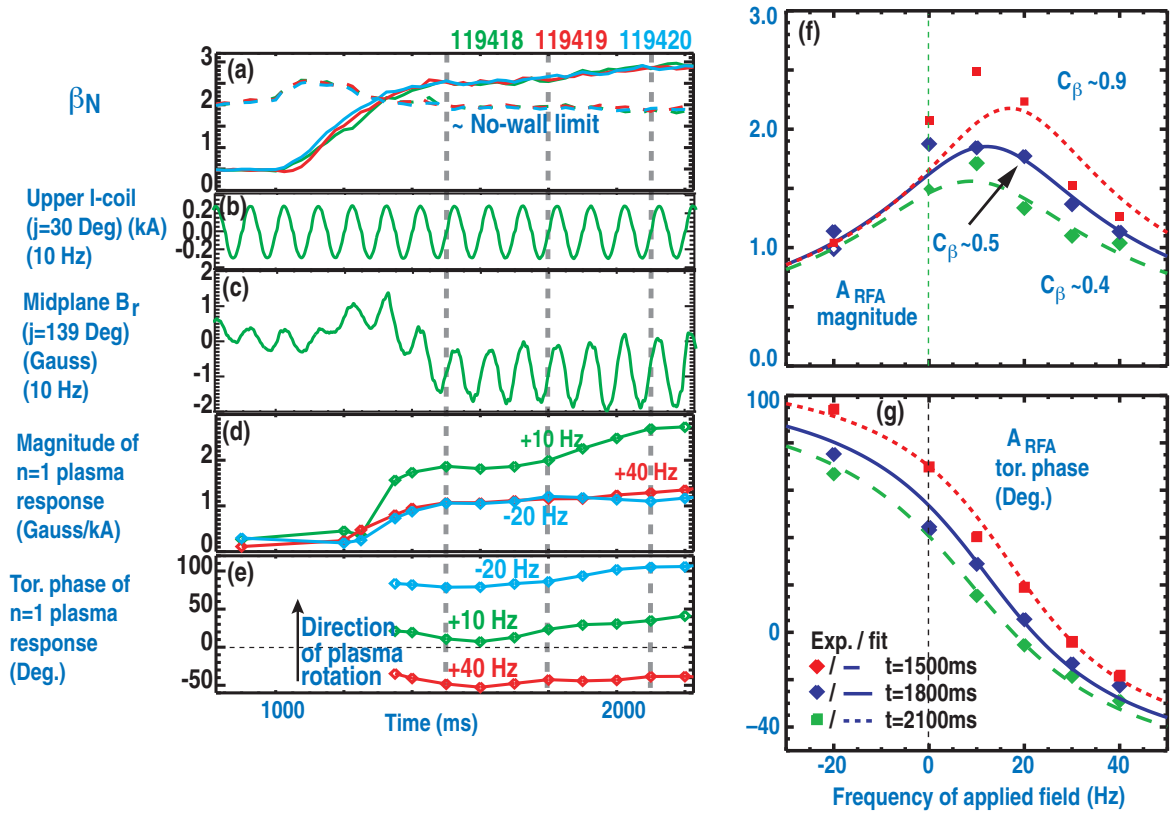

FIG. 31. Evolution of plasma signals during the MHD spectroscopy experiment in DIII-D. (a) β_N is raised above the estimated no-wall limit. The application of (b) a rotating $n = 1$ field leads to (c) a perturbation of the magnetic field. (d) Magnitude and (e) phase of the $n = 1$ plasma response at the applied frequency normalized to the applied current (reference [105, 106]). [(a-e) Reprinted courtesy of IAEA, Nucl. Fusion **45**, 368 (2005).] The RFA spectra obtained by the method of MHD spectroscopy. Magnitude (f) and phase (g) of the $n = 1$ A_{RFA} measured with midplane saddle loops and fitted to analytic formula (reference [105, 106]). [(f,g) Reprinted courtesy of IAEA, adapted from Nucl. Fusion **45**, 368 (2005).]

the phase of the $n = 1$ plasma response. The RFA spectra, measured at two times during the discharges corresponding to two different values of β_T, are compared to the single mode prediction from equation (27) and shown on the right side of figure 31. One important point to notice is that the measurements show the predicted resonance. The resonance becomes sharper as β_T increases, consistent with weaker damping. Fitting two free complex parameters equivalent to c_s and γ_0 into equation (27) leads to good agreement. The values of c_s resulting from both fits are similar (within 10%), consistent with a factor that depends only on the geometry of the sensors and the mode.

Good agreement between the measured spectrum and the fit confirms that the interaction between the RWM and externally supplied magnetic fields is well-described by a single mode model [compare with section 3.4.3]. The frequency response was similarly found in NSTX [91]. Consequently, the fit parameter yields an absolute measurement of the plasma condition, which should be related to the evolution of plasma rotation on its evolution path (c.f. section 2.7). For a fast rotating plasma, this is quite unrelated to the no-wall marginal stability point. The coherent detection technique allows for a small perturbation amplitude compared to pulsed techniques (section 3.4.2), only trading off in time resolution, which is limited to the period of the applied frequency. This is the extension of the technique of "active MHD spectroscopy", previously applied at frequencies above 10 kHz [134], to frequencies of a few tens of Hertz.

To explore the nature of the damping mechanism, an experiment is performed to see whether there is a size dependence between DIII-D and JET on the damping process involved in the RWM [135]. The magnitude and phase of the plasma response appears independent of the size and wall property of the device. The critical stability seems to follow the generic picture given in figure 18 but with a larger dissipation coefficient $\kappa_{\|} = 1$ in the sound wave damping model to bring the sound wave damping curve to be more in line with the kinetic damping curve.

3.6. Identification of damping due to NTV in NSTX

Dissipation of plasma toroidal angular momentum due to applied non-axisymmetric magnetic fields and their plasma-induced components increased by resonant field amplification and RWM destabilization has been identified in experiments on the NSTX by Zhu and Sabbagh [109]. The measured decrease of plasma toroidal angular momentum is compared to calculations of non-resonant drag torque based on the theory of neoclassical toroidal viscosity. Quantitative agreement between experiment and theory is found when the effect of toroidally trapped particles is included. The neoclassical toroidal viscosity (section 3.2.2) is due to the symmetry breaking of the perturbation field. The banana orbits are assumed to be collisionless for the toroidally trapped particles but collisional for the helically trapped particles. It has two regimes, the "ν" and the "$1/\nu$" regime.

Shown in figure 32 is the NTV during amplification of $n = 1$ nonaxisymmetric field configuration in NSTX. The procedure used is to first evaluate the plasma response using the DCON code and then use the eigenfunction and the measured level of plasma displacement as input to the NTV torque expressions given in reference [108]. This is then compared with the experimentally derived torque. Shown in (a) is the evolution of β_N, with the shaded region corresponding to $\beta_N > \beta_N^{no-wall}$, together with the maximum

current in the non-axisymmetric field coils; (b) the $n = 1$ plasma response measured by poloidal field sensors; (c) comparison of the measured torque $d(I\Omega_\phi)/dt$ profile to the theoretical integrated NTV torque during RFA; and (d) similar comparison during RWM evolution (reference [109]). We note that the neoclassical torque is proportional to the square of the modulus of the perturbing magnetic field and is also weighted by the square of the toroidal mode number of the perturbing field. They are concentrated near the mode rational surfaces.

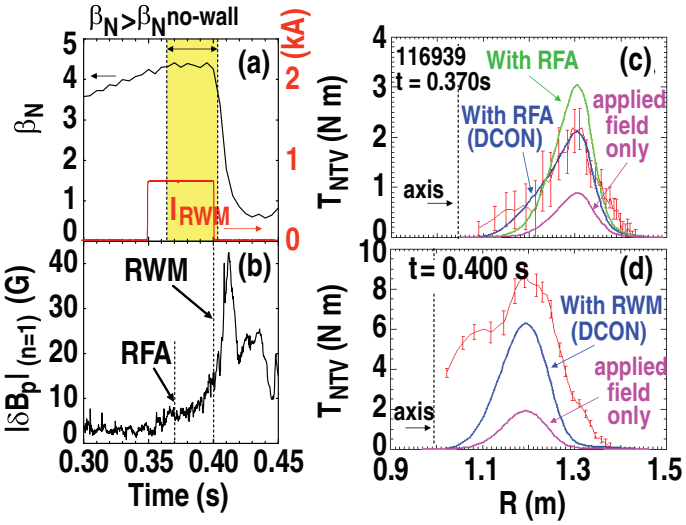

FIG. 32. Experiments on NSTX which verified the NTV during amplification of $n = 1$ non-axisymmetric field configuration: (a) evolution of β_N, computed in the period when $\beta_N > \beta_N^{no-wall}$, and maximum current in non-axisymmetric field coils; (b) $n = 1$ plasma response measured by poloidal field sensors; (c) comparison of measured $d(I\Omega_\phi)/dt$ profile to theoretical integrated NTV torque during RFA; and (d) similar comparison during RWM evolution (reference [109]). [Reprinted courtesy of APS, Phys. Rev. Lett. **96**, 225002 (2006).]

Non-resonant magnetic braking by $n = 3$ fields was also shown in reference [109]. Since the NTV torque created by this field scales linearly with plasma rotation instead of inversely as for $n = 1$ resonant magnetic braking, rotation bifurcation as described in section 2.7 cannot occur by the $n = 3$ field application by itself. Therefore, non-resonant magnetic braking by NTV was shown to be a powerful tool to modify the plasma rotation profile to study the properties of RWM marginal stability versus plasma rotation. This technique was used to create very low rotation [90] and profile modification for RWM studies in NSTX without rotation bifurcation [91], and is now used as a general tool for various physics studies in the device, including perturbative transport experiments.

3.7. Dynamic error field correction

In order to maintain plasma rotation and to have a sustained rotational stabilization of the RWM, we need to eliminate the resonant component of the external magnetic field, which could be present in the tokamak discharge environment in the phase when plasma

β_T is near and above the no-wall limit. The error field is produced by the non-perfection in the coil systems that are needed to initiate and maintain the discharge. The currents in these coils need to change in response to the variation in the plasma equilibrium such as the increase in β_T. Therefore, the error field evolves dynamically throughout the discharge history and needs to be compensated dynamically (figure 33). There are many components of these error fields, the most dangerous one is the component which resonantly excites the RWM and gives rise to large damping of the rotation and defeats rotational stabilization. The time scale of change of the external error field is, therefore, the same as the evolution time scale of the plasma equilibrium. In principle the equilibrium evolution time scale is still much longer than the time scale of the RWM. Therefore, the requirement on the feedback system for dynamic error field compensation is much less severe than that for the nonlinear suppression of the RWM. However, dynamic error field correction is an important topic because even if C_β is relatively small, which is the operation regime envisaged for ITER, this is still an unavoidable problem. In the following, we will see that this phenomenon also affords a special opportunity to explicitly separate out the time scales of the different components of the error field that affects the dynamics of the RWM.

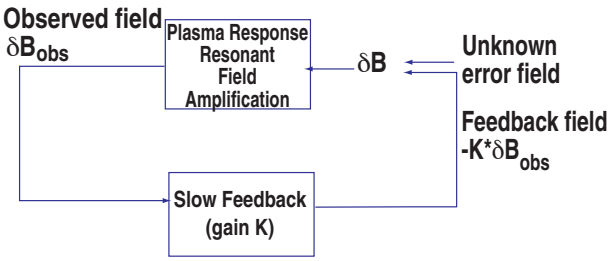

FIG. 33. Dynamic error field correction utilizes the resonant field amplification A_{RFA} of the stable RWM to minimize the effect of external error field on the plasma.

3.7.1. Poloidal field structure dependence in dynamic error field correction. The first set of experiments that showed the importance of the resonant component of the external field in affecting the stability of the plasma is provided by deliberately varying the connection angle between the upper and lower I-coils in the error field suppression experiment. As shown in figure 34, depending on the connection angle between the upper and lower I-coils, we may use the I-coils to produce different spectra of the external fields for the purpose of cancelling the "resonant component" of the error field. Conversely, an inappropriately prepared compensation field will destabilize the plasma.

Shown in figure 34(a) is the result of an experiment [136] on a steady-state plasma rotationally stabilized against the RWM with β_N above the no-wall limit ($\beta_N \geq 3.5$). It shows the variation of the measured time-averaged amplitude and the toroidal phase of the $n = 1$ component of the coil current for error field compensation. We note

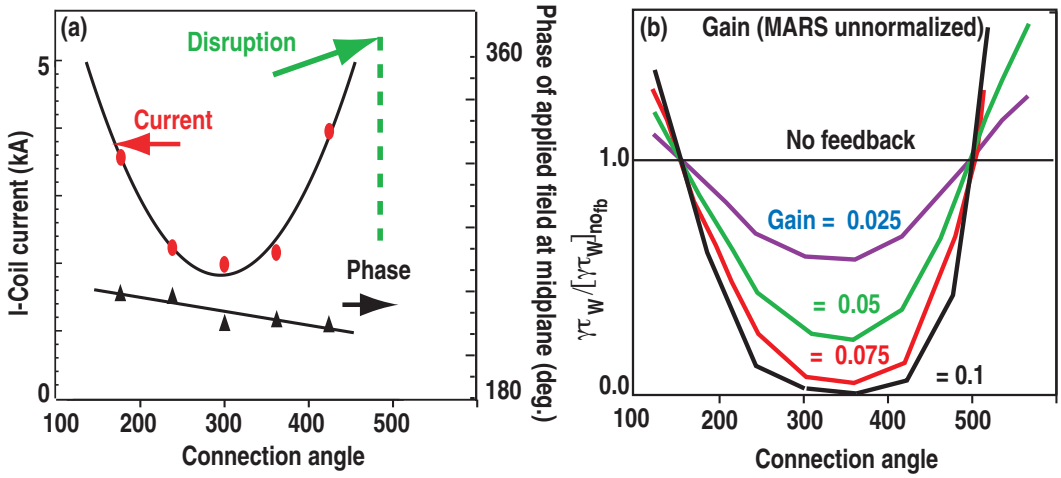

FIG. 34. (Left) experimentally measured magnitude and toroidal phase of feedback currents in I-coil as a function of the connection angle in DIII-D. Disruption is observed at an angle of 480 degrees (reference [136]). (Right) simulation using MARS of dependence of the stability of the plasma vs coil connection angle parameterized by different levels of gain.

that the required current has a minimum around $\Delta\phi_{connect}$ = 240–300 degrees. This minimum and the absolute phase of the I-coil current show the optimum spectrum of the I-coil amplitude and phase that could be used to cancel the resonant component of the unknown error field.

It is interesting to note that with different $\Delta\phi_{connect}$ settings, the toroidal phase of plasma response changes weakly showing that the unknown error field does not change much in this set of experiments. Based on these observations, the connection angle was set to $\Delta\phi_{connect}$ = 240–300 degrees for most of the magnetic feedback experiments on DIII-D. It has also been shown that when the I-coil connection is maximally unfavorable — at 420 degrees, the applied error field correction actually led to disruption as shown as the vertical dotted line in figure 34(a). This phenomenon should be compared with the phase-flip experiment in HBT-EP in section 3.4.4.

3.7.2. Theoretical modeling on the importance of the poloidal structure of the external correction field. The optimized connection angle $\Delta\phi_{connect}$ = 240–300 degrees in figure 34(a) is consistent with a number of modeling results.

First, a study including the structure of the RWM was made with the normal mode analysis (NMA) approach [121] with the DCON-VACUUM code to simulate feedback with I-coils. In this simulation, the feedback process used the complete set of normal modes of the plasma obtained during the open loop simulation. The unstable RWM was used to observe the role of plasma and feedback-coil coupling on the mode growth rate. To feedback-stabilize the RWM, the preferred connection angle was found to be $\Delta\phi_{connect}$ = 240–300 degrees.

Second, the same conclusion was obtained from results based on analysis using the MARS-F code as shown in figure 34(b). The mode used here is an unstable RWM and the dependence of the growth rate on the coupling between the mode and the feedback coil geometry was again the dominant factor. Shown are curves with fixed gain (unnormalized). A larger reduction in the growth rate was obtained with better coupling between the applied field and the unstable mode, which is qualitatively similar to experiment.

3.7.3. Demonstration of error field compensation and dynamic error field correction using internal vs. external coils. The basic ansatz of dynamic error field correction in high β_T regimes is that by detecting the enhanced plasma response to the resonant component of the external error field we may dynamically supply a compensating "resonant component" of an external field to reduce the resonant component of the unknown total external error field to the required level. This compensation, called dynamic error field correction, should be independent of the geometry of the external coils that produced the field and was verified in DIII-D (figure 35) using two different field patterns made available by two independent coil systems, namely C-coils and I-coils (figure 25). In the early time period of the discharge, the initial error field correction is provided with three pairs of C-coils located outside the vacuum vessel on the midplane. The C-coils current was reduced linearly in time to zero. At the same time the feedback was switched to the I-coils located off-midplane, allowing the I-coils current to adjust the error field compensation. In this experiment the upper three pairs of I-coils were connected with the lower three pairs with a 240 degree toroidally-phase shift. The $m = 2 - 3$ components are dominant.

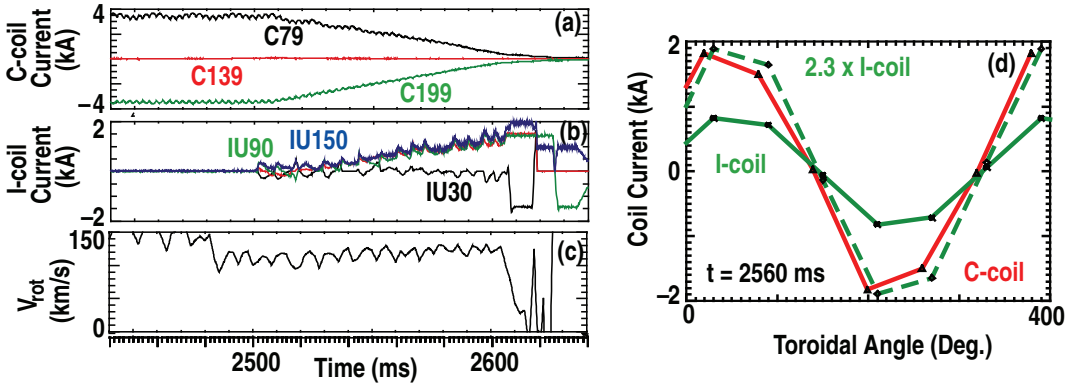

FIG. 35. Experimental demonstration of the principle of dynamic error field compensation in DIII-D. In this experiment, the error field correction provided by the C-coils [with currents in various coil pairs shown in (a)] is gradually replaced by the currents in I-coils [shown in (b)]. Plasma rotation in the discharge shown in (c) remains fairly constant, and the toroidal distribution of currents in C- and I-coils are the same as shown in (d) (reference [136]). [Reprinted courtesy of IOP, Nucl. Fusion **45**, 1718 (2005).]

By this procedure, the I-coils current replaced the C-coils current for error field correction. The plasma rotation was sustained at the same level as the initial value. No reduction of plasma rotation illustrated the fact that the reduction of midplane C-coil field was well-compensated with the increase of off-midplane I-coil field.

At a fixed time, the toroidal phase of the coil current was well-matched between the I-coil and C-coil with a multiplier of 2.3 between the two coil currents [figure 35(d)]. This indicated that only the magnitude of the resonant component of the correction field varied, not the phase.

3.8. Enhanced experimental operation through dynamic error field correction

Error field reduction was achieved in many devices and led to higher β_T and β_N, reported in DIII-D [122] and NSTX [77, 137].

3.8.1. Achieving the ideal kink limit. Figure 36 shows the achievement of high β_N close to the ideal wall β_T limit in DIII-D by using dynamic error field correction magnetic feedback [86]. The achieved β_N was twice the no-wall β_N limit and is, therefore, close to the ideal-wall pressure limit. This is the first achievement of the ideal-wall pressure limit at such a high level of $\beta_N/\beta_N^{no-wall}$. The discharge used a modest current ramp with continuously decreasing q throughout the plasma cross section. The discharge termination occurred at $q_{95} \sim 3.1$ and was accompanied by a fast growing $n = 1$ mode precursor. The observed e-folding growth time of $300\,\mu$s ($<< \tau_w \sim 3000\,\mu$s) for the precursor represents the onset of an ideal kink. The ideal MHD stability computation with a series of numerical equilibria reconstructed from experimental data indicates that the experimental configuration is within 10% of the ideal wall β_T limit. In the dynamic error field correction feedback process, the demand signal to the feedback system was a response signal to a gradual change to the currents in the equilibrium maintaining coil. This indicates that the signal detected by the poloidal sensors are from RFAs excited by some residual resonant component of the non-axisymmetric (error) field, which evolves in time as β_T evolves.

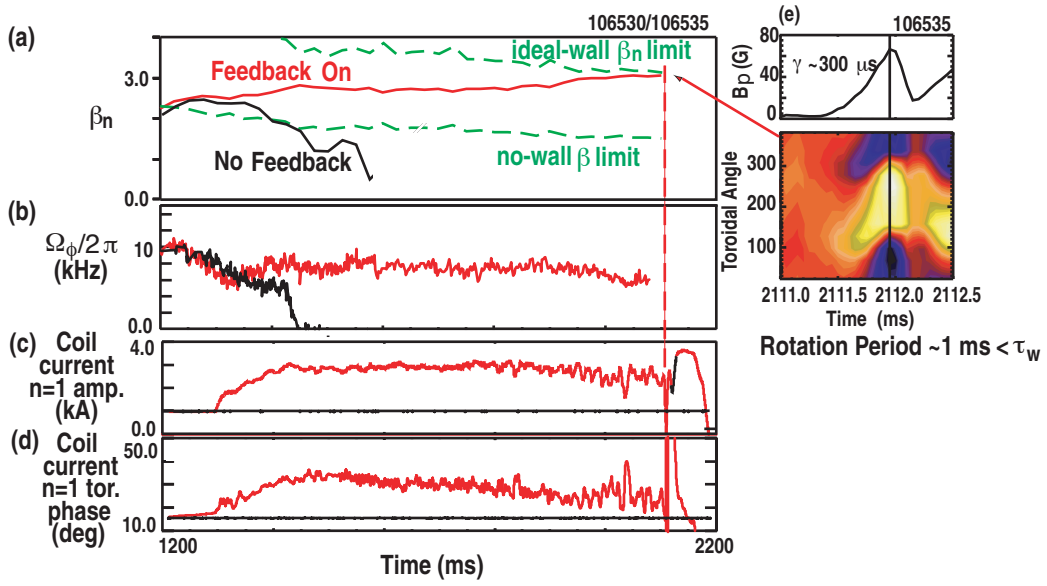

FIG. 36. Experimental achievement of high-pressure plasma in DIII-D close to the ideal MHD limit. Shown in (a) are the traces of the plasma pressure (β_N) versus time in two discharges with/without dynamic error filed correction. The estimated ideal-wall and no-wall limits were verified by the GATO code using experimentally measured pressure and safety factor q-profile. (b) The evolution in time of the rotation frequency for the two discharges with and without feedback. (c) The amplitude of the $n = 1$ radial magnetic field supplied by the C-coil system. Note that with no feedback, the current is preset to be 1 kA. (d) The toroidal phase of the $n = 1$ radial magnetic field supplied by C-coil. (e) Growth of the $n = 1$ poloidal field perturbation near the ideal MHD limit. The growth time of the mode is observed to be 300 μs; within this duration its toroidal phase angle also undergoes a 180 degrees shift (references [124, 133]). [Reprinted courtesy of IOP, Plasma Phys. Control. Fusion **44**, B339 (2002).]

Another more interesting demonstration of the equilibrium related nature of the error field in DEFC from feedback is provided by the experiment shown in figure 37 on DIII-D. The experiment was conducted with feedback off, and with the C-coil currents preprogrammed to those determined by the feedback system while feedback was turned on. The discharge behavior as shown in figure 37 followed the evolution of the discharge with feedback on (figure 36). The achieved values of β_N and plasma rotation frequency were identical to the plasma with feedback on. This evidence suggests that the resonant component of residual non-axisymmetric field contributed significantly to the mode amplification and consequently reduced the rotation velocity. Once the compensation was made, the RFA did not grow and the plasma did not slow down. Plasma rotation was able to suppress the onset of RWM up to the ideal MHD β_N. This result was found to be reproducible.

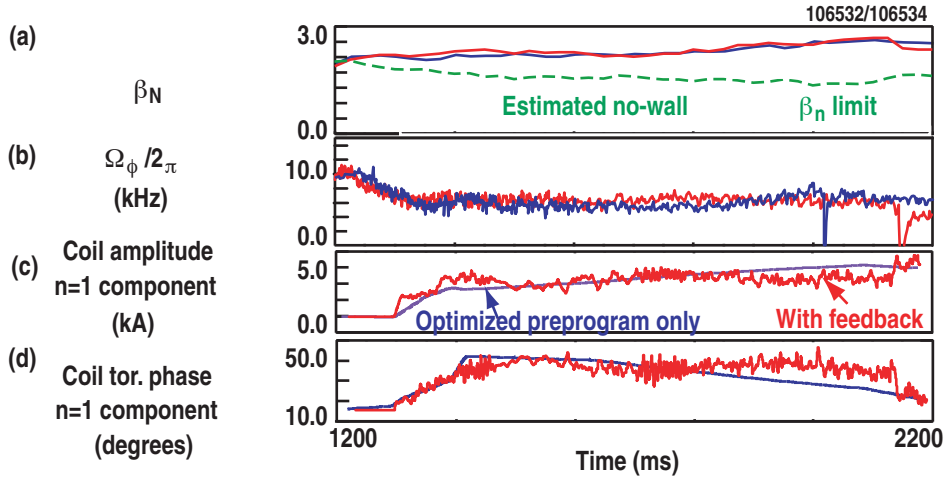

FIG. 37. Experimental achievement of high β_N discharge in DIII-D with pre-programmed coil current and comparison with the case using dynamic error field correction feedback. Two traces are shown, red is with feedback and blue is without. Shown in (a) is plasma pressure β_N (b) is the plasma rotation, in (c) the amplitude of the $n = 1$ component of the coil current, and in (d) the toroidal phase angle of the $n = 1$ component of the coil current (references [124, 133]). [Reprinted courtesy of IOP, Plasma Phys. Control. Fusion **44**, B339 (2002).]

3.8.2. Sustainment of rotational stabilization. Sustained wall stabilization for the XK mode has been demonstrated in an advanced tokamak discharge with high normalized β and high bootstrap current in DIII-D [124, 138]. β exceeds the calculated no-wall limit of $\beta_N \sim 4l_i$ for almost one second, and reaches a maximum near the estimated ideal-wall stability limit at $\beta_N \sim 6l_i$. Here plasma rotation plays a major role in the stabilization, with the non-axisymmetric coils (C-coils) providing feedback-controlled correction of the $n = 1$ error fields that would otherwise slow the plasma rotation.

Similar results were demonstrated by Sabbagh et al in NSTX without [88], and with $n = 1$ RWM feedback control and $n = 3$ error field correction [91], with values of $\beta_N \sim 11l_i$ [90].

3.9. Nonresonant external perturbation-induced toroidal rotation

As shown in section 3.2.2, the presence of an error field in the plasma breaks the toroidal symmetry of the plasma configuration and gives rise to the NTV torque [108]. This torque has been identified in experiments in NSTX [109] (section 3.6). Another consequence of the NTV theory is the presence of a toroidal-driven flow given by

equation (21) due to the non-axisymmetric fields and reported by Shaing [108, 111, 114]. The importance of the non-axisymmetric error field to the locking threshold (the minimum amplitude of the error field to cause the plasma to lock to the wall) in plasmas has been emphasized by Cole *et al.* in reference [117]. In the work by Garofalo in 2008 [107], the first observation of plasma acceleration driven by the application of static non-resonant error fields was reported. It also resulted in improvement in the global energy confinement time.

Toroidal rotation benefits the tokamak by flow shear stabilization of turbulence, screening of error fields, and stabilization of neoclassical tearing modes and RWMs. However, a self-heated burning plasma with little toroidal momentum injection will have negligible inertial torque. Toroidal momentum sinks will exist in a burning plasma, including torques from unavoidable magnetic field errors. Although the braking effect of static magnetic field asymmetries is well-known as discussed extensively in section 3.1.1, predictions that they can lead to an increase in rotation frequency (neoclassical offset) was not noted before 2008. When a large non-resonant $n = 3$ field is applied to a plasma with small neutral beam torque in DIII-D, the measured toroidal rotation of impurity ions and the calculated main ion toroidal rotation both increase in the electron diamagnetic drift direction. The magnitude, direction and radial profile of the offset rotation are consistent with theory as is the suppression of the rotation increase at low β.

The offset rotation rate is about 1% of the Alfvén frequency, more than double the rotation needed for stable operation at high β above the no-wall kink limit in DIII-D [100] and JT-60U [101] (section 2.6). An important consequence is that the non-resonant field torque in a fusion plasma from high-n fields for ELM suppression [139] may not present a problem, but instead may generate a plasma rotation sufficient to benefit confinement and stability in a fusion reactor!

3.10. Discussion on error field amplification and dynamic error field correction

Because the error field can greatly influence the plasma rotation, which in turn determines the stability of the RWM, research on error field is closely related to the research on RWM. This close relationship is accentuated because the plasma can have an amplified (resonant) response to the external error field. The research on error field and its amplification has resulted in improved understanding not only of the interaction between the plasma and an external perturbation field, but also the plasma state during its development of an RWM. This area of research has largely been phenomenological in nature, but is gradually evolving towards being more quantitative. Eventually, research in this area can greatly help us understand the dynamics of the plasma, including differentiating between the various plasma models.

The recent concentration of activity in this area started with the observed puzzle by Garofalo [53] of correlation between plasma rotation slowing down and speeding up near the $\beta_N^{no-wall}$ limit. It was subsequently explained by Boozer as the phenomenon of enhanced plasma response (RFA) approaching a "marginal stability" limit [55]. It was proposed that RFA can be described in terms of two simple parameters of s for stability and α for damping torque which are characteristics of the plasma state.

Ensuing experiments showed that RFA was observed in all experiments, including DIII-D, JET, NSTX, HBT-EP etc. Special experiments were designed to study the nature of the RFA. It showed that the RFA carries the helicity of the plasma, increases in amplitude with β_N and has its inherent natural frequency. It has to be emphasized that some of these equilibria are in the high rotation state studied in section 2. The important result was that these studies revealed that RFA can be described in terms of a single mode. Also, it is not necessarily true that all the plasmas were being close to some "marginal stability" state. Rather, RFA could be related more to the adjustment of this single mode to be in equilibrium with both the resistive wall and the background plasma. Interpreted in this way, the "rotation equilibrium" is lost, i.e. we should observe a rotation bifurcation when the "viscous torque" between this mode and the background plasma cannot balance with the electromagnetic torque between the mode and the external resistive wall. On the other hand, the true RWM instability is when the torque balance can be maintained, but still no neighboring equilibrium exists. There is still free energy to be expended to drive the flux diffusion through the resistive wall. This picture is qualitatively supported by the results from RFA and shows that the research results on RFA corroborates with those given in section 2. [Note this picture of the development of the RWM is very similar to that proposed by Gimblett *et al.* [54], except that the "mode" in question most likely is not a RP-RWM but rather a IP-RWM and there are other (kinetic) effects that affect the overall stability of the mode]. If this picture is firmed up quantitatively, we can claim to have made a great advance towards the predictability of the stability of RWM (c.f. section 2.8) The amplitude of the extra mode is usually quite small, therefore aspects of linear theory could remain valid.

Development of the technique of MHD spectroscopy [105] affords a method to probe the plasma with minimum amount of perturbation. It allowed detailed comparison of the experiment with computer modeling. For instance, the ongoing work by Lanctot verified that both IPEC and MARS-F can be used to model the RFA at low β_N [140]. Generalization to plasma conditions above the no-wall limit and with different plasma models is being actively pursued. This is the possible contribution of the major advance in RFA to the understanding of RWM.

It is worthwhile to mention that after understanding that the plasma slowing down is mainly due to the "resonant" response due to this mode, it was demonstrated experimentally this mode may be compensated for in various means, on the equilibrium evolution time scale, to allow the plasma remain stable to the RWM to achieve high performance at high rotation values.

Together with developments in the understanding of perturbed magnetic field in plasmas, the dynamics of particles in these fields were investigated quantitatively, demonstrating that the symmetry breaking fields give rise to the NTV and the non-resonant part also imparts a toroidal flow to the plasma. This effect is also demonstrated in experiments quantitatively. It is proposed that this effect can be used to provide counter current rotation of the plasma for the stabilization of the RWM. These represent recent developments towards a more quantitative understanding of the RFA in its relation to the RWM.

All the above indicates that this field is entering a new phase. It is expected that much progress will come from the study of error fields through even more coupling between theory, modeling and experiment in the near future. It is also expected that this effort will directly benefit the understanding and stabilization of the RWM. For instance it should be able to allow us establish the nature of rotational stabilization, i.e. whether type (a) in the scheme of classification of Gimblett and Hastie [54], is a good classification for the behavior of plasma in RWM.

4. RWM Stabilization with Magnetic Feedback

4.1. Introduction

When $\beta_N > \beta_N^{no-wall}$, and the toroidal rotation is not sufficiently large, the plasma is expected to be unstable to the RWM. In this case, we have to rely on magnetic feedback to stabilize the plasma. In general, feedback is a very useful branch of knowledge and it is being increasingly recognized as necessary and important for the fusion device. Two different sections of the IEEE Control Systems Magazine [141, 142] were recently devoted to a review of the feedback study of fusion plasmas. The feedback of the RWM aims at making the resistive wall mimic an "ideal wall". To study the plasma stability during feedback, we have to consider not only the response of the plasma to the perturbation under consideration, but also have to include the response of all other components involved in the feedback process. These components are the mode identification (sensors), control logic, power supply and feedback coils. A schematic of this closed loop feedback relationship is shown in figure 38. A collection of the useful concepts of the control theory that are employed for the feedback stabilization is given in Appendix D.

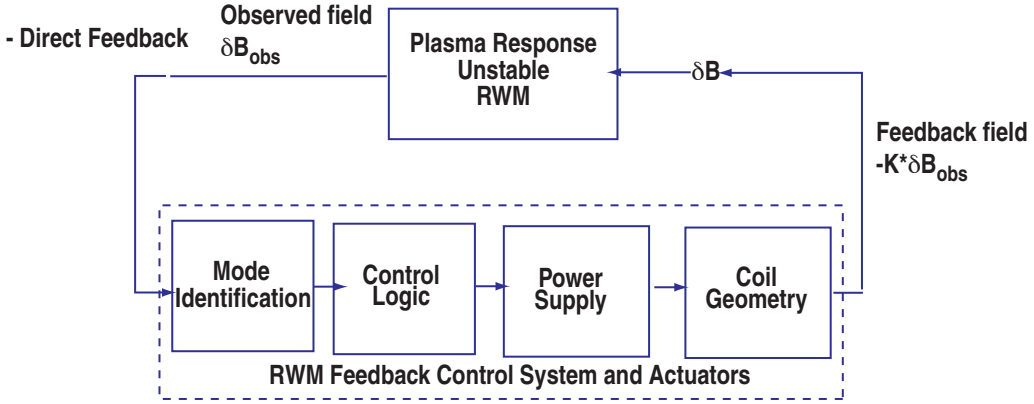

FIG. 38. Schematic block diagram of flow of the signal during direct feedback. Currents in the feedback coils are determined by a sequence of processes and factors that are labeled by the blocks for mode identification, control logic, power supply, and coil geometries etc.

4.2. The first analysis of feedback stabilization of tokamaks by Liu and Bondeson.

The toroidal calculations of RWM feedback control were first presented by Liu and Bondeson in 2000 [143]. The results showed that the high β_T, $n = 1$ RWM can be stabilized even with a simple arrangement of actuator and sensor coils. The feedback

geometry used is shown in figure 39. [This should be contrasted with the original configuration proposed by Bishop [32] shown in figure 7(b) and its implementation for RFPs to be shown in figure 56.] It was found sufficient to use one toroidal array of feedback coils and one array of sensor coils located at one poloidal location. This is because such a simple coil set couples well to the high-β_T $n = 1$ kink which balloons on the outboard side of the torus. Although the sensors have to be placed inside the conducting shell, the feedback coils can readily be placed outside, and their optimal extent poloidally is about one quarter of the poloidal circumference. Complex gain, which mimics the effect of a rotating shell [17] and makes the mode rotate, can decrease the gain required for stabilization. But real gain still plays the more important role.

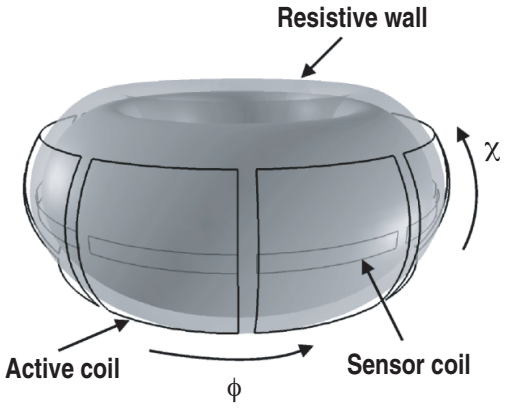

FIG. 39. Dynamic error field correction utilizes the resonant field amplification A_{RFA} of the stable RWM to minimize the effect of external error field on the plasma.

4.3. Analysis, theory and codes for feedback stabilization

4.3.1. Choice of sensor and feedback logic There are a large number of choices of the magnetic signal to be used for mode identification. This could be either the radial or poloidal components of the perturbed magnetic field: either compensated or uncompensated for its direct coupling from the wall or coil currents. Similarly, there is also a large choice of feedback schemes. The actuators could be programmed to nullify the projected perturbation signals at either the plasma or the wall.

A number of the more common control logics and choices of sensor signals are listed in Table III.

Strait [144] made a simple and elegant analysis on the effectiveness of different sensor and feedback configurations by using the relationships between the fluxes at the plasma and the resistive wall. The most important conclusions of his analysis are summarized in figure 40 for different feedback schemes using gain G on plasma mode with growth rate γ normalized to the resistive wall time τ_w. The top left of this figure shows that an ideal B_p sensor can be very effective (with $G \leq 1$) in stabilization of all

Table III. Feedback logic and flux and method used for stabilization

Logic	Type of Flux and Method of Utilization
Smart shell	Uses total radial flux just outside or inside the wall: feedback tries to produce "pseudo-ideal wall" at the observation location [32].
Fake rotating shell	Uses radial flux: the feedback currents are toroidally shifted relative to the observed mode pattern imitating the phase shift induced by toroidal rotation [58].
Explicit mode	Uses the radial flux compensated by the flux due to direct coupling between the coil and the sensors [144].
Mode control	Uses poloidal flux that is due to the unstable RWM and optimally decoupled from the applied B_r field from the feedback coils [86].

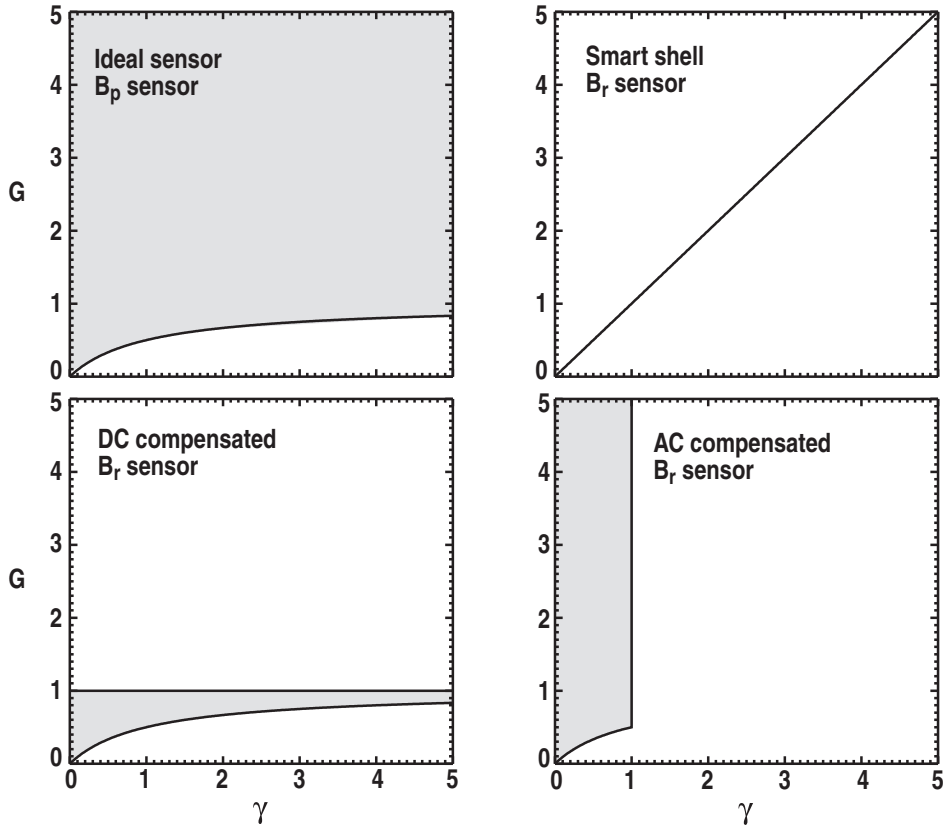

FIG. 40. Summary of analysis by Strait on the effectiveness of sensor and feedback schemes in magnetic feedback. The range of gain values G (dashed) to stabilize a mode is plotted against the open-loop growth rate γ of the unstable RWM. The top left panel is for ideal B_p sensor, top right for Smart shell feedback with B_p sensor, lower left for dc compensated B_r sensor, and lower right for ac compensated B_r sensor (reference [144]). [Reprinted courtesy of IOP, Nucl. Fusion **43**, 430 (2003).]

modes with $\gamma \to \infty$. On the top right, the figure shows that even with the smart shell logic but using B_r sensor, $G \to \infty$ as $\gamma \to \infty$. Therefore, it is not as efficient as the B_p sensor. The dc compensated B_r sensor can be as efficient as the B_p sensor. This is shown in the bottom left panel. However, ac compensated B_r sensor is the least efficient and is also limited in the range of the growth rates of the RWM it can stabilize, i.e. $\gamma \leq 1$.

The computational studies of the superior performance of poloidal sensors were first demonstrated in using MARS-F [67]. Subsequent calculations with several codes [121, 145, 146] confirmed this advantage of the poloidal sensors. Work with the MARS-F code has shown that control can be made robust with respect to variations in plasma pressure, current and rotation [95, 147, 148], if the active coils have a single coil in the poloidal direction located at the outboard midplane (e.g., as the C-coil in DIII-D). A single poloidal coil toroidal array covering about 20% of the poloidal circumference [67] works well over a large range of plasma currents. Multiple active coils in the poloidal direction are useful when radial sensors are used [121, 146, 149], but surprisingly do not bring substantial improvements for poloidal sensors [149].

The advantage of the poloidal sensor versus the radial sensor in feedback was also noted by Pustovitov. He also pointed out that it is even more preferable to use a combination of poloidal and radial sensors [150].

In RFX (a reversed field pinch device in Italy), a control algorithm, the clean-mode control (CMC) was developed to control the effect of the $m = 1$ resistive-kink and tearing modes directly, similar to "mode control" in tokamaks rather than "virtual shell control". This approach can remove the systematic error affecting magnetic measurements due to the aliasing of the sideband harmonics produced by the active coils. It decreases deformation of the last closed magnetic surfaces and prevents wall locking systematically. The resultant pattern of plasma wall interaction moved toroidally during the discharge and resulted in a more even distribution of the plasma-wall interaction [151].

4.3.2. Extended energy principle for magnetic feedback of an ideal-stationary plasma. For feedback, the plasma stability problem necessarily has to be extended to include the external circuit and feedback control elements. With idealization, these elements can still be modeled concisely and the full feedback problem studied for its analytic properties.

An example of the theoretical approach in this direction is given by Chu *et al.* [121]. In this work, feedback stabilization of the RWM in a general feedback configuration is formulated in terms of the normal modes of the plasma-resistive wall system. The growth/damping rates and the eigenfunctions of the normal modes are determined by an extended energy principle for the plasma during its open loop operation. The dynamics

of the feedback system is completed by the prescription of the feedback logic. During the closed loop operation, the extended energy principle further determines the interactions between the feedback coils with the open loop eigenfunctions and the stability of the full system.

This formulation, given in Appendix E, has been implemented numerically and applied to the DIII-D tokamak. It is found that feedback with poloidal sensors is more effective than feedback with radial sensors. Using radial sensors, [figure 41(a)] increasing the number of feedback coils from a central band on the outboard side to include an upper and a lower band can substantially increase the effectiveness of the feedback system. The strength of the RWM that can be stabilized is increased from $\gamma\tau_w = 1$ to 30. (γ is the growth rate of the RWM in the absence of feedback and τ_w is the resistive wall time constant.) Using poloidal sensors, just one central band of feedback coils is sufficient for the stabilization of the RWM with $\gamma\tau_w = 30$.

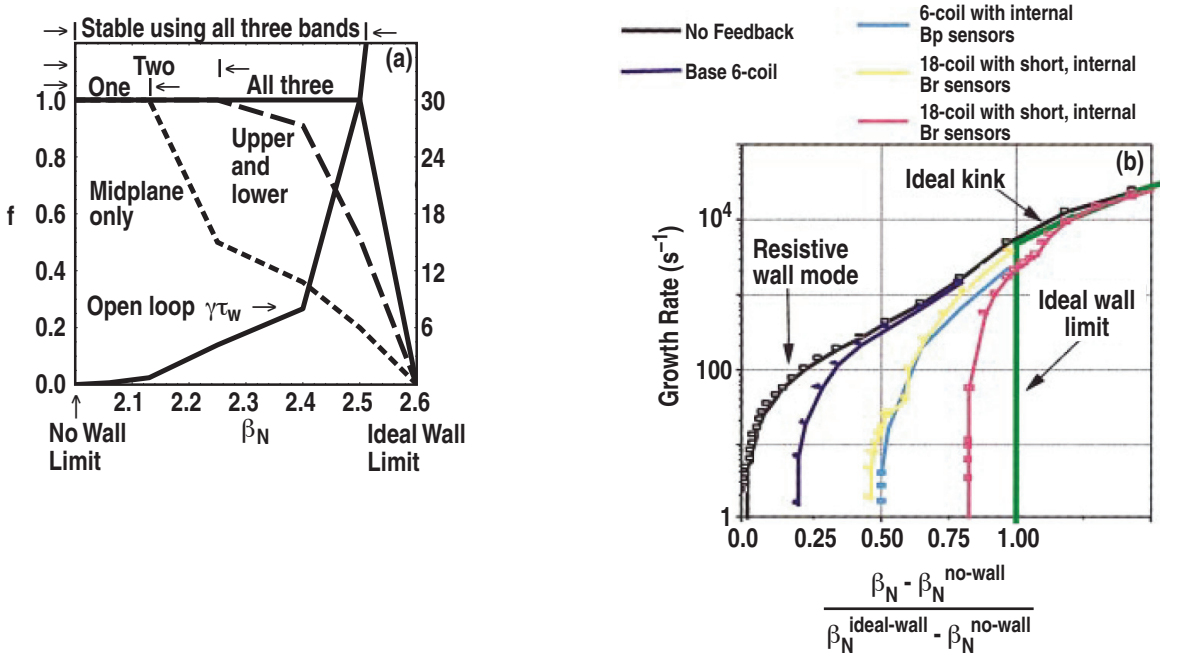

FIG. 41. (a) Application of the NMA code to the study of the effectiveness of feedback using different feedback and sensor coils using B_r in DIII-D. f is the effectiveness factor. $f = 1$ for stability. In this figure f is plotted as a function of β_N for one, two, and three bands of radial sensors and coils. It is seen that using one midplane coil, the RWM is stabilized only for $\beta_N \leq 2.13$. Using the upper and lower bands, the RWM is stabilized for $\beta_N \leq 2.25$. Using all three bands of coils stabilizes $\beta_N \leq 2.5$. At this value of β_N, the strength of the RWM has a growth rate of $\gamma\tau_w$ of 30 (reference [121]). [Reprinted courtesy of IAEA, Nucl. Fusion **43**, 441 (2003).] (b) Summary of VALEN calculations of optimized feedback configurations in DIII-D for both smart shell and mode control feedback logic (references [146, 156]). [Reprinted courtesy of AIP, Phys. Plasmas **8**, 2170 (2001).]

We note that a similar approach of separating the feedback problem into the coupled open-loop and closed-loop problems has been adopted by the STARWALL-OPTIM [152] 3D code package (section 4.3.4).

Another work in this spirit was by Bondeson *et al.* [153]. The large aspect ratio model for the current driven XK is applied to study the control of the RWMs. Comparison with toroidal computations indicates that the cylindrical instabilities react in similar ways to pressure driven modes, when the feedback and sensor coils are placed on the low field side of the torus. However, higher gain is required in the cylindrical case.

4.3.3. Necessary simplification for practical application of control methods Interaction between the plasma and the RWM feedback systems uses magnetic sensors (and sometimes other signals) to gain information on the amplitude of the unstable RWM. This signal is processed through the control logic to generate the control currents in a set of feedback coils. Although it is demonstrated that the complete solution of the feedback problem is possible in terms of the full set of normal modes, in practice, the number of "modes" has to be limited to be practical. For toroidal systems, the transfer functions are sums over infinitely many isolated poles [121, 148, 154], corresponding to the RWM growth-rates in the absence of feedback. The transfer functions can be well approximated in the entire unstable half plane by the Pade approximation using three-pole (or even two-pole for poloidal sensors) [148]. Adopting the Pade approximation makes the system more amenable to well-established analysis methods developed in control theory.

4.3.4. Codes for magnetic feedback At present, there are four codes that have been developed for the study of the magnetic feedback problem in toroidal geometry. These are the CARMA(MARS-CARIDI), NMA, VALEN and STARWALL-OPTIM.

- CARMA results from the coupling of the MARS [148] code to the 3D CARIDI [155] eddy current code. The MARS code is described in more detail in references [62, 66, 67, 68]. Aside from feedback stabilization, it can also be used to study rotational stabilization of an RWM with a general toroidal rotation profile. It now includes the full diamagnetic and magnetic drift of the particles self-consistently.
- The NMA [121] code is a complete solution of the 2D feedback problem of RWM with the full 2D geometry of the sensor and coil structure. The advantage of NMA is its conceptual conciseness. The disadvantage is that it can not handle either plasma rotation, nor the 3D geometry of the sensor and feedback coils. More details of this code is given in section 4.3.2 and Appendix E.

- VALEN [146] is specifically constructed to study feedback stabilization of the RWM. The advantage of VALEN is that it allows a full model of the 3D structure of the external coils. Therefore, it is an extremely useful design tool. It is described in more detail in Appendix F and reference [146]. This code has been used to design new (and optimum) feedback systems [77] and for the interpretation of experimental results [88]. Here, it was found that off-midplane control coils situated near passive conducting plates lead to inferior feedback performance compared to a midplane-located coil set. Another example of these optimization studies with the VALEN code is its application to the design of the internal feedback coils (I-coils) for DIII-D feedback experiments [156]. The issue it resolved was the advantage and/or disadvantage in using a single poloidal segment ($\sim$6 toroidal control coils on the midplane) vs. three poloidal segments ($\sim$18 control coils located at the midplane and above/below the midplane) for feedback experiments. The results from VALEN are summarized in figure 41(b), in which the growth rates of the RWM with different coil set and different sensor and feedback schemes are plotted as a function of C_β (x-axis). The six midplane coils on DIII-D (a basic smart shell feedback scheme) and proportional gain raise C_β only 20% towards the ideal wall β_T limit, consistent with the modest feedback performance expected for such a system. The use of shorter sensors located inside the vacuum vessel and the existing six control coil system projects to about 30% toward the ideal wall limit. The use of a toroidal array of midplane mounted B_p sensors improves the projected performance of the existing six control coil set further to about 50% toward the ideal wall limit. For an 18 coil set in three poloidal segments which was proposed for installation on DIII-D, the basic smart shell projected performance is improved to 50% toward the ideal wall limit. The use of a toroidal array of midplane-mounted B_p sensors improves the projected performance of an 18-control coil set to about 80% towards the ideal wall limit. These results can be compared with that obtained by NMA given in figure 41(a) [121].
- STARWALL and OPTIM. This code couples the fully three-dimensional stability code STARWALL [152], and the feedback optimization code OPTIM [152]. It was developed to compute the growth rates of RWMs in the presence of non-axisymmetric, multiply-connected wall structures and to model the active feedback stabilization of these modes. The unique feature of this code is that it can take several toroidal harmonics simultaneously into account. Therefore, it can compute both the open-loop and closed-loop RWMs in the presence of non-axisymmetric, multiply connected wall structures. This code uses the approach similar to NMA [121] and separates the RWM and feedback stabilization into two parts:

the open- and the closed-loop problems. In the open-loop part, a complete set of eigenfunctions of the plasma resistive wall system is determined. The feedback coils are included in the resistive wall configuration. During the open loop operation, the feedback coils are additional passive resistive elements without an applied external voltage. The OPTIM code then finds an optimal set of feedback parameters that would make the system stable. The code has been applied to study the effect of toroidal mode coupling caused by multiply connected wall structures.

4.4. Experiments on magnetic feedback stabilization.

4.4.1. Internal sensors and mode control logic lengthen discharge duration. All feedback sensors employed in these experiments are magnetic field or flux sensors and, in principle, can determine the magnetic field components at any location beyond the plasma boundary for feedback control. The types and locations of control sensors are crucial for feedback control (section 4.3.1). The optimization depends on the toroidal phase relationship between the mode, external applied field and eddy field. Preference arises from: (1) the sensitivity of the sensors to the mode itself or the total field/flux, (2) local value of fields measured by the magnetic pickup probe or spatially averaged flux loop, (3) resilience to the expected noise or error field, and (4) easiness for eliminating the $n = 0$ equilibrium field.

In the early history of feedback control, the "smart shell" or "virtual shell" with radial flux loop sensors was used where the feedback aims to preserve the total radial flux at the sensor location. Since the RWM is driven by the joule loss on the wall, the recharging of the lost flux should slow down the growth rate and the feedback control current with some toroidal phase shift which should make the RWM stable.

Sensor preference was examined experimentally in DIII-D [86, 156]. Shown in figure 42(a) are results using the "smart shell" feedback algorithm. It shows that internal saddle (B_r) loops are more effective than external loops in extending the plasma duration. Figure 42(b) compares results for feedback with δB_r and δB_p sensors and without feedback. Using the δB_p sensors and the "mode control" algorithm, the increase in plasma duration was almost five times as long as that achieved using the internal saddle loops and the "smart shell" algorithm. These show a clear advantage of internal sensors and sensing the mode itself compared to the external sensors or total flux. It seems the "smart shell" does not perform as well as originally proposed with a simple model [32].

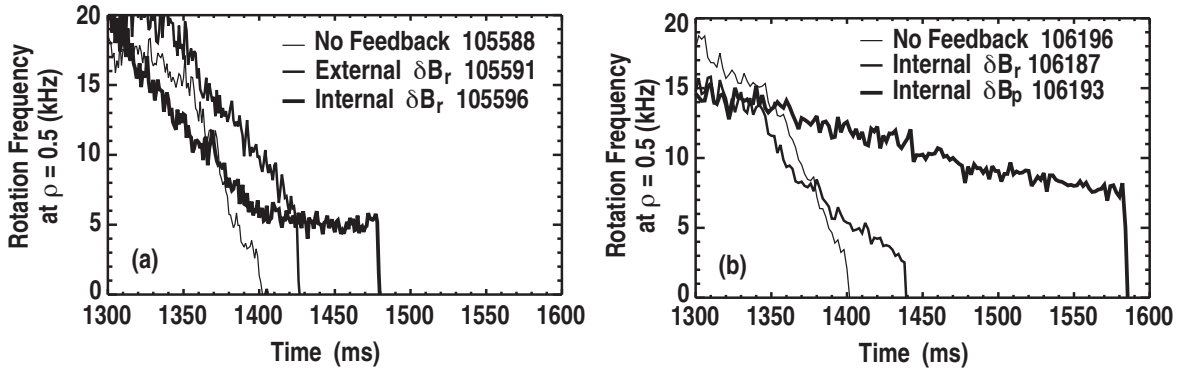

FIG. 42. Comparison of stabilized plasma duration for a variety of feedback conditions in DIII-D (reference [86]). [Reprinted courtesy of Proceedings of 28th EPS Conference on Controlled Fusion and Plasma Physics, Funchal, Portugal, ECA Vol. 25A (EPS, Petit-Lancy, 2001) Paper P4.008, http://www.cfn.ist.utl.pt/EPS2001/fin/authors/nav/AutJ01fr.html.]

An entirely different approach for sensors is the combination of sensor measurements and the use of the system model. Here, the belief is that the feedback does not require an exact knowledge of the system status as long as the system is contained within a stable domain. One approach is the use of the Kalman filter [157] which is composed of a set of mathematical equations that allows a system to find an optimized state based on measurements and models. For example, if the sensor measurement has noise, the system will be controlled using pre-set system eigenvalue, rather than only by sensor signals. The experimental verification of its feasibility combined with predicted growth rate is reported [157].

4.4.2. Achieving higher C_β at lower plasma rotation by I-coil feedback. To gain an appreciation of the achievement of rotational and feedback stabilization, the experimentally achieved C_β are summarized in figure 43. Shown are representative shot trajectories of plasma rotation (at the $q \sim 2$ surface) vs. C_β. The marginal stability criterion was computed using the MARS-F code [67] for a generic set of equilibria typical for these discharge conditions. Without feedback, the discharge terminated below the estimated critical rotation frequency [trajectory(a)]. With I-coil feedback a proper choice of gains increased C_β to $0.8-1.0$ [trajectories (b1),(b2)] even when the plasma rotation was gradually reduced well below the predicted critical rotation. The trajectory (b1) was terminated by a fast non-oscillatory RWM. The discharge represented by trajectory (b2) reached higher C_β even with lower rotation down to 30 km/s.

For comparison, a typical discharge trajectory of the best performance plasmas using C-coil feedback is included [trajectory (d)]. C_β achieved in experiments using the C-coils is near the RWM stable boundary predicted by MARS-F. We conclude that feedback with I-coils produced higher plasma pressure when compared to that using C-coils even when the plasma rotation was significantly reduced. Feedback with the I-coils at near-zero rotation can sustain the plasma at ∼40% above the no-wall limit, i.e. $C_\beta \sim 0.4$ for ≥100 ms. This range of $C_\beta \sim 0.4 - 0.5$ is consistent with both MARS-F and VALEN predictions for a non-rotating plasma taking into account the characteristics of the power supply used in the present experiments [158].

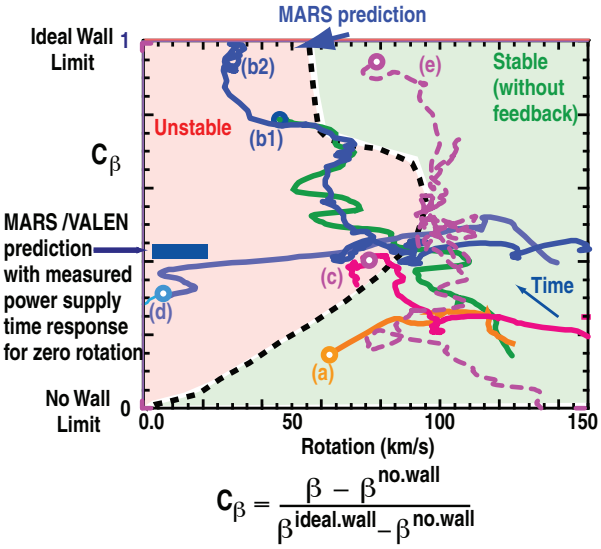

FIG. 43. Summary of achieved stabilization results in DIII-D in the rotation- C_β plane. (a) Without feedback, (b1,b2) with I-coil feedback, (c) feedback with C-coils, and (d) with I-coil feedback and strong $n = 1$ braking. The onsets of the RWMs are marked by small circles. The dotted line through the middle of the figure is the critical threshold for rotational stabilization computed by MARS-F (reference [136]). [Reprinted courtesy of IAEA, Nucl. Fusion **45**, 1715 (2005).]

4.4.3. Simultaneous activation of dynamic error field correction and direct feedback. It was demonstrated that during dynamic error field correction, the most important component of the error field to eliminate is mainly the resonant component to the stable XK. Whereas during direct feedback, the important goal is to suppress the self-generated XK of an unstable plasma. When error field correction is made in a less-optimized manner, the resonant component of the error field is not completely eliminated. A residual error field remains. It still couples to the "stable" XK. When the plasma approaches marginal stability, the coupling increases and appears as a self-generated instability and has to be suppressed by direct feedback. In this situation, the dynamic error field correction and direct feedback presumably has to take place simultaneously. This circumstance is especially true during the increase in C_β. When the RWM stability condition is marginally stable, the dynamic error field correction takes place. With increasing C_β, the direct

feedback is needed to stabilize the RWM. In figure 44 [159] is shown the comparison of discharge performance between feedback using I-coil only and feedback with both I-coil and C-coil in DIII-D. In this case, the I-coil was used to stabilized the RWM excited by the edge localized modes (ELMs) and the C-coil was used for dynamic error field correction.

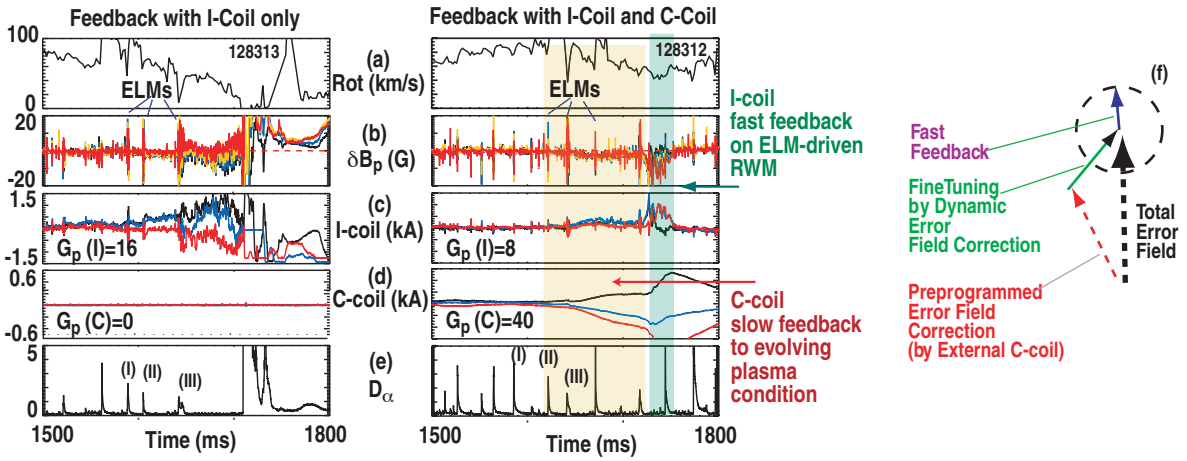

FIG. 44. β_N collapse during frequent ELMs with I-coil vs I- and C-coil feedback in DIII-D. Left column: feedback with I-coil only can suppress ELM-induced RWM for a few ELM cycles. (Right column) simultaneous operation with both the I-coil (fast feedback) and C-coil (slow feedback) reduces accumulation in amplitude of RWM. (a) plasma rotation at q 2. (b) δB_p magnetic sensor signal (c) I-coil currents (d) C-coil currents (e) D_α signal (au). [(a-e) Reprinted courtesy of IOP, Nucl. Fusion **49**, 125003 (2009).] (f) Schematic showing the simultaneous action of both fast and slow feedback (reference [159]). [(f) Reprinted courtesy of IAEA, Nucl. Fusion **45**, 1715 (2005).]

4.4.4. Achieving high plasma β by using feedback in NSTX. Feedback control of $n = 1$ RFA and unstable RWMs was first demonstrated in low rotation plasma by Sabbagh in 2006 [90], and is now used as a routine tool since 2008 on NSTX. It was found that on the average, the discharge pulse duration was increased. Also, the discharges were able to reach higher β. This is shown in figure 45 [92]. The averaged value of β_N achieved during the flattop phase of the discharge was plotted against the averaged value of the internal inductance l_i. It is seen that the discharges reach higher averaged β_N values with feedback control on versus those with feedback control off.

Open loop $n = 3$ error field correction is also used in these plasmas to broaden the rotation, yielding a stable, steady-state profile.

4.4.5. Achieving reproducibility in feedback stabilization of the current driven RWM. Reproducible stabilization of RWM is extremely useful to investigate the feedback performance. This was achieved in the case of a current-driven RWM excited at $q_{95} \sim 4$ through a strong plasma current ramp. The resulting helical mode structure is basically similar to the pressure driven RWM in AT plasmas.

Figure 46 shows the feedback performance, where the mode amplitude at the plasma edge for the $q_{95} \sim 4$ plasma was used as a measure of the mode growth rate. The increase of proportional gain reduced the mode amplitude from ∼20 to the level of ∼2 Gauss. The addition of derivative gain was effective in further suppressing the mode. During the feedback process, both the feedback current and the mode amplitude decreased simultaneously. It is different from the case of dynamic error field correction in which the setting of a finite coil current leads to the reduction of the mode amplitude. Based on the response of the mode to the derivative gain and the relation between the mode amplitude and coil currents, the feedback on the current-driven RWM can be identified as functioning as a direct feedback rather than dynamic correction against a static error field.

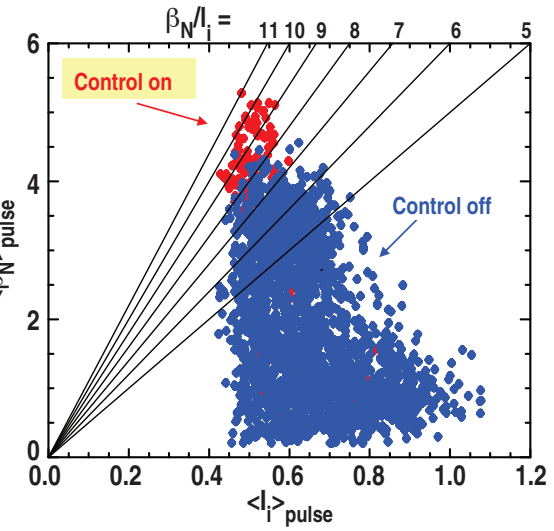

FIG. 45. Value of $< \beta_N >_{pulse}$ vs. plasma internal inductance $< l_i >_{pulse}$ averaged over the I_p flat top interval for shots with at least 0.2 s duration ($\geq$ 60 RWM growth times) in NSTX (reference [92]). [Reprinted courtesy of IOP, Nucl. Fusion **50**, 025020 (2010).]

Through a detailed analysis of the experimental data, the distinctive roles of dynamic error field correction (DEFC) and magnetic feedback are identified. It is also concluded that DEFC cannot be used to replace the role of direct magnetic feedback [160].

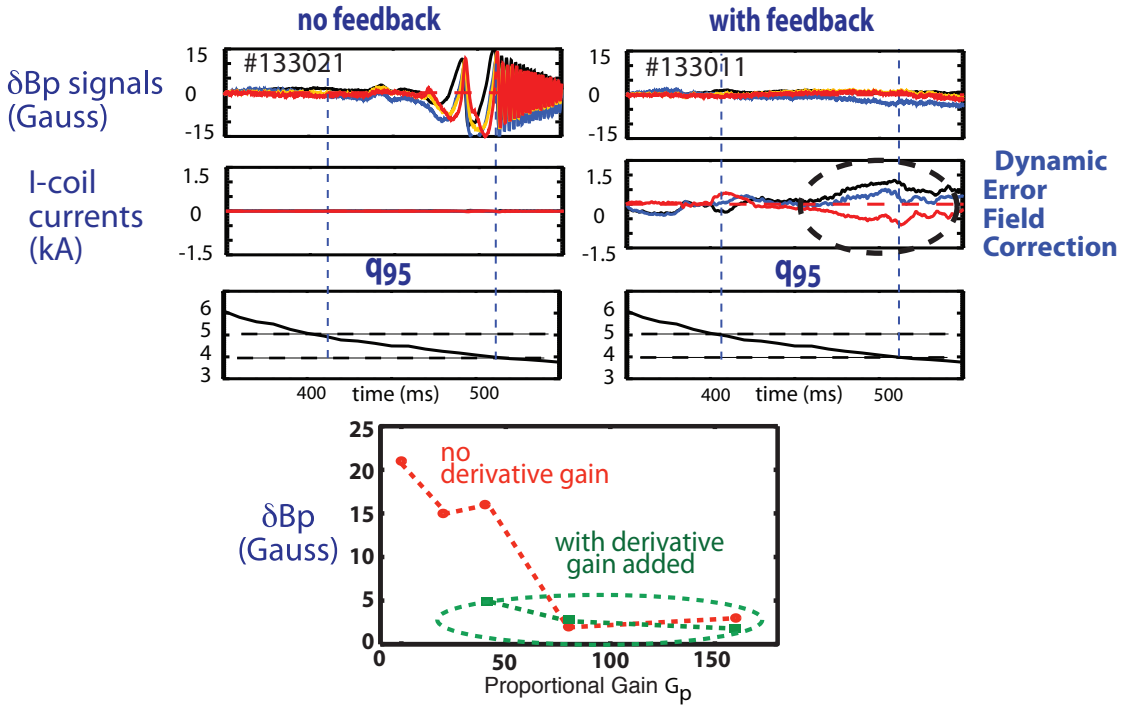

FIG. 46. Shown are the comparison in the development of the RWM for a low β plasma in DIII-D between discharges without derivative gain feedback (left panels) with the case of with derivative gain (right panels). The top panel is the time trace of the δB signal (in Gauss), the middle is the feedback coil current, the bottom is the safety factor at 95% flux q_{95}. The last panel on the bottom is the comparison of δB_p between the two different methods of feedback gains. It is seen that without the derivative gain, the plasma developed a tearing mode when q dropped below 5 towards 4; while with feedback, the growth of the mode is inhibited. Instead, the current in the I-coil shows more activity with derivative feedback, showing the presence of active dynamic error field correction (references [159]). [Reprinted courtesy of IOP, Nucl. Fusion **49**, 125003 (2009).]

4.4.6. Verification of the open loop growth rate Although the full feedback process is complicated by the various external components mentioned in the introduction section 4.1, its maximum performance can be revealed from the its "abnormal termination" during the close-loop operation. A collection of the "open loop" growth rate of modes during "abnormal termination" of the closed-loop operation using I-coils for the stabilization of RWMs are shown in figure 47 These modes grow near the termination of the discharge and the feedback system exhausts the available current to control the mode. At that moment, the plasma rotation decreased to near zero due to the strong magnetic torque of the uncontrolled RWM and the observed growth

rate is expected to correspond to the theoretical growth rate without either rotational or magnetic feedback stabilization, equivalent to the open loop growth rate $\gamma_{open}\tau_w$. These observed growth rates are in good agreement with model predictions. Shown in figure 47 is the comparison of this prediction with computations using the VALEN code. A similar comparison was obtained for the MARS-F code. These results suggested that the feedback system with I-coils in DIII-D could suppress RWM with growth rates up to $\gamma_{open}\tau_w \sim 25$.

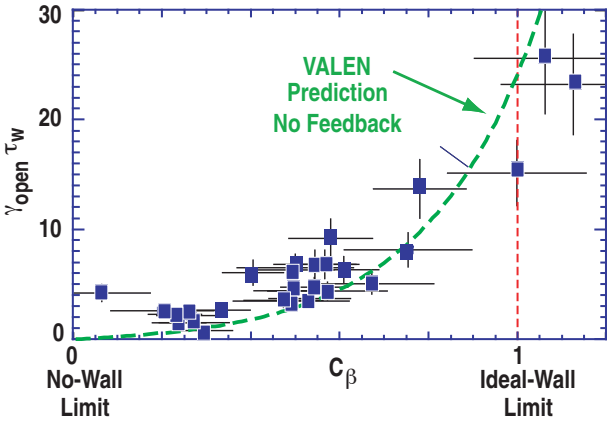

FIG. 47. Experimentally measured openloop growth rate of the unstable RWM as a function of C_β in DIII-D. Shown in dotted line was the value predicted by VALEN code (reference [122]). [Reprinted courtesy of AIP, Phys. Plasmas **11**, 2505 (2004).]

4.5. Deformation (non-rigidity) of the plasma during RWM feedback stabilization and error field correction

In general, the plasma deformation is not expected to remain fixed in shape (rigid) during magnetic feedback stabilization and/or error field correction. This non-rigidity is largely a measure of the "practical limit" of effectiveness of the coupling of the feedback coil to the unstable mode vs. the other stable modes. Evidence of RWM non-rigidity was reported in NSTX by Sabbagh *et al.*[90]. An ideal feedback coil would couple only to the unstable mode and does not couple to the stable modes. This can be demonstrated using the formulation of NMA (Appendix E).

As shown in the formulation of NMA, the state of the plasma-coil system can be completely described by a set of normal modes with given patterns $\{\delta B_{ni}\}$ on the plasma surfaces and the resistive wall and with amplitudes $\{\alpha_i\}$.

A good example is given by the plasma and coils in DIII-D. This system is especially interesting due to the fact that it has two sets of external coils (the C-coils and the I-coils) that were used for feedback and error field corrections. The geometry of these coils are shown as the blue window frame structures outside of the plasma in figure 48. Without feedback and with the growth of the RWM, the pattern of normal perturbed magnetic field δB_n on the plasma surface and on the resistive wall are given in (a) and (b) in figure 48. Note that this is the state of the system when

$$\begin{aligned} \alpha_1 &= 1 \quad , \\ \alpha_i &= 0 \qquad i \neq 1 \quad . \end{aligned} \tag{28}$$

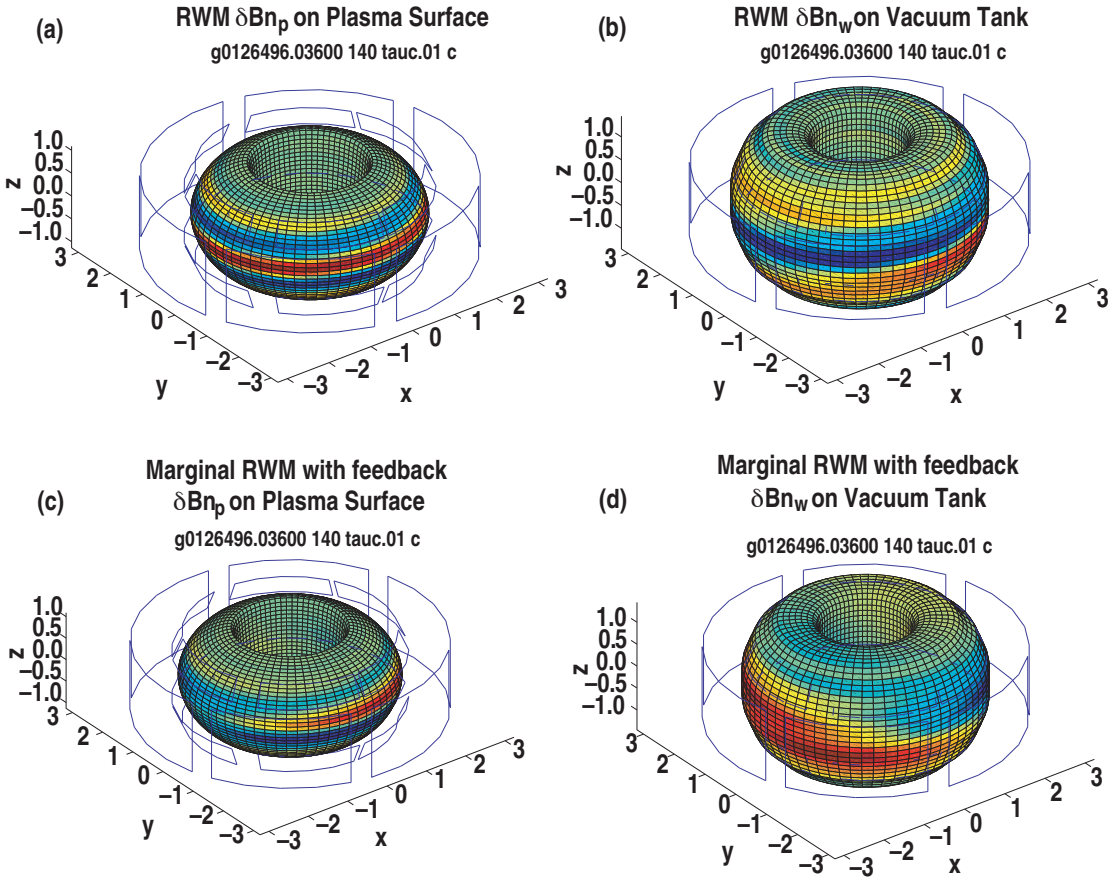

FIG. 48. Example of the open loop eigenfunction are shown in the upper panel. (a) the pattern of the normal component of the perturbed magnetic field δB_n on the plasma surface, on the right is δB_n on the resistive wall. It is seen that the perturbed fields show the helicity of the equilibrium magnetic field. It has a tighter pitch on the plasma boundary than on the resistive wall (b)due to the fact that higher harmonic components decays faster away from the plasma boundary. This mode structure does not change greatly with C_β. The structure of the RWM at marginal stability with feedback using C-coil for a plasma with $C_\beta = .85$ are shown in the lower panel. (c) is the pattern of the normal magnetic field on the plasma surface and (d) is that on the resistive wall. It is interesting to note that the helicity of the perturbed magnetic field on the resistive wall now has a helicity opposite to that on the plasma surface or opposite to that of the original plasma equilibrium. The light blue lines are the C- and I-coils in DIII-D.

Here, the unstable RWM is denoted as mode 1 . On the left is the pattern of δB_n on the plasma surface, on the right is δB_n on the resistive wall. It is seen that the perturbed fields show the helicity of the equilibrium magnetic field. It has a tighter pitch on the plasma boundary than on the resistive wall due to the fact that higher harmonic components decay faster away from the plasma boundary. This mode structure does not change greatly with C_β. Of course, it also does not depend on whether the C-coils or I-coils are used for feedback stabilization.

During feedback, the external feedback current I_c couples not only to the unstable RWM, but also to all the stable RWMs, i.e. the i'th mode with $i > 1$. The RWMs are excited to the amplitude given by the solution of equation (E.4).

$$\alpha_i = \frac{E_i^c I_c}{s - \gamma_i} \quad . \tag{29}$$

Here E_i^c denotes the excitation of RWM mode i by the current I_c. It depends on the interaction energy between the magnetic field produced by I_c with mode i. s is the frequency variable in the frequency domain, γ_i is the growth (damping) rate of mode i. At marginal stability $s = 0$, the amplitudes of excitation of different modes are therefore proportional to E_i^c/γ_i. The growth (damping) rates γ_i depend on the equilibrium under consideration and the external resistive wall. They can not be easily modified. Whereas E_i^c, the coupling of the stable modes to the external coils, can be judiciously chosen to be minimized. A good feedback coil set should be designed to maximize coupling to the unstable mode while reducing them for all the stable modes. With optimal design, the stable modes would not be excited to a large amplitude, and the RWM remain quite "rigid" during the feedback process.

For the unstable RWM shown in figure 48, the non-rigidity of the RWM during feedback has been compared between using C-coils vs. using I-coils. It is found that the mode pattern of the total δB_n during feedback does not change substantially for the I-coils feedback, whereas this is not true for using C-coils feedback. An extreme example is shown for the δB_n during C-coils feedback in the (c) and (d) in figure 48. It is interesting to note due to the extreme non-rigidity, the helicity of the perturbed magnetic field on the resistive wall now has a helicity opposite to that on the plasma surface or opposite to that of the original plasma equilibrium. This is evidence that C-coils is much less effective than the I-coils for feedback.

Another indication of the non-rigidity of the plasma during feedback comes from the use of Pade approximation (section 4.3.3). It was found that during feedback, the plasma response can be approximated by using three or even two (but not one) poles [148] in the Pade approximation. This is different from the situation in RFA, in which usually one pole in the Pade approximation is sufficient. A system that can be described by one pole can be readily stabilized.

4.6. Discussions on feedback stabilization

Substantial progress has been achieved in modeling and experiments on the feedback stabilization of the RWM. It is now recognized that for the tokamak, the magnetic feedback configuration could be much simpler than originally envisioned by Bishop. Simple feedback geometry with feedback coils inside the resistive wall could be very efficient. Much of the technology developed in general feedback theory can be readily

applied to the feedback problem for the tokamak. Different feedback logic has been analyzed and experimentally tested. Many codes have been developed for the analysis of feedback experiments. Feedback was found to be helpful in achieving high plasma performance. At the moment, pure feedback stabilization of unstable tokamaks has been demonstrated for the pressure driven RWM in NSTX reported by Sabbagh [90] and positively identified for the current driven RWM in DIII-D. Detailed identification of plasma response at high β_T to different feedback components durring various feedback shemes remain unlcear. Part of the difficulty is the existence of other modes in the high β tokamak. Due to the low rotation threshold for the RWM found in section 2, it is possible that the rotation could be maintained through the neoclassical toroidal viscosity induced by a non-resonant error field. In this case, direct feedback stabilization of the RWM is not needed. However, the RWM can be destabilized through its coupling to other MHD instabilities (section 5.2). Feedback stabilization is still needed for other instabilities and is also needed to prevent the destabilization of the RWM by these instabilities. What has been learned up to now can readily be applied to the feedback stabilization of other instabilities that couple strongly to a nearby resistive wall. Some of these candidates could be the neoclassical tearing mode or other very low n modes with a substantial edge component in ITER.

5. RWM in ITER, Future Tokamaks, Stellerators and RFPs

5.1. ITER

An important goal of ITER [1] is to demonstrate steady-state-compatible operation at moderate fusion gain with $Q_{DT} = 5 - 10$. Operation in "steady-state" regimes in ITER entails operation at high normalized pressure ($\beta_N \sim 3$). It was predicted that β_N is less than the no-wall limit for steady state with $Q_{DT} = 5$, but for $Q_{DT} = 10$, it is possible that the RWM could be destabilized. A typical representative ITER steady-state scenario was given by Polevoi [161] as Scenario 4. In this scenario, the plasma current is 9 MA, with major radius $R = 6.35\,\mathrm{m}$, minor radius $a = 1.85\,\mathrm{m}$, elongation at the separatrix $E = 1.97$, triangularity $\delta = 0.58$, with normalized plasma β or $\beta_N = 2.57$ and internal self-inductance $l_i = 0.63$. The rotation profile was computed using the ASTRA transport code [161].

Since the base design of ITER was not in the advanced tokamak regime, the RWM control issue is regarded as an issue of secondary importance to the control of the ELMs. However, as explained in the previous section, dynamic error field correction is still an unavoidable issue. A model of the 3D representation of the preliminary design resistive wall structure for ITER is shown in figure 49(a) [162]. The pattern of the eddy current produced by the RWM on the 3D resistive vessel is shown in figure 49(b) [162].

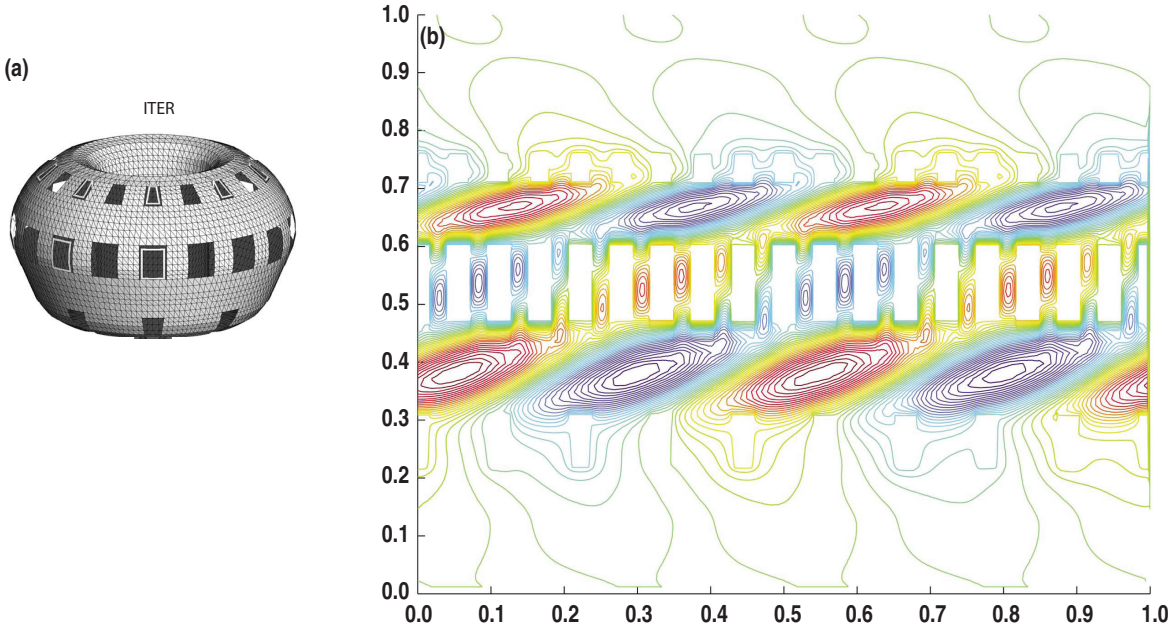

FIG. 49. (a) 3D representation of the preliminary design resistive wall structure for ITER. (b) Contour plot of the current potential (Φ) on the ITER wall produced by RWMs. The eddy current $\vec{j}$ is given by $\vec{j} = \vec{n} \times \vec{\nabla}\Phi$, and $\vec{n}$ is the exterior normal. The vertical and horizontal axes of the flat projections of the walls indicate the poloidal and toroidal directions, respectively (reference [162]). [Reprinted courtesy of AIP, Phys. Plasmas **15**, 056110 (2008).]

The in-vessel coils [139] for ELM control (figure 50) are proposed to be used for RWM and error field control.

Comparison of the performance of the coil configurations using the VALEN-3D [146] code with a single-mode shows superior performance when all three toroidal rows of coils are used (stabilized at $\beta_N = 3.74$) compared with midplane coils (stabilized $\beta_N = 3.39$). The use of just the top and bottom row of coils enables stabilization at $\beta_N = 3.63$. The required current for RWM control appears to be modest compared with the ELM control requirements.

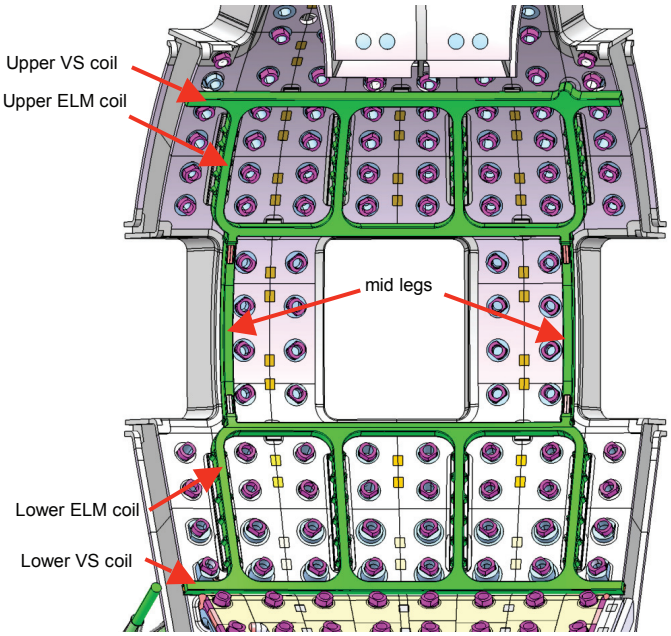

FIG. 50. Proposed design of in-vessel coils for vertical stabilization and ELM control in ITER. The ELM control windings can also be used for resistive wall stabilization (reference [139]). [Reprinted courtesy of IAEA, Proceedings of 22nd IAEA Fusion Energy Conference, Geneva, Switzerland (IAEA, Vienna, 2008) Paper IT/1-2, http://www-pub.iaea.org/MTCD/Meetings/fec2008pp.asp.]

Using the rotation profile predicted by Polevoi for ITER in advanced tokamak operation, the rotational stabilization of the RWM was studied. The results are shown in figure 51. Shown is the real part of the RWM eigenvalue for the ITER advanced tokamak plasmas as a function of C_β and plasma rotation frequency ω_0, predicted by the self-consistent kinetic calculations. Only precessional resonance damping is included. The black dots indicate stable RWMs with practically vanishing growth rates.

5.2. Future RWM issues for existing tokamaks — coupling of RWM to other instabilities

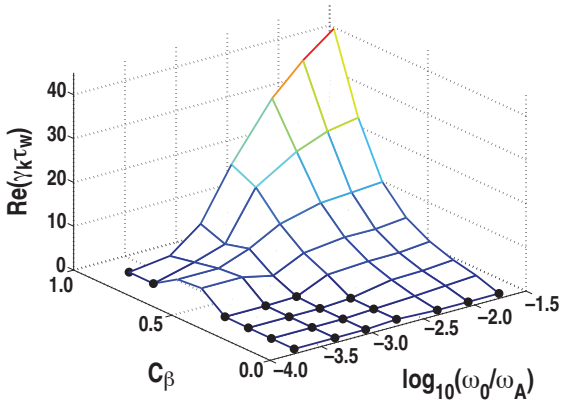

FIG. 51. Rotational stabilization of the RWM in ITER operated in the advanced tokamak regime computed by using the MARS-F code (reference [163]). [Reprinted courtesy of IAEA, Proceedings of 22nd IAEA Fusion Energy Conference, Geneva, Switzerland (IAEA, Vienna, 2008) Paper TH/P9-26, http://www-pub.iaea.org/MTCD/Meetings/fec2008pp.asp.]

Although the critical plasma rotation in low rotation tokamaks was found to be significantly lower [100, 101, 102, 164] than theoretically predicted by Bondeson [31], stable steady-state operation in this low rotation regime is not unconditionally guaranteed. That is, despite the simultaneous operation of slow dynamic error field correction and fast feedback suppression, the ELM-triggered RWM [159] at high normalized β has been observed. Thus, issues remain on how to stabilize the tokamak in this low rotation regime. Various MHD events occur in high β_N discharges, producing a wide spectra of toroidal and poloidal magnetic field patterns. These modes such as ELMs and fishbone-like bursting mode [159, 165] (the fishbone is an internal kink instability of the plasma destabilized by energetic particles), begin to couple to the RWM branch near the no-wall stability limit. When the RWM stability condition becomes marginal at high β and low rotation, these modes can couple directly or indirectly with the RWM pattern, leading to a rapid, forced excitation of RWM on the time scale of the driving MHD event (MHD-driven RWM). A similar possible interaction of the ideal mode with the tearing mode was noted previously. Brennan proposed that exceeding the stability of an ideal mode leads to the excitation of the tearing mode [166]. Quite often, the MHD-driven RWM amplitude can be relatively large, however, the mode itself can remain in a marginally-stable regime. On the other hand, this MHD-driven RWM decays very slowly over tens of milliseconds, potentially leading to a β_N collapse. Feedback is useful to quench the mode amplitude before any serious impact takes place.

On JT60-U, the dynamics and stability of the RWM in high β plasmas was studied in detail [165, 167]. To suppress an $n = 1$ RWM that limits the achievable β_N in the regime $\beta_N \geq \beta_N^{no-wall}$, the plasma rotation is kept larger than the critical rotation. $\beta_N \sim 3.0$ has been sustained for $\sim$1 s; $\beta_N \sim 2.8$ for $\sim$5 s. In the high β_N regime, the MHD instabilities related to the RWM, i.e. an $n = 1$ bursting mode and a slowly growing

mode, have been observed. These modes sometimes induced plasma rotation damping and triggered the RWM. It was conjectured that the bursting mode could be related to the presence of energetic particles. In detailed analysis, it was found that the slowly growing mode can reduce the rotational shear around the $q = 2$ surface and finally trigger the RWM. These results show the rotational shear at the rational surface is also important in determining the plasma stability as well as the plasma rotation speed. Moreover, plasma rotation braking owing to the RWM was observed. It was found that the RWM distortion can clearly induce the plasma rotation braking inside the $q = 2$ surface. The details of these developments are shown in figure 52. Waveforms of the discharge with a slowly growing mode are shown in: (a) temporal evolution of β_N and $d\beta_N/dt$, (b) $n = 1$ magnetic perturbations detected by saddle loops and (c) D_α emission, (d) q, and (e) toroidal rotation profiles with the precursor frequency (reference [165]).

A similar detailed sequence of events were also obtained on the DIII-D tokamak [80]. The effect of energetic particles has also been shown by MARS-K to be stabilizing for the RWM. However, new instabilities could also be excited [168].

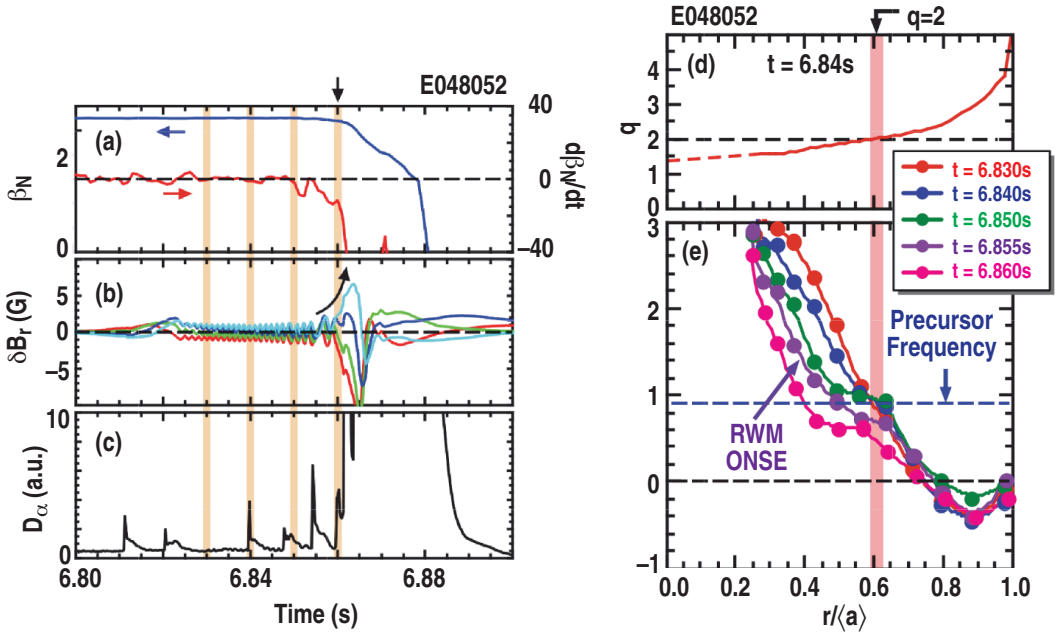

FIG. 52. Waveforms of discharge with a slowly growing mode in JT-60U: (a) temporal evolution of β_N and $d\beta_N/dt$, (b) $n = 1$ magnetic perturbation measured by saddle loops and (c) D_α emission (d) q and (e) toroidal rotation profiles with the precursor frequency (reference [165]). [Reprinted courtesy of IAEA, Proceedings of 22nd IAEA Fusion Energy Conference, Geneva, Switzerland (IAEA, Vienna, 2008) Paper EX/5-2, http://www-pub.iaea.org/MTCD/Meetings/fec2008pp.asp.]

On NSTX, the dynamics and stability of the RWM in high β_N plasmas (some cases with $\beta_N > 7$ was studied by Sabbagh et al. [77, 88, 90]. Similar interaction with other MHD modes was apparent, including the transformation of the RWM into a saturated internal kink during active feedback control, with the eventual observation of an NTM at the $q = 2$ surface, and the damping of both modes [77]. RWM non-rigidity was reported at high β_N during $n = 1$ feedback [90]. Fishbone-like modes appear at β_N over the no-wall ideal β limit, but do not always coincide with RWM destabilization. Recent research pointed out that the energetic particles provide key components to determine the rotation frequency of the RWM in NSTX [169].

Therefore, the coupling with other instabilities, including ELMs, the $q = 2$ fishbone, the collapse of the rotational shear and rotation profiles in the low rotation regime, and effect of energetic particles are the main research topics for the tokamaks in the near future.

5.3. KSTAR and coil geometry designed to satisfy multiple feedback functions

The Korea Superconducting Tokamak Advanced Research (KSTAR) with $R/a = 1.8\,\mathrm{m}/0.5\,\mathrm{m}$ [170, 171], is designed to develop a steady-state-capable advanced superconducting tokamak. As shown in section 3.1 all future reactor-oriented devices have to implement dynamic error field correction to ensure stable operation. One of the design issues is, therefore, the coil geometry which produces the non-axisymmetric field for dynamic error field correction. Similarly, we have to design and construct the additional coils for RWM control. The coils for these two functions have to satisfy various practical engineering constraints. This could be an issue especially when the available space for coil installation is limited. The requirements for RWM suppression are also different whether the device was aimed at a proto-reactor-type of operation with moderate β_N or for pursuing fundamental advanced tokamak physics research with higher β_N.

One of the choices is the approach of multi-purpose segmented non-axisymmetric coils, which should, in principle, be the most practical and economical. These segmented coils carry out simultaneously several functions. As long as the $n = 0$ and $n = 1$ modes remain rigid and mutually decoupled, a compact design can be made. KSTAR serves as an important example of this design philosophy. This is in contrast to the approach of using separate coils for dynamic error field correction and direct feedback proposed in FIRE [172] and JT60-SA.

In KSTAR, the non-axisymmetric coils are arranged with an extreme goal of "multiple-purpose" design. The single coil system carries out the functions of vertical $n = 0$ positional control, plasma radial control, $n = 1$ RWM and error field correction. In addition, passive stabilizing plates are located above and below the midplane.

The four quadrant segmented coils are shown in figure 53. Advantages of multi-purpose coils are: (a) reducing total coil Ampere-turns, (b) simplification of coil installation and maintenance, and (c) capability of helical magnetic perturbation. Potential disadvantages are: (a) complex control system, (b) burden to the power supply for handling the frequency range from lower frequency of change in equilibrium to the higher frequency needed for unstable RWM feedback control. According to a cylindrical model [173], although the coils are located only in quadrants, the wide poloidal coverage allows the possibility of both $n = 1$ and $n = 2$ RWM control at high β_T.

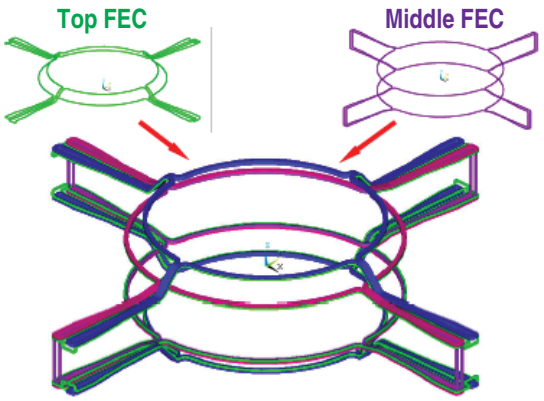

FIG. 53. The multiple feedback function design of the FEC feedback coils in KSTAR. The top and middle coils are also shown (references [170, 171]).

The computed stable operating space of KSTAR, including the performance of RWM stabilization by the in-vessel control coils(IVCC) and passive stabilizing plates is examined by Katsuro-Hopkins [174]. It is shown that the $n = 1$ no-wall limit can be exceeded by a factor of 2 with passive RWM stabilization, and VALEN code calculations show that the midplane IVCC coil can stabilize the plasma at β close to the ideal with-wall stability limit.

5.4. JT60-SA and high μ conducting wall

The design of JT60-SA (upgrade of JT-60U) is an example of reactor-study in which the design is carried out for stabilization of the RWM with both rotational stabilization and feedback stabilization. The feedback of the RWM with relatively fast ($\gamma_{open}\tau_w \geq 1$) growth rates is pursued with internal coils within the environment of low radio-activation ferritic material (with high μ), a most promising candidate for wall material for a DEMO reactor. The specific contribution of this study is the impact of high μ metal on the stability of the RWM.

The critical β_T is found to decrease ~10% by the application of the ferromagnetic effect with $\mu/\mu_0 \sim 2$. (μ and μ_0 are the permeabilities of the ferromagnetic wall and vacuum, respectively.) The stability window [31] exists for the standard aspect ratio tokamak even with high permeability, but does disappear for high aspect ratio tokamaks.

In particular, the stability of the RWM is studied for a wall with a thickness of $0.05a$ and $\mu/\mu_0 = 2$, and assuming that the ferritic material is sufficiently saturated. First, even without considering the effect of the resistivity of the external wall, the effect of the ferromagnetic wall is to reduce the critical β_T to around ~90% from the standard non-ferritic metallic wall. This is due to the concentration of the perturbation flux in the wall through the ferromagnetic effect. Second, the increase in permeability of the resistive wall decouples the ideal XK from the flux diffusion of the resistive wall. As shown in section 2.3.2, rotational stabilization results from the coupling of these two branches by the effects of toroidal plasma rotation and ion sound wave damping through the toroidal effect. It is therefore reasonable to observe that the maximum rotation frequency needed to stabilize the RWM tends to increase due to the increase in size of the unstable region with increasing relative permeability of the wall. It is also found that the rotation frequency of the unstable RWM becomes an increasing function of the wall radius, which has a different tendency from the case without additional permeability [175, 176].

The effect of relative permeability on the stability window that was opened by the effects of toroidal plasma rotation and sound wave damping term is shown in figure 54. The growth rates for plasma rotation with $V = 0.5V_{pA}$ (V_{pA} being the poloidal Alfvén velocity) are shown with closed symbols. The dotted region in the figure denotes the unstable region of ideal kink mode. The stability window is opened for $V \geq 0.5V_{pA}$. Note that the curve of the growth rates crosses zero in the ideal kink unstable region for $V = 0.4V_{pA}$. Increments of mode rotation frequency shown by open symbols in the figure and reduction of the width of stability window tend to become larger for higher values of relative permeability as seen in the case of $\mu = 5\mu_0$. It was found that the maximum rotation frequency in the RWM unstable region tends to increase as the unstable region is enlarged with increasing relative permeability. It was suggested from the analysis that more careful phase control would be required for active feedback control of the RWM with a ferromagnetic wall.

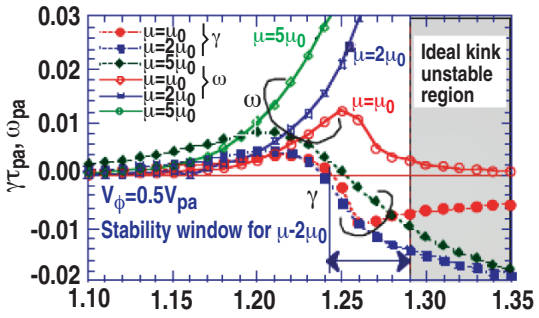

FIG. 54. Growth rate and mode frequency for the designed JT60-SA as a function of the normalized wall radius for three relative permeabilities where the toroidal rotation velocity is 0.5 times poloidal Alfvén velocity (references [177, 178]). [Reprinted courtesy of IAEA, Proceedings of 22nd IAEA Fusion Energy Conference, Geneva, Switzerland (IAEA, Vienna, 2008) Paper FT/P7-7, http://www-pub.iaea.org/MTCD/Meetings/fec2008pp.asp.]

The VALEN code [146] was used to study the effect of passive stabilizer plates together with internal feedback coils using the coil geometry in JT60-SA. The VALEN code showed that with the stabilizing plate and the vacuum vessel geometry with finite resistivity, the passive plate provided most of the stabilization and the effect of the resistivity in the vacuum vessel wall was relatively minor. The active feedback control of coils on the back of the stabilizing plate increased the maximum normalized β_T value to 3.8 from 2.8.

The effect of inserting ferromagnetic material on the resistive wall for the purpose of compensating the inherent error fields has also been tested experimentally with success [179]. In this case, higher β_N was achieved experimentally, presumably due to the reduction of the error field and was not due to the effect of ferromagnetic material on the RWM.

5.5. Stellerator.

In magnetic fusion research, helical systems (stellerators) have made steady progress in the past two decades. The plasma parameters obtained in helical devices have become comparable to those of tokamaks. Results from the large helical device — LHD [180] showed prospective plasma qualities close to those of large tokamaks. Configuration design studies of helical systems have also been proposed as a possible improvement to the tokamak — owing to the great freedom in the geometry of 3D helical system structures. In such new configurations, the primary objective is to improve neoclassical transport by reducing orbit losses of helical ripple trapped particles and to explore more compact high β_T configurations. The concept of the quasi-axisymmetric stellerator, which has a magnetic field structure with tokamak-like symmetry [181, 182] is one of these new proposals.

A low aspect ratio stellerator CHS-qa has been designed on the basis of such a quasi-axisymmetric concept [183, 184, 185]. The flux surfaces and rotational transform and pressure profiles are shown in figure 55(a) and 55(b). As well as good neoclassical transport characteristics, MHD stability for high β_T equilibrium is very important in making the new concept promising for fusion reactors.

Due to the fact that substantial currents are present in these quasi-symmetric stellerators such as CHS-qa, they are still unstable to the XK mode. The stability of the RWM has been studied by Merkel *et al.* [152]. The growth rate as a function of wall resistivity is shown in figure 55(c). They found that the XK can be stabilized by a perfectly conducting ($\sigma = \infty$) closed wall at $b/a = 1.3$. For a wall with $\sigma \neq \infty$, one gets a RWM. The structure of the most unstable mode changes with decreasing

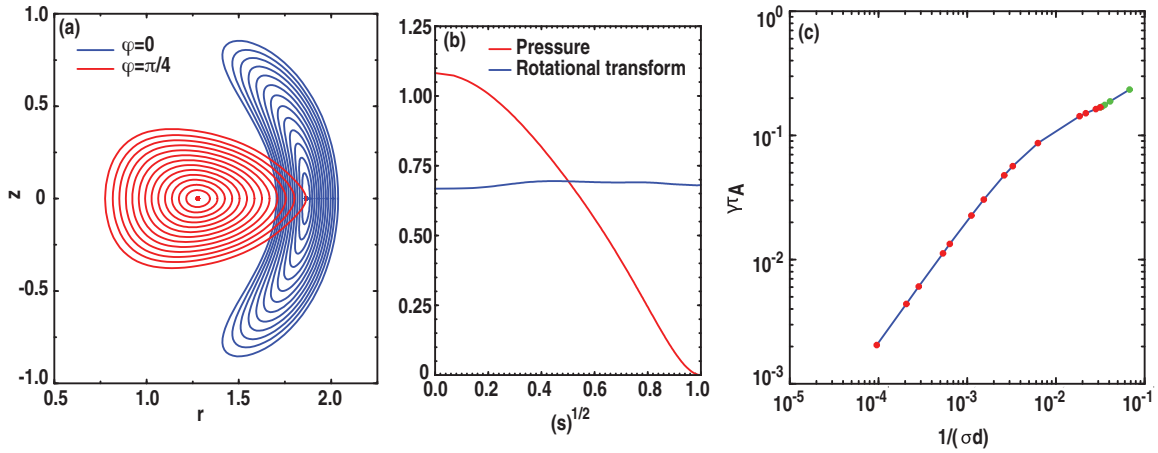

FIG. 55. Flux surfaces (a), rotational transform (b), pressure (b) of a quasi-axisymmetric equilibrium with $\langle\beta\rangle = 0.013$, $B_0 = 0.9$ T, current $I = 280$ kA. (c) Growth rates of a RWM for the quasi-axisymmetric equilibrium in CHS-qa(reference [152]). [Reprinted courtesy of Proceedings of 31st EPS Conference on Controlled Fusion and Plasma Physics, London, United Kingdom, ECA Vol. 28G (EPS, Petit-Lancy, 2001) Paper P1.208, http://epsppd.epfl.ch/London/html/mindex.htm.]

resistivity. For high resistivity, the $(m, n) = (2, 1)$ harmonic with even parity dominates; for low resistivity the $(m, n) = (5, 3)$ harmonic with odd parity dominates. Except the STARWALL [152], most the 3D MHD stability codes do not have a resistive wall. In 2005, Chu and Ichiguchi [186] proposed a method of computing the growth rates of the RWMs in 3D configurations by utilizing results from ideal stability codes to estimate the dissipation in the resistive wall. These studies are still in their infancy but it is possible that RWM control will be required to achieve high β_T in stellerators, assuming transport losses are not too high.

5.6. RFP.

The RFP is a confinement system formed by the self-organization of a large toroidal current. It relies on an external conducting wall to maintain plasma stability with respect to the external and (internal) kink modes. Therefore, the subject of stabilization of the RWM is of particular importance for RFP. An early important paper on this subject was given by Gimblett [15].

The main RWMs in the RFP are intrinsic, non-resonant, current-driven kink modes that are largely unaffected by sub-Alfvénic plasma rotation [187]. RWMs have been observed in the previous decades [16, 188]. More recently, RWMs are studied in EXTRAP-T2R [189, 190, 191, 192] and in RFX-mod [151, 193, 194, 195]. More description on the details of results from the EXTRAP-T2R are also given in the works of reference [196] on the effect of magnetic sideband on control, [197] on the open loop and RFA experiments and modeling, and [198] on advance control. The feedback coil system used in these experiments is shown in figure 56. Note the similarity of the actual configuration of the coils in comparison to the smart shell proposed by Bishop [32] and shown in figure 7(b).

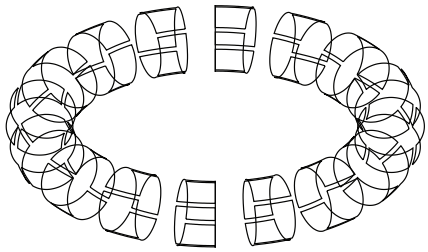

FIG. 56. Schematic drawing of the active coil layout on the torus of EXTRAP-T2R showing the 16 toroidal positions with four saddle coils, each coil spanning $\theta = 90\,\mathrm{deg}$ poloidally and $\phi = 11.25\,\mathrm{deg}$ toroidally (reference [189]). This should be compared with that shown in figure 7(b) conceptualized by Bishop. [Reprinted courtesy of APS, Phys. Rev. Lett. **93**, 225001 (2004).]

In EXTRAP-T2R, active feedback stabilization of multiple independent RWMs is experimentally demonstrated in a reversed field pinch plasma. The operating ansatz for feedback, incorporating a thin wall, used to stabilize RWM growth is the same for the tokamak and RFP. However, since the RFP differs from the tokamak in that the poloidal and toroidal magnetic fields are of the same order of magnitude, the RFP has a different RWM spectrum and, in general, a range of modes are always unstable. Therefore, the requirement of simultaneous feedback stabilization of multiple independent RWMs arise for the RFP configuration.

Simultaneous feedback stabilization of multiple modes was studied and demonstrated in EXTRAP-T2R and shown in the left of figure 57. It reduced the coupling of unstable modes through the "sideband" harmonics generated by the feedback coils. The reduction of RWM amplitudes lead to a delay in the braking of the plasma rotation. This is measured by the tearing mode rotation, resulting in a significant prolongation of the discharge pulse. A reproducible simultaneous suppression of several nonresonant RWMs is achieved. Coupling of the different modes due to the limited number of the feedback coils is observed, in agreement with theory [196].

The feedback scheme of wise-shell in which a selected number of modes are feedback on, instead of the intelligent shell [32] has been employed. It is found that the wise-shell scheme is superior. The error field amplification has been observed which enhanced magnetic diffusion. The enhancement has been found to agree with the theory of Pustovitov [199] and is shown on the right of figure 57.

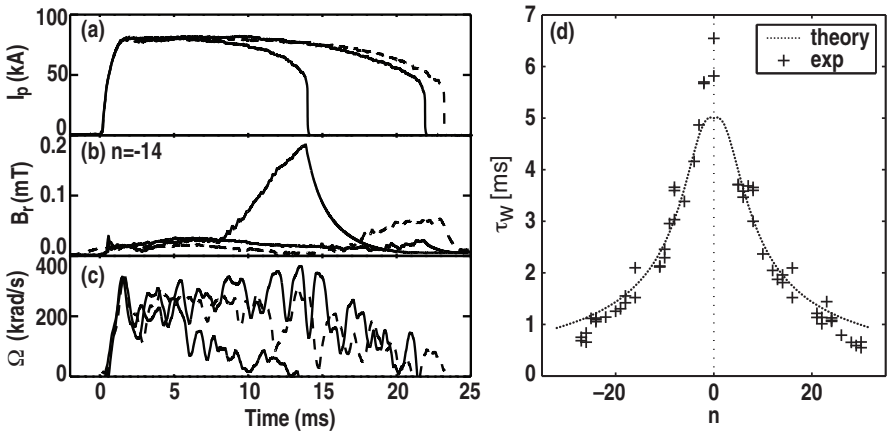

FIG. 57. Flux surfaces (a), rotational transform (b), pressure (b) of a quasi-axisymmetric equilibrium with $\langle\beta\rangle = 0.013$, $B_0 = 0.9$ T, current $I = 280$ kA. (c) Growth rates of a RWM for the quasi-axisymmetric equilibrium in CHS-qa(reference [152]). [Reprinted courtesy of Proceedings of 31st EPS Conference on Controlled Fusion and Plasma Physics, London, United Kingdom, ECA Vol. 28G (EPS, Petit-Lancy, 2001) Paper P1.208, http://epsppd.epfl.ch/London/html/mindex.htm.]

The largest RFP device, RFX-mod ($R = 2\,\mathrm{m}$, minor radius $a = 0.46\,\mathrm{m}$, maximum current 1.78 MA) is equipped with a special feedback system. It has 48 (toroidal direction) x 4 (poloidal direction) = 196 coils and the same number of sensors, with every coil being independently controlled. The coil and sensor system covers completely the external plasma boundary. The coil system can generate magnetic field harmonics with poloidal mode numbers m range from -2 to 2, and toroidal mode number ranges from 0 to 24. This system can stabilize all harmonics of the RWM at the same time, or can selectively stabilize some of the harmonics while leaving the others growing in specific time intervals [193, 194].

In RFX-mod, it is possible to make the perturbed B_r equal to zero at the plasma boundary for multiple harmonics. This control system can therefore not only stabilize the RWM but also the tearing mode (dynamo mode) and simulate an ideal wall near the plasma boundary. This is an additional but important purpose of the feedback system [151]. Therefore it largely reduces the plasma-wall interaction and results in a significant prolongation of the discharge. The direct coupling between the tearing mode and the RWM has not yet been observed.

It has been demonstrated that a complex proportional gain can be used to rotate a selected RWM in a given direction. Reversing the phase of feedback rotates the RWM in the opposite direction. This is shown in figure 58 [195].

Through the development of a new control algorithm, named clean mode control (CMC), the control of the effects of the $m = 1$ resistive-kink and tearing modes (TMs) on the reversed field pinch RFX-mod has significantly improved, compared to the previous virtual shell (VS) operations. The CMC algorithm is based on the real-time removal of a systematic error affecting magnetic measurements due to the aliasing of the sideband harmonics produced by the active coils. CMC brings several advantages over VS: the non-axisymmetric deformation of the last closed magnetic surface decreases; wall unlocking of TMs is systematically obtained; TM phase locking is weakened, the plasma wall interaction pattern moves during each discharge and it is more uniformly toroidally distributed, assuming a helical pattern [151]. It is noted that due to this new control algorithm, control of not only the RWM, but also the tearing (dynamo) modes becomes feasible [200].

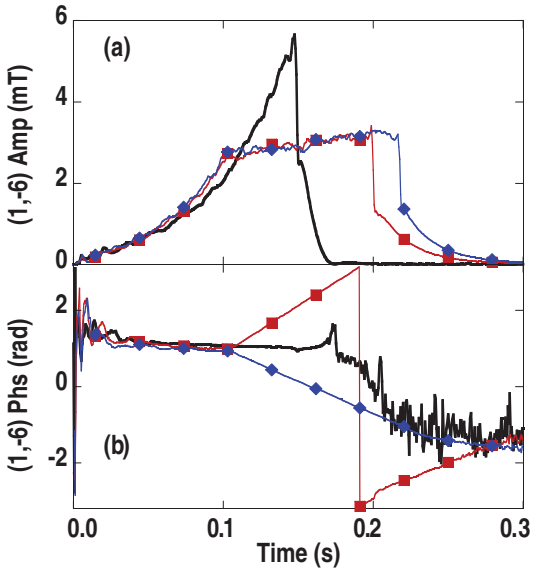

FIG. 58. Effect of a complex proportional gain on RFX-mod: (a) mode amplitudes (b) mode phases. Black full traces represent a reference shot where (1,-6) RWM is free to grow up to 0.13 s and then is fully controlled. Squares and diamonds traces show the effect of the application of complex proportional gains: the rotation of a selected RWM can be induced in both opposite directions (feedback in action from 0.1 s) [195]. [Reprinted courtesy of APS, Phys. Rev. Lett. **101**, 195005 (2008).]

6. Summary and Discussion

In this work, we presented a brief review on the development and progress in the stabilization of the XK and RWM. In the last two and half decade, especially towards the latter part of this period, there has been tremendous progress in this area, not only in experiment and theory but also in modeling and technology.

For tokamaks, the stabilizing effect of the external resistive wall can be made effective not only transiently, as in the 1980s, but also at quasi-steady state. This situation was brought about by slowing down the rotation of the plasma, lengthening the time scale of the instability, that allowed us to utilize the precessing motion of the trapped particles. During the course of this understanding, many theories have been developed and compared with experimental findings. Maintaining plasma rotational torque balance has been found to be particularly important in allowing the plasma to evolve stably toward the marginal stability of the RWM. The rotational equilibrium could be spoiled by minute error fields which induce resonant response from the plasma which slows the plasma down. Portions of the general behavior of plasma during this evolution path can be described by simple analytic models when these models are constructed judiciously. But it is not clear that a completely analytic approach can model all aspects of this development.

A number of computer codes have been built to allow us to very closely model the behavior of the plasma during the development of the RWM. These codes include the detailed dynamics of the particles and their interaction with the electromagnetic perturbations. Thus, the theoretical description of the interaction between the plasma and the perturbing electromagnetic field has gone beyond the fluid theory. In particular, the plasma flow and dissipation described by the usual fluid theory is not expected to be sufficient. MHD plus kinetic or full kinetic description of the plasma is desirable. These codes are also expected to model the detailed three-dimensional structure of the external conducting or feedback structures. Further development of these codes will give us even more comprehensive capabilities for the modeling of the RWMs for future devices.

However, the stabilization effect that has been demonstrated experimentally has not been found to be robust. This is mainly because near the beta limit, the tokamak can also develop other instabilities. These instabilities can excite the RWM. To turn the stabilization effects found up to now into robust, reproducible tools for the everyday operation of the tokamak should be the next area of research on the RWM for the tokamak.

The RWM is a very important research topic for the RFP. Recent advances in RFP experiments showed that it is an ideal test bed for developing and implementing advanced control strategies for the RWM. In fact, given the negligible effect of plasma rotation on the stability of the RWM, the action of a set of active control coils activated by a digital controller is the only viable approach to suppress growth of the RWM. Modern RFP experiments are provided with extensive sensor arrays allowing detailed description of the magnetic boundary condition for the control of RWM. This proved to be very useful for benchmarking complex numerical codes against experimental data for 3-D effects on stability of the RWM [201]. This would be useful for both the tokamak and RFP configurations. Much of the results indicate that fluid theory still holds valid for RFP plasmas. Fluid theory uses phenomenological transport (dissipation) coefficients. These coefficients need to be derived from first principle theories for the RFP plasmas to make the results scalable with respect to various global parameters. With the advent of a new device and new feedback hardware, much progress is expected in the near future.

We thus come to an interesting situation where reliable fluid theoretical models allow us detailed study of the feedback stabilization of the RFP where complicated feedback schemes have been tried and proven successful. Whereas in tokamaks, advanced plasma conditions allow us probe the kinetic behavior of plasma at very low frequency. It is expected that in the final plasma condition approaching to the fusion reactor, both advanced plasma conditions and advanced feedback are needed. It should be our goal to integrate these results and apply them to future fusion devices, such as KSTAR, JT60-SA, ITER,..., etc.

References

[1] ITER Overview and Summary Nucl. Fusion **39**, 2137 (1999)

[2] Strait E. J., Phys. Plasmas **1**, 1415 (1994)

[3] Hender T. C., Wesley J. C., Bialek J., Bondeson A., Boozer A. H., Buttery R. J., Garofalo A., Goodman T. P., Granetz R. S., Gribov Y., Gruber O., Gryaznevich M., Giruzzi G., Gunter S., Hayashi N., Helander P., Hegna C. C., Howell D. F., Humphreys D. A., Huysmans G. T. A., Hyatt A. W., Isayama A., Jardin S. C., Kawano Y., Kellman A., Kessel C., Koslowski H. R., LaHaye R. J., Lazzaro E., Liu Y. Q., Lukash V., Manickam J., Medvedev S., Mertens V., Mirnov S. V., Nakamura Y., Navratil G., Okabayashi M., Ozeki T., Pacagnella R., Pautasso G., Porcelli F., Pustovitov, V. D., Riccardo V., Sato M., Sauter O., Schaffer M. J., Shimada M., Sonato P., Strait E. J., Sugihara M., Takechi M., Turnbull A. D., Westerhof E., Whyte D. G., Yoshino R., Zohm H. and the ITPA MHD, Disruption and Magnetic Control Topical Group, Nucl. Fusion **47**, S128 (2007)

[4] Strait E. J., Lao L. L., Taylor T. S., Chu M. S., Lee J. K., Turnbull A. D., Allen S. L., Brooks N. H., Burrell K. H., Callis R. W., Carlstrom T. N., Chance M. S., Colleraine A. P., Content D., DeBoo J. C., Ferron J., Greene J. M., Groebner R. J., Heidbrink W. W., Helton F. J., Hill D. N., Hong R.-M., Hosogane N., Howl W., Hsieh C. L., Jackson G. L., Jahns G. L., Kellman A. G., Kim J., Kinoshita S., Lazarus E. A., Lomas P., Luxon J. L., Mahdavi M. A., Neyatani Y., Ohkawa T., Osborne T. H., Overskei D. O., Ozeki T., Perry M., Petersen P. I., Petrie T. W., Phillips J. C., Porter G. D., Schissel D. P., Scoville J. T., Seraydarian R. P., Shimada M., Simonen T., Snider R. T., Stambaugh R. D., Stav R. D., St. John H., Stockdale R. E., Stroth U., and Wood R., Plasma Physics and Controlled Fusion Research 1988, Vol. 1 (International Atomic Agency, Vienna, 1989), p. 83 (1989)

[5] Bernstein I. B., Frieman E. A., Kruskal M. D., and Kulsrud R. M., Proc. R. Soc. London **A244**, 17 (1958)

[6] Shafranov V. D., Sov. Phys.-Tech. **15**, 175 (1970).

[7] Frieman E. A., Greene J. M., Johnson J. L. Weimer K. E., Phys. Fluids **16**, 1108 (1973)

[8] Gruber R., Troyon F., Berger D., Bernard L. C., Rousset S., Schreiber R., Kerner W., Schneider W., and Roberts K., Comp. Phys. Comm. **21**, 323 (1981)

[9] Grimm R. C., Dewar R. C., and Manickam J., J. Comput. Phys. **49**, 94 (1983)

[10] Bernard L. C., Helton F. J., Moore R. W., Comput. Phys. Comm. **24**, 377 (1981)

[11] Degtyarev L., Martynov A., Medvedev S., Troyon F., Villard L., and Gruber R., Comput. Phys. Comm. **103**, 10 (1997)

[12] Troyon F., Gruber R., Saurenmann H., Semenzato S., and Succi S., Plasma Phys. Control. Fusion **26**, 209 (1984)

[13] Pfirsch D. and Tasso H., Nucl. Fusion **11**, 259 (1971)

[14] Freidberg J. P., *Ideal Magnetohydrodynamics* (New York: Plenum) p .309 (1987)

[15] Gimblett C. G., Nucl. Fusion **26**, 617 (1986)

[16] Alper B., Bevir M., Bodin H. A. B., Bunting C. A., Carolan P. G., Cunnane J., Evans D. E., Gimblett C. G.,Hayden R. J., Hender T. C., Lazaros A., Moses K. W., Newton A. A., Noonan P. G., Paccagnella R., Patel A., Tsui H. Y. W. and Wilcock P. D., Plasma Physics Controlled Fusion **31** 205 (1989)

[17] Gimblett C. G., Plasma Physics Controlled Fusion **31** 2183 (1989)

[18] Stambaugh R. D., Moore R. W., Bernard L. C., Kellman A. G., Strait E.J., Lao L. L., Overskei D. O., Angel T., Armentrout C. J., Baur J. F., Blau F. F., Bramson G., Brooks N. H., Burrell K. H., Callis R. W., Chase R. P., Colleraine A. P., Cottrell G., Deboo J. C., Ejima S., Fairbanks E. S., Fasolo J., Fox C. H., Gilleland J. R., Groebner R. J., Helton F. J., Hong R. M., Hsieh C. L., Jahns G. L., Kahn C. L., Kim J., Knowles D., Lee J. K., Lee P., Lieber A. J., Lohr J. M., McColl D. B., Meyer C. H., Newman D. E., Ohkawa T., Ohyabu N., Petersen P. I., Petrie T. W., Pfeiffer W. W., Phillips J. C., Rottler L. C., Schissel D. P., Scoville J. T., Seraydarian R. P., Sleaford R. W., Smith J. F., Snider R. T., Stav R. D., St. John H., Stockdale R. E., Tooker J. F., Vaslow D., Wesley J. C., Wojtowicz S. S., Wong S. K. and Zawadski E. W., Plasma Physics and Controlled Fusion Research 1984, Vol. 1 (IAEA, Vienna, 1985) p. 217

[19] Okabayashi M., Bol K., Chance M., Couture P., Fishman H., Fonck R. J., Gammel G., Heidbrink W. W., Ida K., Jaehnig K. P., Jahns G., Kaita R., Kaye S. M., Kugel H., LeBlanc B., Manickam J., Morris W., Navratil G. A., Ohyabu N., Paul S., Powell E., Reusch M., Sesnic S., and Takahashi H., Plasma Physics and Controlled Fusion Research 1986, Vol. 1 (IAEA , Vienna, 1987) p. 275

[20] Huysmans G. T. A., Hender T. C., Alper B., *et al.*, Nucl. Fusion **39**, 1489 (1999).

[21] Nave M. F. F., Smeulders P, Hender T. C., Lomas P. J., Alper B., Bak P., Balet B.,Christensen J. P., Clement S., de Esch H. P. L., Hawkes N., Huysmans G. T. A., Jones T. T. C., Konig R., Lawson K., Lingertat L., Maas A., Obrien D. P., Rookes A., Sartori R., Stamp M. F., Schunke B., Thomas P. R., Thomsen K., Nucl. Fusion **37**, 809 (1997).

[22] Ishida S., Takeji S., Isayama A., Isei N., Ishii Y., Ozeki T., Fujita T., Kamada Y., and Neyatani Y., Control. Fusion and Plasma Physics **21A**, 489 (1997).

[23] Tsunematsu T., Takeda T., Matsuura T., Kurita G., and Azumi M., Comput. Phys. Comm. **19**, 179 (1980)

[24] Turnbull A. D., Brennan D. P., Chu M. S., Lao L. L., Snyder P. B., Fusion Sci. and Technol. **48**, 875 (2005)

[25] Okabayashi M., Fredrickson E. D., Manickam J., Taylor G., Batha S. H., Bell M. G., Budny R. V., LeBlanc B., Levinton F. M., Jackson J., McGuire K. M., Nazikian R., Zarnstorff M. C., Nucl. Fusion **38**, 1149 (1998)

[26] Jahns G. L., Chance M. S., Kaye S. M., Manickam J., Takahashi H., LeBlanc B., Morris A. W., Reuch M., Sesnic S., Nucl. Fusion **28**, 881 (1988)

[27] Callen J. D., Hegna C. C., Rice B. W., Strait E. J., Turnbull A. D., Phys. Plasmas **6**, 2963 (1999)

[28] Zarnstorff M. C., Bell M. G., Bitter M., Goldston R. J., Grek B., Hawryluk R. J., Hill K., Johnson D., McCune D., Park H., Ramsey A., Taylor G. and Wieland W., Phys. Rev. Lett. **60**, 1306 (1988).

[29] Kessel C., Manickam J., Rewolt G., and Tang W. M., Phys. Rev. Lett. **72**, 1212 (1994)

[30] Turnbull A. D., Taylor T. S., Lin-Liu Y. R., and St. John H., Phys. Rev. Lett. **74**, 718 (1995)

[31] Bondeson A. and Ward D. J., Phys. Rev Lett. **72**, 2709 (1994)

[32] Bishop C. M., Plasma Phys. Control. Fusion **31**, 1179 (1989)

[33] Betti R. and Freidberg J. F., Phys. Rev. Lett. **74**, 2949 (1995)

[34] Fitzpatrick R. and Aydemir A. Y., Nucl. Fusion **36**, 11 (1996)

[35] La Haye R. J., Bondeson A., Chu M. S., Garofalo A. M., Liu Y. Q., Navratil G. A., Okabayashi M., Reimerdes H. and Strait E. J., Nucl. Fusion **44**, 1197 (2004)

[36] Finn J. M., Phys. Plasmas **2**, 3782 (1995)

[37] Betti R., Phys. Plasmas **5**, 3615 (1998)

[38] Bondeson A. and Xi H. X., Phys. Plasmas **4**, 2081 (1997)

[39] Coppi, B., Galvao R., Pellat R., Rosenbluth M. N.and Rutherford P. H., Sov. J. Plasma Phys. **2**, 533 (1976)

[40] Rice J. E., Lee W. D., Marmar E. S., Basse E. S., Bonoli P. T., Greenwald M. J., Hubbard A. E., Hughes J. W., Hutchinson I. H., Ince-Cushman A., Irby J. H., Lin Y., Mossessian D., Snipes J. A., Wolfe S. M., Wutkitch S. J., and Zhurowich K., Phys. Plasmas **11**, 2427 (2004)
[41] deGrassie J. S., Rcie J. E., Burrell K. H., Groebner R. J., and Solomon W. M., Phys. Plasmas **14**, 056115 (2007)
[42] Nave M. F. F. and Wesson J. A., Nucl. Fusion **30**, 2575 (1990)
[43] Hender T. C., Fitzpatrick R., Morris A. W., Carolan P. G., Durst R. D., Edlington T., Ferreira J., Fielding S. J., Haynes P. S., Hugill J., Jenkins I. J., La Haye R. J., Parham, B. J., Robinson D. C., Todd T. N., Valovic M., and Vayakis G., Nucl. Fusion **32**, 2091 (1992)
[44] Jensen T. H., Leonard A. W., and Hyatt A. W., Phys. Fluids **B5**, 1239 (1993)
[45] Fitzpatrick R., Nucl. Fusion **33**, 1049 (1993)
[46] Guo S. C. and Chu M. S., Phys. Plasmas **8**, 3342 (2001)
[47] Guo S. C. and Chu M. S., Phys. Plasmas **9**, 4685 (2002)
[48] Guo S. C. and Chu M. S., Phys. Plasmas **11**, 4050 (2004)
[49] Gates D. A. and Hender T. C., Nucl. Fusion **36**, 273 (1996)
[50] Fitzpatrick R., Phys. Plasmas **5**, 3325 (1998)
[51] Gimblett C. G., Hastie R. J., Theory of Fusion Plasmas, J. W. Connor, E. Sindoni, and J. Vaclavik Eds. (SIF Bologna) p. 319 (1999)
[52] Fitzpatrick R., Phys. Plasmas **9**, 3459 (2002)
[53] Garofalo, A. M., Turnbull A. D., Austin M. E., Bialek J., Chu M. S., Comer K. J., Fredrickson E. D., Groebner R. J., La Haye R. J., Lao L. L., Lazarus E. A., Navratil G. A., Osborne T. H., Rice B. W., Sabbagh S. A., Scoville J. T., Strait E. J., and Taylor T. S., Phys. Rev. Lett. **82**, 3811 (1999)
[54] Gimblett C. G. and Hastie R. J., Phys. Plasmas **11**, 1019 (2004)
[55] Boozer A. H., Phys. Rev. Lett. **86**, 5059 (2001)
[56] Gimblett C. G. and Hastie R. J., Phys. Plasmas **7**, 5007 (2000)
[57] Freidberg J. P. and Betti R., Phys. Plasmas **8**, 383 (2001)
[58] Fitzpatrick R. and Jensen T. H., Phys. Plasmas **3**, 2641 (1996)
[59] Taylor J. B., Connor J. W., Gimblett C. G., Wilson H. R., and Hastie R. J., Phys. Plasmas **8**, 4062 (2001)
[60] Hegna C. C., Phys. Plasmas **11**, 4230 (2004)
[61] Hu B. and Betti. R., Phys. Rev. Lett. **93**, 105002 (2004)
[62] Chu M. S., Greene J. M., Jensen T. H., Miller R. L., Bondeson A., Johnson R. W., and Mauel M. E., Phys. Plasmas **2**, 2236 (1995)
[63] Okabayashi M., Pomphrey N., and Hatcher R., Nucl. Fusion **38**, 1607 (1998)
[64] Okabayashi M., Bialek J., Chance M. S., Chu M. S., Fredrickson E., Garofalo A. M., Hatcher R. E., Jensen T. H., Johnson L. C., La Haye R. J., Navratil G. A., Lazarus E. A., Scoville J. T., Strait E. J., Turnbull A. D., Walker M., and the DIII-D Team, J. Plasma Fusion Reseach Series **5**, 42 (2002)
[65] Pustovitov V. D., Phys. Plasmas **14**, 082506 (2007)
[66] Bondeson A., Vlad G., Lutjens H., Phys. Fluids **B4**, 1889 (1992)
[67] Liu Y. Q., Bondeson A., Fransson C. M., Lennartson B., and Breitholtz C., Phys. Plasmas **7**, 3681 (2000)
[68] Liu Y. Q., Chu M. S., Chapman I. T., Hender T. C., Phys. Plasmas **15**, 112503 (2008)
[69] Bondeson A. and Chu M. S., Phys. Plasmas **3**, 3013 (1996)
[70] Zheng L. J. and Kotschenreuther M., J. Computational Physics **211**, 748 (2006)
[71] Zheng L. J., Kotschenreuther M. T., and Van Dam J.W., Proceedings of 22nd IAEA Fusion Energy Conf., Geneva, Switzerland (IAEA, Vienna, 2008) Paper TH/P9-32

[72] Glasser A. H., Chance M. S., Bull. Am. Phys. Soc. **42**, 1848 (1997)
[73] Zheng L. J. and Kotschenreuther M. T., Phys. Plasmas **12**, 072504 (2005)
[74] Tokuda S., Shiraishi J., Kagei Y., Aiba N., Proceedings of 22nd IAEA Fusion Energy Conf., Geneva, Switzerland (IAEA, Vienna, 2008) Paper TH/P9-32
[75] Frieman E. A. and Rotenberg M., Rev. Mod. Phys. **32**, 989 (1960)
[76] Berkery J. W., Sabbagh S. A., Betti R., Hu B., Bell R. E., Gerhardt S. P., Manickam J. and Tritz K., Phys. Rev. Lett. **104**, 035003 (2010)
[77] Sabbagh S. A., Bialek J. M., Bell R. E., Glasser A. H., LeBlanc B. P., Menard J. E., Paoletti F., Bell M. G., Fitzpatrick R., Fredrickson E. D., Garofalo A. M., Gates D. A., Kaye S. M., Lao L. L., Maingi R., Mueller D., Navratil G. A., Stutman D., Zhu W., and the NSTX Research Team, Nucl. Fusion **44**, 560 (2004)
[78] Strait E. J., Taylor T. S., Turnbull A. D., Ferron J. R., Lao L. L., Rice B. W., Sauter O., Thompson S. J., and Wroblewski D., Phys. Rev. Lett. **74**, 2483 (1995)
[79] Taylor T. S., Strait E. J., Lao L. L., Mauel M. E., Turnbull A. D., Burrell K. H., Chu M. S., Ferron J. R., Groebner R. J., LaHaye R. J., Rice B. W., Snider R. T., Thompson S. J., Wroblewski D.,and Lightly D.J., Phys. Plasmas **2**, 2390 (1995)
[80] Reimerdes H., Garofalo A. M., Jackson G. L., Okabayashi M., Strait E. J., Chu M. S., In Y., La Haye R. J., Lanctot M. J., Liu Y. Q., Navratil G. A., Solomon W. M., Takahashi H., Groebner R. J., Phys. Rev. Lett. **98**, 055001-1 (2007)
[81] Takeji S., Tokuda S., Fujita T., Suzuki T., Isayama A., Ide S., Ishii Y., Kamada Y., Koide Y., Matsumoto T., Oikawa T., Ozeki T., Sakamoto Y., and the JT-60 Team, Nucl. Fusion **42**, 5 (2002)
[82] Matsunaga G., Takechi M., Kurita G., Ozeki T., Kamada Y., and the JT-60 Team, Plasma Phys. Control. Fusion **49**, 95 (2007)
[83] Takeji S., *et al.*, J. Plasma Physics and Fusion Research **78**, 447 (2002)
[84] Kurita G., Tuda T., Azumi M., Ishida S., Navratil G. A., Sakurai S., Tamai H., Matsukawa M., Ozeki T., Chu M. S., Chance M. S., and Miura Y., Nucl. Fusion **46**, 383 (2006)
[85] Okabayashi M., Pomphrey N., Manickam J., Ward D. J., Bell R. E., Hatcher R., Kaita R., Kaye S. M., Kugel H. W., LeBlanc B., Levinton F. M., Roberts D. W., Sesnic S., Sun Y., Takahashi H., McGuire K. M., Nazikian R., Zarnstorff M. C., Nucl. Fusion **36**, 1167 (1996)
[86] Johnson L. C., Okabayashi M.,Garofalo A. M., Strait E. J., Bialek J., Chance M. S., Chu M. S., Fredrickson E. D., La Haye R. J., Manickam J., Nagy A., Navratil G. A., Snider R. T., Scoville J. T., Turnbull A. D., and Walker M. L., Proceedings of 28th EPS Conf. on Control. Fusion and Plasma Physics, Funchal, 2001, ECA Vol. 25A (European Physical Society, 2001) p. 1361
[87] Chance M. S., Phys. Plasmas **4**, 2161 (1997)
[88] Sabbagh S., Sontag A. C., Bialek J. M., Gates D. A., Glasser A. H., Menard J. E., Zhu W., Bell M. G., Bell R. E., Bondeson A., Bush C. E., Callen J., Chu M. S., Kaye S. M., Lao L. L., LeBlanc B. P., Liu Y., Maingi R., Mueller D., Shaing K. C., Stutman D., Tritz K., Zhang C., Nucl. Fusion **46** , 635 (2006)
[89] Lao L. L., Ferron J. R., Groebner R. J., Howl H., St. John H., Strait E. J., and Taylor T. S., Nucl. Fusion **30**, 1035 (1990)
[90] Sabbagh S. A., Bell R. E., Menard J. E., Gates D. A., Sontag A. C., Bialek J. M., LeBlanc B. P., Levinton F. M., Tritz K. and Yuh H., Phy. Rev. Lett. **97**, 045004 (2006)
[91] Sontag A. C., Sabbagh S. A., Zhu W., Menard J. E., Bell R. E., Bialek J. M., Bell M. G., Gates D. A., Glasser A. H,, LeBlanc B. P., Shaing K. C., Stuttman D., and Tritz K., Nucl. Fusion **47**, 1005 (2007)
[92] Sabbagh S. A., Berkery J. W., Bell R. E.,Bialek J. M., Gerhardt S. P., Menard J. E., Betti R., Gates D. A., Hu B., Katsuro-Hopkins O. N., LeBlanc B. P., Levinton F. M., Manickam J., Tritz K. and Yuh H., Nucl. Fusion **50**, 025020 (2010)

[93] Hammet G. W. and Perkins F. W., Phys. Rev. Lett. **64** , 3019 (1990)
[94] Antonsen T. M. Jr. and Lee Y. C., Phys. Fluids **25**, 132 (1982)
[95] Bondeson A., Liu Y. Q., Gregoratto D., Franson C. M., and Gribov Y., Plasmas Phys. Control. Fusion **45** , A253 (2003)
[96] Kuvshinov B. N. and Mikhailovskii A. B., Plasma Phys. Report **24** , 623 (1998)
[97] Gregoratto D., Bondeson A., Chu M. S., and Garofalo A. M., Plasma Phys. and Control. Fusion **42** , 768 (2002)
[98] Liu Y. Q., Bondeson A., Chu M. S., Favez J. Y., Gribov Y., Gryaznevich M., Hender T. C., Howell D. F., La Haye R. J., and Lister J. B., Nucl. Fusion **45**, 1131 (2005)
[99] Chu M. S., Bondeson A., Chance M. S., Liu Y. Q., Garofalo A. M., Glasser A. H., Jackson G. L., La Haye R. J., Lao L. L., Navratil G. A., Okabayashi M., Reimerdes H., Scoville J. T., and Strait E. J., Phys. Plasmas **11**, 2497 (2004)
[100] Strait E. J., Garofalo A. M., Jackson G. L., Okabayashi M., Reimerdes H., Chu M. S., Fitzpatrick R., Groebner R. J., In Y., La Haye R. J., Lanctot M. J., Liu Y. Q., Navratil G. A., Solomon W. M., Takahashi H., and the DIII-D Team, Phys. Plasmas **14**, 056101 (2007)
[101] Takechi M., Matsunaga G., Aiba N., Fujita T., Ozeki T., Koide Y., Sakamoto Y. , Kurita G., Isayama A., Kamada Y., and the JT-60 Team, Phys. Rev. Lett. **98** 055001-2 (2007)
[102] Garofalo A. M., Jackson G. L., La Haye R. J., Okabayashi M., Reimerdes H., Strait E. J., Ferron J. R., Groebner R. J., In Y., Lanctot M. J., Matsunaga G., Navratil G. A., Solomon W. M., Takahashi H., Takechi M., Turnbull A. D., and the DIII-D Team, Nucl. Fusion **49**, 1121 (2007)
[103] Liu Y. Q., Chapman I. T., Chu M. S., Reimerdes H., Villone F., Albanese R., Ambrosino G., Garofalo A. M., Gimblett C. G., Hastie R. J., Hender T. C., Jackson G. L., Okabayashi M., Pironti A., Portone A., Rubinacci G., and Strait E. J., submitted to Phys. Plasmas, (2008)
[104] Reimerdes H., Garofalo A. M., Jackson G. L., LaHaye R. J., Okabayashi M., Strait E. J., Ferron J. R., Groebner R. J., In Y., Lanctot M. J., Matsunaga G., Navratil G. A., Solomon W. M., Takahashi H., Takechi M., Turnbull A. D., and the DIII-D Team, Bull. Am. Phys. Soc. **53**, 202 (2008)
[105] Reimerdes H., Chu M. S., Garofalo A. M., Jackson G. L., La Haye R. J., Navratil G. A., Okabayashi M., Scoville J. T., and Strait E. J., Phys. Rev. Lett. **93**, 135002 (2004)
[106] Reimerdes H., Bialek J., Chance M. S., Chu M. S., Garofalo A. M., Gohil P., In Y., Jackson G. L., Jayakumar R. J., Jensen T. H., Kim J. S., La Haye R. J., Liu Y. Q., Menard J. E., Navratil G. A., Okabayashi M., Scoville J. T., Strait E. J., Szymanski D. D., and Takahashi H., Nucl. Fusion **45**, 368 (2005)
[107] Garofalo A. M., Burrell K. H., DeBoo J. C., deGrassie J. S., Jackson G. L., Lanctot M., Reimerdes H., Schaffer M. J., Solomon W. M., and Strait E. J., Phys. Rev. Lett, **101**, 195005 (2008)
[108] Shaing K. C., Phys. Plasmas **10**, 1443 (2003)
[109] Zhu W., Sabbagh S. A., Bell R. E., Bialek J. M., Bell M. G., LeBlanc B. P., Levinton F. M., Menard J. E., Shaing K. C., Sontag A. C., Yuh H., Phys. Rev. Lett. **96**, 225002 (2006)
[110] Boozer A. H., Phys. Plasmas **10**, 1458 (2003)
[111] Shaing K. C., Phys. Rev. Lett. **87**, 245003 (2001)
[112] Shaing K. C., Phys. Plasmas **9**, 3470 (2002)
[113] Shaing K. C., Hirshman S. P., and Callen J. D., Phys. Fluids **29**, 521 (1986)
[114] Shaing K. C., Phys. Fluids **B5**, 3841 (1993)
[115] Shaing K. C., Sabbagh S. A., and Chu M. S., Nucl. Fusion **50**, 025022 (2010)
[116] Fitzpatrick R., Nucl. Fusion **33**, 3325 (1993)
[117] Cole A. J., Hegna C. C., and Callen J. D., Phys. Rev. Lett. **99**, 065001 (2007)
[118] Park J. K.,Menard J. E., Shaffer M. J., Boozer A. H., Hawryluk R. J., Reimerdes H., Evans T., the NSTX Research Team and DIII-D Research Team, Phys. Rev. Lett. **99**, 065001 (2007)

[119] Chu M. S., Chan V. S., Chance M. S. Edgell D. H., Garofalo A. M., Glasser A.H., Guo S. C., Humphreys D. A., Jensen T. H., Kim J. S., LaHaye R. J., Lao L. L., Navratil G. A., Okabayashi M., Perkins F. W., Reimerdes H., St. John H. E., Soon E., Strait E. J., Turnbull A. D., Walker M. L., and Wong S. K., Nucl. Fusion **43**, 196 (2003)

[120] Chance M. S., Chu M. S., Okabayashi M., and Turnbull A. D., Nucl. Fusion **42**, 295 (2002)

[121] Chu M. S., Chance M. S., Glasser A. and Okabayashi M., Nucl. Fusion **43**, 441 (2003)

[122] Strait E. J., Bialek J. M., Bogatu I. N., Chance M. S., Chu M. S., Edgell D. H., Garofalo A. M., Jackson G. L., Jayamumar R.J., Jensen T. H.,Katsuro-Hopkins O., Kim J. S., LaHaye R. J., Lao L. L., Makowski M. A., Navratil G. A., Okabayashi M., Reimerdes H., Scoville J. T., Turnbull A. D., and the DIII-D Team, Phys. Plasmas **11**, 2505 (2004)

[123] Jackson G. L., Anderson P. M., Bialek J., Cary W. P., Campbell G. L., Garofalo A. M., Hatcher R., Kellman A. G., La Haye R. J., Nagy A., Navratil G. A., Okabayashi M., Pawley C. J., Reimerdes H., Scoville J. T., Strait E. J., and Szymanski D. D., Proceedings of 30th EPS Conf. on Controlled Fusion and Plasma Phys., St. Petersburg Vol. ECA 27A (2003) Paper P-4.47; www.ioffe.run/EPS2003

[124] Garofalo A. M., Jensen T. H., Johnson L. C., La Haye R. J., Navratil G. A., Okabayashi M., Scoville J. T., Strait E. J., Baker D. R., Bialek J., Chu M. S., Ferron J. R., Jayakumar J., Lao L. L., Makowski M. A., Reimerdes H., Taylor T. S., Turnbull A. D., Wade M. R., and Wong S. K., Phys. Plasmas **9**, 1997 (2002)

[125] Hender T. C.,Gryaznevich M., Liu Y. Q., Bigi M., Buttery R. J., Bondeson A., Gimblett C. G., Howell D. F., Pinches S. D., Baar M., de Varies P., and JET EFDA Contributors, Proceedings of 20th IAEA Fusion Energy Conf., Vilamoura, Portugal (IAEA, Vienna, 2004) EXP/P2-22(2004)

[126] Gryaznevich M. P., Gimblett C. G., Hender T. C., Howell D. F., Pinches S., La Haye R. J., Liu Y. Q., and Bondeson A., APS 2003 Albuquerque, New Mexico, RP1.036 (2003); http://www.aps.org/meet/DPP03/baps/S2080036.html

[127] Liu Y. Q., Chu M. S., Garofalo A. M., La Haye R. J., Gribov Y., Gryaznevich M., Hender T. C., Howell D. F., and de Vries P., Phys. Plasmas **13** 056120 (2006)

[128] Ivers T. H., Eisner E., Garofalo A., Kombargi R., Mauel M. E., Maurer D., Nadle D., Navratil G. A., Sankar M. K. V., Su M., Taylor E., and Xiao Q., Bartsch R. R., Reass W. A., and Wurden G. A., Phys. Plasmas **3** , 1926 (1996)

[129] Cates C., Shilov M., Mauel M. E., Navratil G. A., Maurer D., Mukherjee S., Nadie D., Bialek J., and Boozer A. H., Phys. Plasmas **7**, 3133 (2000)

[130] Maurer D. A., Bialek J., Boozer A. H., Cates C., Katsuro-Hopkins O., Liu Y., Mauel M. E., Navratil G. A., Pederson T. S., Shilov M., Stillits N., Proceedings of 19th IAEA 2002 Fusion Energy Conf., Lyon, France, (IAEA, Vienna) CD-ROM, Paper TH/P3-13

[131] Mauel M. E., Bialek J., Boozer A. H., Cates C., James R., Katsuro-Hopkins O., Klein A., Liu Y., Maurer D. A., Maslovsky D., Navratil G. A., Pedersen T. S., Shilov M., and Stillits N., Nucl. Fusion **45**, 245 (2005)

[132] Shilov M., Cates C.,James R., Klein A., Katsuro-Hopkins O., Liu Y., Mauel M. E., Maurer D. A., Navratil G. A., Pedersen T. S., and Stillits N., Phys. Plasmas **11**, 2573 (2004)

[133] Okabayashi M., Bialek J., Chance M. S., Chu M. S., Fredricksen E. D., Garofalo A. M., Hatcher R., Jensen T. H., Johnson L. C., La Haye R. J., Navratil G. A., Reimerdes H., Scoville J. T., Strait E. J., Turnbull A. D., Walker M. L., and the DIII-D Team, Plasma Phys. Control. Fusion **44**, B339 (2002).

[134] Fasoli A., Borba D., Bosia G., Campbell D. J., Dobbing J. A., Gormezano C., Jacquinot J., Lavnchy P., Lister J. B., Marmillod P., Moret J. M., Santaglustina A., and Sharapov S., Phys. Rev. Lett. **75**, 645 (1995)

[135] Reimerdes H., Hender T. C., Sabbagh S. A., Bialek J., Chu M. S., Garofalo A. M., Gryaznevich M. P., Howell D. F., Jackson G. L., La Haye R. J., Liu Y. Q., Menard J. E., Navratil G. A., Okabayashi M., Pinches S. D., Sontag A. C., Strait E. J., Zhu W., Bigi M., Baar M. de, Vries P. de, Gates D. A., Gohil P., Groebner R. J., Mueller D., Raman R., Scoville J. T., Solomon W. M., the DIII-D Team, JET-EFDA Contributors, and the NSTX Team, Phys. Plasmas **13**, 056107 (2006)

[136] Okabayashi M., Bialek J., Bondeson A., Chance M. S., Chu M. S., Garofalo A. M., Hatcher R., In Y., Jackson G. L., Jayakumar R. J., Jensen T. H., Katsura-Hopkins O., La Haye R. J., Liu Y. Q., Navratil G. A., Reimerdes H., Scoville J. T., Strait E. J., Takechi M., Turnbull A. D., Gohil P., Kim J. S., Makowski M. A., Manickam J., and Menard J., Nucl. Fusion **45**, 1718 (2005)

[137] Menard J. E., Bell M. G., Bell R. E., Fredrickson E. D., Gates D. A., Kaye S. M., LeBlanc B. P., Maingi R., Mueller D., Sabbagh S. A.,, Stutman D., Bush C. E., Johnson D. W., Kaita R., Kugel H. W., Maqueda R. J., Paoletti F., Paul S. F., Ono M., Peng Y.-K. M., Skinner C. H., Synakowski E. J., and the NSTX Research Team, Nucl. Fusion **43**, 330 (2003)

[138] Garofalo A. M., Strait E. J., Johnson L. C., La Haye R. J., Lazarus E. A., Navratil G. A., Okabayashi M., Scoville T., Taylor T. S., and Turnbull A. D., Phys. Rev. Lett. **89**, 235001 (2002).

[139] Hawryluk R., Proceedings of 22nd IAEA Fusion Energy Conf., Geneva, Switzerland (IAEA, Vienna, 2008) Paper IT/1-2 (2008)

[140] Lanctot, M. J., Reimerdes H., Garofalo A. M., Chu M. S., Liu Y. Q., Strait E. J., Jackson G. L., La Haye R. J., Okabayashi M., Osborne T. H., and Schaffer M. J. Phys. Plasmas **17**, 030701 (2010)

[141] Pironi A. and Walker M. L, IEEE Control Systems Magazine **25**, 24-92 (2005)

[142] Pironi A., Walker M. L, IEEE Control Systems Magazine **26**, 30-91 (2006)

[143] Liu Y. Q. and Bondeson A., Phys. Rev. Lett. **84**, 907 (2000)

[144] Strait E. J., Bialek J., Bogatu N., Chance M. S., Chu M. S., Edgell D., Garofalo A. M., Jackson G. L., Jensen T. H., Johnson L. C., Kim J. S., La Haye R. J., Navratil G. A., Okabayashi M., Reimerdes H., Turnbull A. D., Walker M.L., and the DIII-D Team, Nucl. Fusion **43**, 430 (2003)

[145] Polevoi A. R. and Gribov Y., J. Plasma Fusion Research Series **5**, 82 (2002)

[146] Bialek J., Boozer A. H., Mauel M. E.and Navratil G. A., Phys. Plasmas **8**, 2170 (2001)

[147] Bondeson A., Liu Y. Q., Gregoratto D., Fransson C. M., Lennartson B., Breitholz C., and Gribov Y., Phys. Plasmas **9**, 2044 (2002)

[148] Liu Y. Q. and Bondeson A., Plasma Phys. Control. Fusion **44**, L21 (2002)

[149] Liu Y. Q., Bondeson A., Gribov Y., and Polevoi A., Nucl. Fusion **44** , 232(2004)

[150] Pustovitov V. D., Plasma Phys. and Controlled Fusion **44**, 295 (2002)

[151] Grando L., Manduchi G., Marrelli L., Marchiori G., Paccagnella R., Piovesan P., Piron L., Soppelsa A., Spizzo G., Zanca P., Proceedings of 22nd IAEA Fusion Energy Conf., Geneva, Switzerland (IAEA, Vienna, 2008) Paper EX/p9-8

[152] Merkel P, Nuhrenberg C., Strumberger E., Proceedings of 31st EPS Conf. on Plasma Physics, London, 2004, Vol. 28G (European Physical Society) P-I208

[153] Bondeson A., Liu Y., Gregoratto D., Gribov Y., Pustovitov V. D., Nucl. Fusion **42**, 768 (2002)

[154] Liu Y. Q., Bondeson A., Gregoratto D., Fransson C. M., Gribov Y., and Paccagnella R., Nucl. Fusion **44**, 77 (2004)

[155] Albanese R. and Rubinacci G., Advances in Imaging and Electron Physics **102**, 1 (1998)

[156] Okabayashi M., Bialek J., Chance M. S., Chu M. S., Fredrickson E. D., Garofalo A. M., Gryaznevich M., Hatcher R. E., Jensen T. H., Johnson L. C., La Haye R. J., Lazarus E. A., Makowski M. A., Manickam J., Navratil G. A., Scoville J. T., Strait E. J., Turnbull A. D., and Walker M. L., Phys. Plasmas **8**, 2071 (2001)

[157] In Y., Kim J. S., Edgell D. H., Strait E. J., Humphreys D. A., Walker M. l., Jackson G. L., Chu M. S., Johnson R., La Haye R. J., Okabayashi M., Garofalo A. M., Reimerdes H., Phys. Plasmas **13**, 062512 (2006)

[158] Garofalo A. M., Jensen T. H., and Strait E. J., Phys. Plasmas **9**, 4573 (2002).

[159] Okabayashi M., Bogatu I. N., Bolzonella T., Chance M. S., Chu M. S., Garofalo A. M., Hatcher R. E., In Y., Jackson G. L., Kim J. S., Marrelli L., Martin P., Navratil G. A., Reimerdes H., Strait E. J., Takahashi H., and Welander A. S., Nucl. Fusion **49**, 125003 (2009)

[160] In Y., Bogatu I. N., Garofalo A. M., Jackson G. L., Kim J. S., La Haye R. J., Lanctot M. J., Marreli L., Martin P., Okabayashi M., Reimerdes H., Schaffer M. J., and Strait E. J., Nucl. Fusion **50**, 042001 (2010)

[161] Polevoi A. R., Medvedev S. Yu, Pustovitov V. D., Mukhovatov V. S., Shimada M., Ivanov A. A., Poshekhonov Yu. Yu, and Chu M. S., Proceedings of 19th IAEA Fusion Energy Conf., Lyon, France, (IAEA, Vienna, 2002) CD-ROM CT/P-08 and http://www.iaea.org/programmes/ripc/physics/fec2002/html/fec2002.htm

[162] Strumberger E., Merkel P., Sempf M., and Gunter S., Phys. Plasmas **15**, 056110 (2008)

[163] Liu Y. Q., Chu M. S., Chapman I. T., Gimblett C. G., Gryaznevich M. P., Hastie R. J., Hender T. C., Howell D. F., Saarelma S. and JET-EFDA Contributors, Proceedings of 22nd IAEA Fusion Energy Conf., Geneva, Switzerland (IAEA, Vienna, 2008) CD-ROM TH/P9-26 and http://www.iaea.org/programmes/ripc/physics/fec2008/html/fec2008.htm

[164] Reimerdes H., Garofalo A. M., Okabayashi M., Strait E. J., Betti R., Chu M. S., Hu B., Jackson G. L., LaHaye R. J., Lanctot M. J., Liu Y. Q., Navratil G. A., Solomon W. M., Takahashi H., Groebner R. J. and the DIII-D Team, Plasma Phys. and Controlled Fusion Research **49**, B349 (2007)

[165] Matsunaga G., Sakamoto Y., Aiba N., Shinohara K., Takechi M., Suzuki T., Fujita T., Isayama A., Oyama N., Asakura N., Kamada Y., Ozeki T., and the JT-60 Team, Proceedings of 22nd IAEA Fusion Energy Conf., Geneva, Switzerland (IAEA, Vienna, 2008) Paper EX/5-2.

[166] Brennan D. P., La Haye R. J., Turnbull A. D., Chu M. S., Jensen T. H., Lao L. L., Luce T. C., Politzer P. A., Strait E. J., Kruger S. E., and Schnack D. D., Phys. Plasmas **10**, 1643 (2003)

[167] Matsunaga G., Aiba N., Shinohara K.,Sakamoto Y., Isayama A, Takechi M., Suzuki T., Oyama N., Asakura N., Kamada Y., Ozeki T., and the JT-60 Team, Phys. Rev. Lett. **103** 045001 (2009)

[168] Liu Y., Chu M. S., Guo W. F., Villone F., Albanese R., Ambrosino G., Baruzzo M., Bolzonella T., Hastie R. J., Hender T. C., Jackson G. L., La Haye R. J., Lanctot M. J., Marchiori G., Okabayashi M., Paccagnella R., Furno Palumbo M., Pironti A., Reimerdes H., Rubinacci G., Soppelsa A., Strait E. J., Ventre S., and Yadykin D., "RWM Control Code Maturity: Progress and Specific Examples," accepted for publication in Plasma Phys. Control. Fusion (2010)

[169] Berkery J. W., Sabbagh S. A., Betti R., Hu B., Bell R. E., Gerhardt S. P., Manickam J., Podesta M., The Role of Kinetic Effects, Including Plasma Rotation and Energetic Particles, in RWM Stability , APS DPP invited talk (2009) submitted to Phys. Plasmas (2010)

[170] Lee G. S. and Ivanov D. P., J. Plasma Fusion Research **5**, 261 (2001)

[171] Lee G. S. and Ivanov D. P., Phys. Plasmas **8**, 3107 (2001)

[172] Meade D., Kessel C. E., Hammett G. W., Jardin S. C., Ulrickson M. A., Titus P., Heitzenroodr P., Nelson B. E., Schultz J. H., Thome R. J., Wesley J. C., Mandrakas J., Navratil G. A., Bialek J., Rognlein T., Mau T. K., Budny R., Gorelenkov N., Rutherford P. H., Young K. M., Schmidt J. .A., Phys. Plasmas and Control. Fusion Research, CD-ROM, Paper FTP2/6 (2002).

[173] Jhang H. and Ku S. H., Proceedings of 32nd EPS Plasma Physics Conf. combined with the 8th International Workshop on Fast Ignition of Fusion Targets, Tarragona, Spain (2005) P1.066

[174] Katsuro-Hopkins O., Sabbagh S. A., Bialek J. M., Park H. K., Bak J. G., Chung J., Hahn S. H., Kim J. Y., Kwon M., Lee G. S., Yoon S. G., You K. I., Glasser A. H., and Lao L. L. Nucl. Fusion **50**, 025019 (2010)

[175] Pustovitov V. D., Phys. Plasmas **16** 052503 (2009)

[176] Bergerson W. F., Hannum D. A., Hegna C. C., Kendrick R. D., Sarff J. S., and Forest C. B., Phys. Rev. Lett. **101**, 235005 (2008)

[177] Kurita G., Tuda T., Azumi M., Ishida S., Takechi S., Sakasai A., Matsukawa M., Ozeki T., and Kikuchi M., Nucl. Fusion **43**, 949 (2003)

[178] Kurita G., Bialek J., Tuda T., Azumi M., Ishida S., Navratil G. A., Sakurai S., Tamai H., Matsukawa M., Ozeki T., Chu M. S., Chance M. S., Miura Y., Phys. Plasmas and Controlled Fusion Research (2004) CD-ROM, Paper FTP7/7

[179] Tsuzuki K, Kamaiya K., Shinohara K., Bakhriari M., Ogawa H., Kurita G., Takechi M., Kasai S., Sato M., Kawashima H., Uehara K., Hoshino K., Kusama Y., Yamamoto M, Shibata T., Kikuchi K., Amemiya H., Sadamoto Y., Nagashima Y., Ejiri A., Hino T., Hirohata Y., Tsutsui H., Shimada R., Ido T., Hamada Y., and the JFT-2M Group, Proceedings of 20th IAEA Fusion Energy Conf., Vilamoura, Portugal (IAEA, Vienna, 2004)

[180] Fujiwara M., Kawahata K., Ohyabu N., Kaneko O., Komori A., Yamada H., Ashikawa N., Baylor L. R., Combs S. K., de Vries P. C., Emoto M., Ejiri A., Fisher P. W., Funaba H., Goto M., Hartmann D., Ida K., Idei H., Ito S., Ikeda K., Inagaki S., Inoue N., Isobe M., Kado S., Khlopenkov K., Kobuchi T., Krasilnikov A. V., Kubo S., Kumazawa R., Leuterer F., Liang Y., Lyon J. F., Masuzaki S., Minami T., Miyajima J., Morisaki T., Morita S., Murakami S., Muto S., Mutoh T., Nagayama Y., Nakajima N., Nakamura Y., Nakanishi H., Narihara K., Nishimura K., Noda N., Notake T., Ohdachi S., Oka Y., Okajima S., Okamoto M., Osakabe M., Ozaki T., Pavlichenko R. O., Petersen B. J., Sagara A., Saito K., Sakakibara S., Sakamoto R., Sanuki H., Sasato H., Sato K., Sato M., Seki T., Shimozuma T., Shoji M., Sugama H., Suzuki H., Takechi M., Takeiri Y., Tamura N., Tanaka K., Toi K., Tokuzawa T., Torii Y., Tsumari K., Watanabe K. Y., Watari T., Yamada I., Yamaguchi S., Yamamoto S., Yokoyama M., Yoshida N., Yoshimura Y., Zhao Y. P., Akiyama R., Haba K., Iima M., Kodaira J., Takita T., Tsuzuki T., Yamauchi Y., Yonezu H., Chikaraishi H., Hamaguchi S., Zmagawa S., Inoue N., Iwamoto A., Kitagawa S., Kubota Y., Maekawa R., Mito T., Murai K., Nishimura A., Chikaraishi H., Takahata K., Tamura H., Yamada S., Yanagi N., Itoh K., Matsuoka K., Ohkubo K., Ohtake I., Satoh S., Satow T., Sudo S., Tanahashi S., Yamazaki K., Hamada Y., and Motojima O., Nucl. Fusion **41**, 1355 (2001)

[181] Nuhrenberg J., Lotz W. and Gori S., Theory of Fusion Plasmas (Proc. Workshop, Varenna, 1994), **Editrice Compositori, Bologna** 3 (1994).

[182] Garabedian P., Phys. Plasmas **3**, 2482 (1996)

[183] Matsuoka K., Okamura S., Fujiwara M., Drevlak M., Merkel P., and Nuehrenberg J., Plasma Phys. Rep. **23**, 542 (1997)

[184] Okamura S., Matsuoka K., Fujiwara M., Devlak M., Merkel P., and Nuerenberg, J., J. Plasma Fusion Research Series **1**, 164 (1998)

[185] Okamura S., Matsuoka K., Nishimura S., Isobe M., Nomura I., Suzuki C., Shimizu A., Murakami S., Nakajima N., Yokayama M., Fujisawa A., Ida K., Itoh K., Merkel P., Drevlak M., Zille R., Gori S., Nuhrenberg J., Stellerator CHS-qa, Nucl. Fusion **41**, 1865 (2001)

[186] Chu M. S., Ichiguchi K. Nucl. Fusion **45**, 804 (2005)

[187] Guo S. C., Freidberg J. P., and Nachtrieb R., Phys. Plasmas **6**, 3668 (1999)

[188] Greene P. and Robertson S., Phys. Fluids **B5**, 556 (1993)

[189] Brunsell P. R., Yadikin D., Gregoratto D., Paccagnella R., Bolzonella T., Cavinato M., Cecconello M., Drake J., Luchetta A., Manduchi G., Marchiori G., Marrelli L., Martin P., Masiello A., Milani F., Ortolani S., Spizzo G. and Zanca P., Phys. Rev.Lett. **93**, 225001 (2004)

[190] Brunsell P. R., Bergsaker H., Cecconello M., Drake J. R., Graveestijn R. M., Hedqvista A. and Malmberg J. A., Plasma Phys. Control. Fusion **43**, 1457 (2001)

[191] Brunsell P. R., Malmberg J. A., Yadikin D. and Cecconello M., Phys. Plasmas **10**, 3823 (2003)

[192] Drake J. R., Brunsell P. R., Yadikin D., Cecconello M., Malmberg J. A., Gregoratto D., Paccagnella R., Bolzonella T., Manduchi G., Marchiori G., Marrelli L., Ortolani S., Spizzo G., Zanca P., Bondeson A., and Liu Y. Q., Nucl. Fusio **45**, 557 (2005)

[193] Ortolani S. and the RFXTeam, Plasma Phys. Contol. Fusion **48**, B371 (2006)
[194] Bolzonella T., Cavinato M., Gaito E., Grando L., Luchetta A., Manduchi G., Marchiori G., Marrelli L., Paccagnella R., Soppelsa A., and Zanca P., Fusion Eng. and Design **82**, 1064 (2007)
[195] Bolzonella T., Igochine V., Guo S. C., Yadikin D., Baruzzo M., and Zohm H., Phys. Rev. Lett. **101**, 165003 (2008)
[196] Brunsell P. R., Yadikin D., Gregoratto D., Paccagnella R., Liu Y. Q., Bolzonella T., Cecconello M., Drake J. R., Kuldepp M., Manduchi G., Marchioni G., Marrelli L., Martin P., Menmuir S., Ortonali S., Rachlew E., Spizzo A., and Zanca P., Plasma Phys. Control. Fusion **47**, B25 (2005).
[197] Gregoratto D., Drake J. R., Yadikin D., Liu Y. Q., Paccagnella R., Brunsell P. R., Bolzonella T., Marchiori G., and Cecconello M., Phys. Plasmas **12**, 092510 (2005)
[198] Brunsell P. R., Olofsson K. E. J., Frassinetti L., and Drake J. R., Phys. Plasmas **14**, 102505 (2007)
[199] Pustovitov V. D., Plasma Phys. Rep. **30**, 187 (2004)
[200] Zanca P., Marrelli L., Manduchi G., and Marchiori G., Nucl. Fusion **47**, 1425 (2007)
[201] Villone F., Liu Y. Q., Paccagnella R., Bonzonella T., and Rubinacci G., Phys. Rev. Lett. **100**, 255005 (2008)
[202] Liu D. H. and Bondeson A., Computer Physics Communications **116**, 55 (1999)
[203] Fitzpatrick R., Phys. Plasmas **8**, 871 (2001)
[204] Gribov Y. and Pustovitov V. D. *Proc. 19th IAEA Fusion Energy Conf., Lyon, France* (Vienna, IEA) CD-ROM CT/P-12 and http://www.iaea.org/programmes/ripc/physics/fec2002/html/fec2002.htm)
[205] Boozer A. H., Phys. Plasmas **5**, 1179 (1998)

Acknowledgments

This work was supported by the US Department of Energy under DE-FG03-95ER54309 and DE-AC02-76CH03073. The authors would like to thank the referee for constructive comments; Dr. Raffi Nazikian for encouragements, Drs. R. J. LaHaye, Y. K. In, Y. Q. Liu, Raffi Nazikian, S. A. Sabbagh and the referee for reading carefully through the manuscript. We acknowledge Dr. S. A. Sabbagh for clarification of the experimental results from NSTX. They would also like to thank their colleagues Drs. J. Bialek, T. Bolzonella, A. M. Garofalo, S. C. Guo, G. L. Jackson, M. Lanctot, G. Matsunaga, G. A. Navratil, H. Reimerdes, K. C. Shaing, E.J. Strait and M. Takechi for constructive comments.

Appendix A. The L_{eff} Lumped Parameter Model

In the lumped parameter model, the plasma, resistive wall, feedback coils and the coils producing the external error field are represented as a system of currents interacting through their mutual inductances. In particular, the circuit representing the perturbed plasma current is approximated as a current I_p, with a lumped effective self-inductance L_{eff}. Because the time-scale of the perturbation is much slower than the dynamic time scale of the plasma, the plasma is assumed to always be in equilibrium. This is represented as a zero net voltage driving the plasma circuit.

$$L_{eff}I_p + M_{pw}I_w + M_{pc}I_c + M_{pE}I_E = 0 \quad . \tag{A.1}$$

In equation (A.1), the I_i's with $i = (p, w, c, E)$ are the currents in the plasma, wall, feedback coil, error field circuits. The M_{ij}'s are the mutual inductances between the i and j circuits. The time scale is set by the resistive wall, therefore the current on the resistive wall satisfies

$$\frac{\partial}{\partial t}(M_{wp}I_p + L_wI_w + M_{wc}I_c + M_{wE}I_E) + R_wI_w = 0 \quad . \tag{A.2}$$

We may first examine the situation without the presence of any external current, i.e. $I_w = I_c = 0$. With $\tau_w = L_w/R_w$, equations (A.1) and (A.2) then gives

$$\gamma_{open}\tau_w = -\frac{1}{1 - \frac{M_{pw}^2}{L_wL_{eff}}} \quad , \tag{A.3}$$

or equivalently

$$L_{eff} = \frac{M_{pw}^2}{L_w}\left(\frac{\gamma_{open}\tau_w}{1 + \gamma_{open}\tau_w}\right) \quad . \tag{A.4}$$

Equations (A.1) and (A.2) coupled with the feedback equations can be used to study both the phenomena of dynamic error field correction and feedback of the RWM. The feedback equations used here are

$$M_{sc}I_c = G\delta\psi_{sp} = GM_{sp}I_p \quad . \tag{A.5}$$

In equation (A.5), the subscript s stands for the sensor. We also assumed that only the perturbed flux from the plasma is picked up by the sensor, i.e., the perturbed flux by the currents directly from the resistive wall, the feedback coil and the external error field producing coils have been properly compensated for. This is the feedback scheme with mode control in RWM. Dynamic error field compensation is the slow time limit of the feedback, i.e., the zero frequency limit of equations (A.1) and (A.2), because the external error field producing circuit operates on a time scale slower even than the time scale of the RWM. In this limit, from equation (A.2)

$$\frac{\partial}{\partial t} = I_w = 0 \quad . \tag{A.6}$$

The current on the resistive wall is not excited. Then it is easy to solve for I_c and I_p in terms of I_E, with the result

$$I_c = -\frac{\hat{G}}{L_{eff} + \hat{G}M_{pc}} M_{pE} I_E \quad , \tag{A.7}$$

$$I_p = -\frac{1}{L_{eff} + \hat{G}M_{pc}} M_{pE} I_E \quad , \tag{A.8}$$

where

$$\hat{G} = G\frac{M_{sp}}{M_{sc}} \quad . \tag{A.9}$$

The meaning of equations (A.7) and (A.8) can be easily obtained by examining the limit when $\hat{G}$ is large. In this limit, from equation (A.8), we observe that the plasma current $I_p = 0$ and from equation (A.7), the sum of the perturbed fluxes by the error field and the feedback coil current at the plasma tends to zero; i.e. the feedback coils are utilized to null out the effect of the error field on the plasma. Note that in general, this is valid only for the error field component that is in resonance with RWM and not the total effect of the external error field. In the single mode approximation for the RWM, this is the "most important" component of the error field.

To investigate feedback stabilization of the RWM, we note that due to the difference in time scale between error field compensation and RWM feedback, we may set $I_E = 0$. First we consider the open loop growth rate $\gamma_{open} = \partial/\partial t$ and let $I_c = 0$. I_p in equations (A.1) and (A.2) can be easily eliminated in favor of I_w to produce the equation

$$\gamma_{open}\frac{1}{R_w}\left(L_w - \frac{M_{pw}M_{wp}}{L_{eff}}\right) I_w + I_w = 0 \quad , \tag{A.10}$$

and reproduces equation (A.4). At steady state, ($I_w = 0$), we may solve for I_p in terms of I_c and obtain

$$I_p = -I_c(M_{pc}/L_{eff}) \quad , \tag{A.11}$$

or equivalently,

$$I_p = -I_c(M_{pc}L_w/M_{pw}^2)(1 + \gamma_{open}\tau_w)/\gamma_{open}\tau_w) \quad . \tag{A.12}$$

The amplification can be defined as the ratio between the flux [from the plasma to wall(obs)] to flux [from coil to the wall(obs)]

$$(M_{pw}I_p)/(M_{cw}I_c) = -(M_{pc}L_w/M_{cw}M_{pw})\left[(1 + \gamma_{open}\tau_w)/\gamma_{open}\tau_w\right] \quad . \tag{A.13}$$

Here, at steady state it does not make a difference whether the RWM amplitude is defined with mode only or with total field. Comments on the coefficient will be made after the full derivation.

We may normalize the open loop growth rate γ_{open} in equation (A.10) by the L/R time of the resistive wall and denote

$$s_{open} = \gamma_{open} \frac{L_w}{R_w} \quad , \tag{A.14}$$

to obtain

$$s_{open} = \frac{L_w L_{eff}}{M_{pw} \hat{M}_{wp}} \quad . \tag{A.15}$$

In equation (A.15), the effective mutual inductance from the plasma current to the flux on the wall is

$$\hat{M}_{wp} = M_{wp} - \frac{L_w L_{eff}}{M_{pw}} \quad . \tag{A.16}$$

Now, we may examine the meaning of L_{eff}. First consider the case of $I_p = 0$. From equation (A.1), this is also equivalent to taking $L_{eff} = -\infty$, then

$$s_{open} = -1 \quad . \tag{A.17}$$

This equation says that the current on the resistive wall decay on the L/R time of the resistive wall. Next if $L_{eff} = L_{eff}^{nw} = 0$, then

$$s_{open} = 0 \quad . \tag{A.18}$$

This corresponds to the marginal stability of the RWM, and the plasma is marginally stable to the XK with the wall at ∞. Third, if $L_{eff} = L_{eff}^{Iw} = [(M_{pw} M_{wp})/L_w]$, then we obtain from equation (A.16), that $\hat{M}_{wp} = 0$; and from equation (A.15) that

$$s_{open} = \infty \quad . \tag{A.19}$$

This corresponds to the ideal wall stability limit of the plasma. Therefore, L_{eff} increases from from the value of $-\infty$ at vacuum up with the presence of plasma and increases with plasma β_T to the no-wall stability limit value of $L_{eff}^{nw} = 0$ and further increases to the value of L_{eff}^{Iw} when the plasma β_T reaches the ideal-wall limit. The range of interest of the RWM is $0 < L_{eff} < L_{eff}^{Iw}$. The range of $L_{eff} > L_{eff}^{Iw}$ belongs to the ideally unstable plasma.

We define ideal feedback for the RWM as when we take the sensor location in equation (A.5) as when the sensor senses the perturbed flux due only to the plasma current I_p. In this case the current in the feedback coil is directly proportional to the plasma current

$$I_c = \hat{G} I_p \quad . \tag{A.20}$$

In equation (A.20) the effective gain factor $\hat{G}$ is given by

$$\hat{G} = G \frac{M_{sp}}{M_{sc}} \quad . \tag{A.21}$$

This relation allows us to eliminate I_p and I_c in favor of I_w in equations (A.1) and (A.2) to solve for the closed loop growth rate

$$s_{cl} = \frac{L_w(L_{eff} + \hat{G}M_{pc})}{(\hat{M_{pw}} + \hat{G}\hat{M_{wc}})M_{pw}} \quad . \tag{A.22}$$

In equation (A.22), the effective mutual inductance between the wall and the feedback coil is given by

$$\hat{M_{wc}} = M_{wc} - \frac{L_w M_{pc}}{M_{pw}} \quad . \tag{A.23}$$

Appendix B. The Fitzpatrick-Aydemir Model

This model was first published in the work of reference [34] and subsequently extended in the work of reference [52]. The model is based on large aspect ratio, cylindrical plasma geometry. It therefore enjoys the advantage of simplicity in geometry. It was employed not only to study the stability of the RWM, but also the time development of the RWM including the torque balance. In this model, an ideal plasma with constant rotation is first bordered by a thin viscous layer and then connected with the external vacuum region. The plasma dynamics is completely captured by the boundary condition relating the logarithmic derivative of the perturbed flux to the growth rate of the instability. This model is summarized here in the notation of the work of reference [52]. The plasma is assumed to have a minor radius a. The stability of the XK mode with an ideal wall located at r_w is governed by the quantity c

$$c = \frac{m/n - q(a)}{s(a)q(a)} \quad , \tag{B.1}$$

with (m, n) being the (poloidal, toroidal) mode number of the instability, $q(r)$ the safety factor and $s(r) = (r/q)(dq/dr)$ is the magnetic shear. The response of the plasma is described by the quantity $\Delta\Psi_a = [rd\psi/dr]_{a-}^{a+}$ and the growth rate of the mode is given by the relationship

$$d\Delta\Psi_a \simeq [(\hat{\gamma} - i\hat{\Omega_\phi})^2 + \nu_*(\hat{\gamma} - i\hat{\Omega_\phi})]\Psi_a \quad , \tag{B.2}$$

where d is the quantity

$$d = \frac{1}{m}\frac{(r_w/a)^{2m} - 1}{(r_w/a)^{2m} + 1} \quad , \tag{B.3}$$

and $\Psi_a = \psi(a)$ is the flux value at the plasma edge, $\hat{\gamma} = \gamma/(n\Omega_0)$ is the normalized growth rate, and $\hat{\Omega_\phi} = \Omega_\phi/\Omega_0$ is the normalized rotation frequency. Here, Ω_ϕ is the plasma toroidal angular velocity within the inertial layer. The normalization frequency Ω_0 is given by

$$\Omega_0\tau_A = \sqrt{\frac{3c}{d}}\left(\frac{cs(a)}{1 - c/d_c}\right) \quad , \tag{B.4}$$

and the equivalent viscosity is given by

$$\nu_* = \frac{12}{5c^2\tau_V n\Omega_0} \quad , \tag{B.5}$$

where the Alfvén time is given by $\tau_A = (R_0/B_\phi)\sqrt{\mu_0\rho(a)}$, and the momentum confinement time is given by $\tau_V = a^2\rho(a)/\mu(a)$, $\rho(r)$ is the plasma mass density, and $\mu(r)$ the perpendicular viscosity. In equation (B.2), the first term inside the square brackets corresponds to plasma inertia, whereas the second term corresponds to viscous dissipation. The parameter ν_* represents the strength of this dissipation.

The L/R time of the resistive wall is defined $\tau_w = \mu_0 r_w \delta_w / \eta_w$, where δ_w and η_w are the wall thickness and resistivity, respectively. The response of the wall is fully described by the quantity $\Delta\Psi_w = [r d\psi/dr]_{r_w-}^{r_w+}$. In the "thin shell" limit, in which $\delta_w/r_w << |\gamma|\tau_w << r_w/\delta_w$, this quantity takes the form

$$d\Delta\Psi_w = \hat{\gamma} S_* \Psi_w \quad , \tag{B.6}$$

where $\Psi_w = \psi(r_w)$, and

$$S_* = d\tau_w n\Omega_0 \quad . \tag{B.7}$$

The large parameter S_* measures the conductivity of the wall.

The quantities $\Delta\Psi_a$ given in equation (B.2) from the inertial layer and $\Delta\Psi_w$ given in equation (B.6) must be asymptotically matched to the outer solution, which is governed by marginally-stable ideal-MHD. This matching procedure yields

$$d\Delta\Psi_a = -(1-\kappa)(1-md)\Psi_a + \sqrt{1-(md)^2}\psi_w \quad , \tag{B.8}$$

$$d\Delta\Psi_w = -(1+md)\Psi_w + \sqrt{1-(md)^2}\psi_a + 2md\Psi_c \quad . \tag{B.9}$$

The parameter κ, which measures the intrinsic stability of the plasma in the absence of rotation is given by

$$\kappa = \frac{(1/d_c) - m}{(1/d) - m} \quad . \tag{B.10}$$

The no-wall stability limit (i.e. the stability limit in the complete absence of a wall) corresponds to $\kappa = 0$, whereas the perfect-wall limit (i.e., the stability limit when the wall becomes perfectly conducting) corresponds to $\kappa = 1$. Note, incidentally, that in the Fitzpatrick-Aydemir model the m, n mode is destabilized by *current gradients* rather than *pressure gradients*. Therefore, κ effectively plays the role of the plasma β_T. The quantity Ψ_c parameterizes the m, n static error-field — Ψ_c is actually defined as the error-field flux at the wall in the absence of plasma.

Neglecting the error-field, equations (B.2), (B.6), (B.8), and (B.9) can be combined to give the following simple cubic dispersion relation:

$$[(\hat{\gamma} - i\hat{\Omega}_\phi)^2 + \nu_*(\hat{\gamma} - i\hat{\Omega}_\phi) + (1-\kappa)(1-md)](\hat{\gamma}S_* + 1 + md) = 1 - (md)^2 \quad . \tag{B.11}$$

It is predicted that there is an unstable region even for $\kappa < 0$. This unstable region divides the stable region below $\kappa < 0$ into a first stable region and a second stable region. It is interesting to note that this region reduces in size when the plasma viscosity ν_* is increased.

Suppose that the plasma is stable ($\hat{\gamma} = 0$, and subject to a static error-field). Hence, $|\Psi_c| \neq 0$. The above set of equations can be combined to give

$$|\Psi_a| = \frac{2md}{\sqrt{1-(md)^2}} \left(\frac{|\Psi_c|}{[(\kappa - \kappa_1)^2 + (\nu_* \hat{\Omega}_\phi / (1-md))^2]^{1/2}} \right) \quad . \tag{B.12}$$

Thus the flux driven at the plasma edge, $|\Psi_a|$, becomes much greater in magnitude than the error-field flux, $|\Psi_c|$, as the effective no-wall stability boundary, $\kappa = \kappa_1$, is approached. The most significant error-field amplification takes place at the boundary of the first stable region.

Appendix C. The MARS Stability Code

MARS is a linear plasma stability code which was first constructed by Bondeson, *et al.* [66] for the study of nonideal plasma instabilities. It is an eigenvalue code with the complex growth rate γ being the eigenvalue. The special feature of this code is that the growth rate enters into the equation directly and not its square as is usually the case of other ideal MHD stability codes, such as ERATO [8], PEST [9], GATO [10] and KINKX [11]. Therefore, MARS is particularly suited for the study of unstable modes with very low growth rates as is the case of resistive MHD modes and the RWMs.

Recognizing that plasma flows are important plasma characteristics which affect plasma stability, the code was extended to include non-uniform plasma rotations by Chu *et al.* [62]. It was further extended to include external coils and various feedback characteristics by Liu *et al.* [67]. It was extended again [68] in 2008 to include the kinetic effect of the diamagnetic and magnetic drifts of the particles for the study of the RWM in the low rotation frequency regime. We note that in the low rotation frequency regime, the rotation frequency of the plasma is at a fraction of a percent of the Alfvén frequency. The magnetic drift frequency of the particles can be estimated to be $\omega_D \sim k_\perp \rho_i v_{th}/R$, with $k_\perp \sim m/r$. Here, m is the poloidal mode number, r is the minor radius, ρ_i is the ion Larmor radius, v_{th} is the ion thermal velocity and R is the major radius. It is easy to show that the ratio of $\omega_D R/v_A$ is of the order of a fraction of a percent. Therefore, these drift motions can be in resonance with the frequency of the mode and provide not only the damping but also modify the potential energy δW_k to enable stabilization of the plasma.

The MARS code adopts the fluid variables as the primary quantities in the study of the plasma stability. The drift motion of the plasma particles can be shown to modify the pressure response and to give rise to an anisotropic pressure response induced by the MHD motion. The set of equations used for describing the perturbed plasma motion is given by

$$\rho(\gamma + in\Omega)\vec{v}_1 = -\vec{\nabla}\cdot\vec{p}_t + \vec{j}_1 \times \vec{B} + \vec{j} \times \vec{b}_1 - \vec{\nabla}\cdot\vec{\Pi}_1 - \rho\vec{U}(\vec{v}_1) \quad , \tag{C.1}$$

$$(\gamma + in\Omega)\vec{b}_1 = \vec{\nabla} \times (\vec{v}_1 \times \vec{B} - \eta\vec{j}_1) + (\vec{b}_1 \cdot \vec{\nabla}\Omega)R^2\vec{\nabla}\phi \quad , \tag{C.2}$$

$$\vec{j}_1 = \vec{\nabla} \times \vec{b}_1 \quad , \tag{C.3}$$

$$(\gamma + in\Omega)p_1 = -(\vec{v}_1 \cdot \vec{\nabla})p - \Gamma p\vec{\nabla}\cdot\vec{v}_1 \quad , \tag{C.4}$$

$$(\gamma + in\Omega)\rho_1 = -(\vec{v}_1 \cdot \vec{\nabla})\rho - \rho\vec{\nabla}\cdot\vec{v}_1 \quad . \tag{C.5}$$

In the above set of equations, (ρ, $\vec{v}$, $\vec{B}$, $\vec{j}$, p_1, $\vec{p}_t$) are the (density, velocity, magnetic field, current, fluid pressure and total pressure). Equilibrium quantities are denoted without suffix, whereas the perturbed quantities have suffix 1 or t. Ω is the (non-uniform) rotation frequency of the plasma at equilibrium and depends only on the equilibrium flux function. $\partial/\partial t = \gamma$ is the complex growth rate, and the toroidal variation of the perturbed quantities is related by $\partial/\partial\phi = in$ to the toroidal mode number n. The density equation, equation (C.5), is decoupled from the rest and can, therefore, be solved separately. We note that the total pressure and the fluid pressure are related by

$$\vec{p}_t = p_1\vec{I} + p_\parallel \hat{b}\hat{b} + p_\perp(\vec{I} - \hat{b}\hat{b}) \quad , \tag{C.6}$$

with p_1 being the isotropic part of the fluid response and $p_\parallel, p_\perp$ the anisotropic part of the pressure response due to the particle drift motions. $p_\parallel$ and $p_\perp$ are obtained by integration from the perturbed distribution function f_L^1

$$p_\parallel = \sum_{e,i} \int d\Gamma m v_\parallel^2 f_L^1 \quad , \tag{C.7}$$

$$p_\perp = \sum_{e,i} \int d\Gamma \frac{1}{2} m v_\perp^2 f_L^1 \quad , \tag{C.8}$$

and

$$\frac{df_L^1}{dt} = f_\epsilon^0 \frac{\partial H^1}{\partial t} - f_{p_\phi}^0 \frac{\partial H^1}{\partial \phi} - \nu_{eff} f_L^1 \quad . \tag{C.9}$$

In equation (C.9), $f^0(\Psi, \epsilon)$ is the equilibrium particle distribution function, which is assumed to be a Maxwellian for the thermal ions and electrons. $\epsilon = \epsilon_k + Ze\Phi$ is the total energy of the particles, with ϵ_k being the kinetic energy, $Ze\Phi$ the potential energy, the angular momentum is $P_\phi = mR^2\dot{\phi} - Ze\Psi$, and H^1 is the perturbed Lagrangian $H^1 = -\epsilon_k H_L exp(-i\omega t + in\phi)$ and

$$H_L = \frac{1}{\epsilon_k}[m v_\parallel^2 \vec{\kappa}\cdot\xi_\perp + \mu(Q_{L\parallel} + \nabla B \cdot \xi_\perp)] \quad . \tag{C.10}$$

A general model dispersion relation was proposed [62] for the above set of equations,

$$(\gamma + in\Omega)^2 K + (\gamma + in\Omega)D + \delta W_p + \frac{\delta W_v^b \gamma\tau_w + \delta W_v^\infty}{\gamma\tau_w + 1} = 0 \quad . \tag{C.11}$$

This cubic equation is a generic dispersion relation for the RWM. The solution of equation (C.11) shown in figure 10 reveals that the mechanism of rotational stabilization of the RWM results from the mode coupling induced by plasma rotation between the unstable XK mode with the stable mode of flux diffusion through the resistive wall. The

generic stability phase diagram of its solution has been given in reference [99] and is determined by the strength of the dissipation parameter D. Note that if we specialize to the RWM, then the kinetic energy term $(\gamma + in\Omega)^2 K$ is negligible. By identifying the total $\delta W_k = \delta W_p + (\gamma + in\Omega)D$ of the plasma, the dispersion relation reduces to

$$\gamma \tau_w = -\frac{\delta W_k + \delta W_v^\infty}{\delta W_k + \delta W_v^b} \quad . \tag{C.12}$$

Equation (C.12) is in the same form as equation (15) and the meaning of the dissipation term is very clear. If D were purely real, it stands for a pure dissipation and is due to the resonant response; whereas if D is complex, part of the perturbed energy is reactive, i.e., stored in the precession motion of the particles.

We note that the fluid equations given above can be written alternatively as

$$\Delta W_{MHD} = \Delta W_p(\vec{\xi}, \Gamma = 0) + \Delta W_k^*(\vec{\xi}) \quad , \tag{C.13}$$

$$\Delta W_k^* = \sum_j (\Delta W_{T_j} + \Delta W_{c_j}) \quad , \tag{C.14}$$

$$\Delta W_c = \int_{circ.} d\vec{x} d\Gamma \left(-\frac{\partial f}{\partial E}\right) \frac{n[\omega_{*n} + (\epsilon_k - 3/2)\omega_{*T} + \omega_E] - \omega}{n\omega_D + (\alpha n q + l)\omega_b - i\nu_e f f - \omega} |\{exp(i\chi'_m) H_1\}|^2 \quad , \tag{C.15}$$

$$\Delta W_T = \int_{trapped} d\vec{x} d\Gamma \left(-\frac{\partial f}{\partial E}\right) \frac{n[\omega_{*n} + (\epsilon_k - 3/2)\omega_{*T} + \omega_E] - \omega}{n\omega_D - i\nu_{eff} - \omega} |\{exp(i\chi'_m) H_1\}|^2 \quad . \tag{C.16}$$

These are the contributions to the δW_k by the circulating and trapped particles.

MARS also implemented several physical models for the dissipation. Aside from the full kinetic response given above, we can also give a specific form to the viscous stress tensor $\vec{\Pi}_1$, with the intention to model the fluid approximations to the ion Landau damping. In particular, two distinct models are given. The first one is the ion "sound wave damping" model first developed by Hammet and Perkins [93]

$$\vec{\nabla} \cdot \vec{\Pi} = \kappa_{||} \sqrt{\pi} |k_{||} v_{th_i}| \rho \vec{v}_1 \cdot \hat{b}\hat{b} \quad . \tag{C.17}$$

The value of $\kappa_{\|} = 0.5$ was usually chosen. The second one is the "kinetic damping" model. This model was used previously to study the damping of the TAE modes by Bondeson and Chu [69]. The kinetic damping model uses the kinetic energy principle with $\omega* = 0$, $\omega_D = 0$.

The details of the numerical implementation in the MARS code can be found in the work of Liu *et al.* [202]. Recently, different plasma models for the background plasma have been proposed as being more suitable for the description of the interaction of the plasma with the RWM. These give different expressions to the viscous stress tensor. The different models include the neoclassical viscosity model [108, 109], etc. These different models need to be further included into the extended MARS code for a more comprehensive comparison with the experiment and for a more reliable prediction for the stability of RWM in future devices.

We mention two other codes with a similar purpose, the AEGIS-K [71] and the MARG2D [74].

Appendix D. Useful Concepts Derived from Control Theories

Liu and Bondeson's work [143] demonstrated the successful application and adoption of the framework of stability and control theory to the problem of feedback stabilization for toroidal plasma instabilities. One of the central concepts in control theory is the transfer function $P(s)$ in the frequency domain. $P(s)$ over the full complex frequency range ($|s| < \infty$) constitutes all the information we have about the system under study. For direct magnetic feedback, $P(s)$ measures the normalized flux or magnetic field $b_s(s)/b_0$ at the sensor position, resulting from the current $I_f(s)$ in the active coils

$$P(s) = [b_s(s)/b_0]\, I_f(s) \quad . \tag{D.1}$$

Here $b_s(s)$ is the field measured by the sensors (subscript s for sensor), $I_f(s)$ is the current in the feedback coils (subscript f for feedback) and the variable s is the Laplace transform variable. The normalization constant b_0 can be chosen as the field at the sensors produced by a 1 A current in the active coils in the absence of the walls and the plasma.

An example of a transfer function $P^r_m(s)$ can easily be written down for a cylindrical plasma with feedback coils at r_f and radial sensors located at r_s [147].

$$P^r_m(s) = \left(\frac{r_s}{r_f}\right)^{|m|-1} \left(\frac{|m|}{s - \Gamma_m}\right) \quad . \tag{D.2}$$

In equation (D.2), m is the poloidal mode number and Γ_m is the normalized growth rate ($\gamma_m \tau_m$, τ_m is the resistive wall time τ_w for the m-th poloidal harmonic) of the RWM in the absence of feedback. Note that the transfer function $P^r_m(s)$ has a simple pole at $s = \Gamma_m = \gamma_m \tau_m$. $P(s)$ is an analytic function of s, and since all physically real systems should be limited in the range of frequencies in which it can respond, one of the general properties of the transfer function is that when $s \to \infty$, $P(s) \to 0$. In the present example, $P^r_m(s)$ also shows that when the system approaches the ideal-wall stability limit, $\Gamma_m = \infty$, the transfer function for radial sensors vanish. This is a special property of the radial sensors which makes them ineffective for stabilization near the ideal stability limit.

In real toroidal geometry, single mode cylindrical theory is not sufficient to describe the full response of the plasma; we need to introduce multiple modes [95, 147, 203] to take into account the shape of the sensor and active coils. The total transfer function was found to be representable as a sum over single-mode transfer functions

$$P_{open}(s) = \sum_m c_m P_m(s) s_m \quad , \tag{D.3}$$

where c_m and s_m are geometrical coefficients characterizing the feedback and sensor coils, respectively. The plasma response $P(s)$ considered here is an inherent property of the plasma with $I_f(s)$ treated as independent, therefore $P(s)$ has the characteristics of the plasma in the open (feedback) circuit. In equation (D.3), we explicitly used the subscript *open* to denote this important notion.

One particularly useful form of the transfer function is obtained by expressing $P(s)$ as the ratio of polynomials such as

$$P_{open}(s) = \frac{(s + s_{n1})(s + s_{n2})}{(s - s_{RWM})(s + s_{d1})(s + s_{d2})} \quad , \tag{D.4}$$

where s_{RWM} is the open loop growth rate of the unstable RWM and other poles and zeros are related to the wall shielding effect and the stable higher order RWMs. This compact polynomial expression is useful for assessing feedback control logic parameters such as gain and time constants. The approximation of a complex transfer function by low order rational functions is called the Pade approximation.

In a real feedback system shown schematically in figure 38, the sensor signal b_s is processed by the plasma control system to generate the b_{pcs}. (The subscript pcs stands for the plasma control system. This system generates digitized feedback signals with proportional, differential or integral gains.)

The b_{pcs} in turn is fed into the power supply to generate the voltage that excites the current I_f in the control coils. This process of obtaining I_f from b_s is in general nonlinear and it is governed by the feedback logic and power supply and is more related to the domain of electrical and control engineering. The stability of the plasma under feedback control can only be understood if we first understand each of the components involved in the feedback. In the present work, we assume that the relationship between I_f and b_s can be approximated by a linear frequency dependent function $K(s)$. Thus conceptually, during closed-loop operation, the following closed-loop relation must be satisfied

$$1 + K(s)P_{open}(s) = 0 \quad . \tag{D.5}$$

If equation (D.5) has no solution for s with a positive growth rate, then the plasma is stable. Here, we emphasized the plasma transfer function by treating it differently from all other components in figure 38. In principle, for closed feedback, each of the components in figure 38 are equally important, and $K(s)$ should be decomposed as the product of the transfer functions $K_i(s)$ of the components, with each component determined by the "open circuit" operation.

The feedback logic for the RWM specifies how the magnetic sensor signals are used to activate the currents in the feedback coils. For example, in the "smart shell logic", the radial flux loop sensors that measure the total perturbed radial flux from B_r at

the wall is used. On the other hand, in the "mode control logic", the B_p sensors that measure the magnetic flux due to the poloidal field B_p are used. The B_p sensors are designed to be decoupled from the predominantly B_r flux produced by the feedback coils and are coupled optimally to the perturbed flux from the unstable RWM. An important difference between these two types of sensors can be observed by noting that in the cylindrical tokamak approximation, the open loop transfer function for poloidal sensors is given by [147]

$$P_m^p(s) = \left(\frac{r_w}{r_f}\right)^{|m|-1} \left[\frac{(2\Gamma_m + |m|)|m|/m}{s - \Gamma_m}\right] \quad . \tag{D.6}$$

Equation (D.6) should be compared with equation (D.2). We note that as the system approaches the ideal-wall stability limit, $\Gamma_m = \infty$, the transfer function $P_m^p(s)$ tends to a constant in contrast to $P_m^r(s)$ for radial sensor, which vanishes. This means that the system remains controllable by using poloidal sensors near the stability limit.

As shown in figure 38, in the controller, several components act in series. Therefore the transfer function $K(s)$ is the product of many different circuit components, each of which can be characterized by its own transfer function. For instance

$$K(s) = K_{ps} K_{pcs} K_{coil} K_{delay} \quad . \tag{D.7}$$

$K_{ps}(s)$ is the response of the power supply (PS), and $K_{coil}(s)$ is the response of the feedback coils. They can be obtained experimentally [158]. System time delay is included by $K_{delay} = exp(-s\tau_{delay})$.

The feedback gain of a PCS controller can be expressed analytically by

$$K_{PCS}(s) = \left[G_p + \frac{G_d s\tau_d}{(1 + s\tau_d)}\right] \frac{1}{(1 + s\tau_p)} \quad , \tag{D.8}$$

where τ_p is the filtering time constant associated with the digitization Nyquist frequency, τ_d is the time derivative constant, and G_p, G_d are the proportional and derivative feedback gains respectively.

The overall closed loop frequency response is expressed by

$$1 + P_{open}(s) K_{PCS}(s) K_{PS}(s) K_{coil}(s) K_{delay}(s) = 0 \quad . \tag{D.9}$$

The stability of the resultant system is determined by equation (D.5) or equation (D.9).

Appendix E. The Normal Mode Approach to Feedback

The basic difference between feedback of the RWM and other more traditional dynamic systems is that the correct plasma response model to the external electromagnetic perturbation is not yet completely known. If we assume a specific model for the plasma response, then the feedback is a completely solvable problem. This was first pointed out by Chu *et al.* [121] for an ideal stationary plasma. In reference [121], the feedback stabilization of the RWM (RWM) of a plasma in a general feedback configuration for the plasma-resistive wall system is formulated in terms of a generalized energy principle.

$$\delta W_g \equiv \delta K + \delta W_p + \delta W_v + D_w + \delta E_c = 0 \quad . \tag{E.1}$$

In equation (E.1), δK is the kinetic energy of the plasma, δW_p is the perturbed free energy of the plasma, δW_v is the perturbed energy of the (various) vacuum regions (between the plasma and the resistive wall and outside the resistive wall), D_w is the energy dissipation of the resistive wall, δE_c is the energy input from the external (feedback) coils. Of these various terms, only δW_p and δE_c could be negative. For slowly-growing or slowly-damped RWM δK is negligible. δW_g is a bilinear functional of the plasma displacement ξ and the perturbed magnetic field δB outside of the plasma in the vacuum region.

During the open loop operation, equation (E.1) reduces to

$$\delta W_r = \delta W_p + \delta W_v + D_w = 0 \quad . \tag{E.2}$$

With thin wall approximation, the dissipation functional D_w is shown to be self-adjoint to the magnetic field penetrated through the resistive wall. Equation (E.2) is, thus, a self-adjoint bilinear functional of $\{\xi, \delta B\}$. Equation (E.2) has a set of orthonormal open-loop eigenfunctions $\{O_i\} = \{\xi, \delta B_i\}$ with open loop growth rates $\{\gamma_i\}$.

$$\delta W_p(i,j) + \delta W_v(i,j) + D_w(i,j) = 0 \quad , \tag{E.3}$$

and $D_w(i,j) = \delta_{i,j}\gamma_i/2$. The set of normal modes determined by equation (E.3) is then used as the basis for closed loop operation, thus, the name NMA (normal mode approach). It has been found from practice that for tokamaks, usually, only one of the modes in the open loop eigenfunctions $\{O_i\}$ can have a positive growth rate, which should naturally be called the unstable RWM. Actually all the other modes should be regarded as the "damped" RWM. If left unchecked (without feedback stabilization), the unstable RWM will grow. It needs to be stabilized by feedback. During feedback, the feedback coils will exchange energy with these RWMs. Depending on the geometry of the feedback coil, the excitation of each of the modes is obtained by substituting the magnetic field produced by the feedback coil into equation (E.1) and utilizing the

relations in equation (E.3). These coefficients form the excitation matrix $\{E_i^c\}$ for the excitation of the $i-th$ mode by the current I_c in the $c-th$ external coil. The resultant minimization gives the equations

$$\frac{\partial \alpha_i}{\partial t} - \gamma_i \alpha_i = \sum_c E_i^c I_c \quad . \tag{E.4}$$

In equation (E.4), α_i is the amplitude of the $i-th$ mode during feedback

$$\{\xi, \delta B\} = \sum_i \alpha_i \{\xi_i, \delta B_i\} \quad . \tag{E.5}$$

The feedback system is completed by the description of the feedback logic. For instance, a set of sensor loops with flux $F_l(\{\alpha_i, I_c\})$ may be utilized to sense the perturbed flux, and the voltage on the feedback coils may then be given by $G_c^l F_l(\{\alpha_i, I_c\})$. Then the current in the feedback coil is given by

$$\left(\frac{\partial}{\partial t} + \frac{1}{\tau_c}\right) I_c = G_c^l F_l\left(\{\alpha_i, I_c\}\right) \quad . \tag{E.6}$$

The feedback system is completely described by equations (E.4) and (E.6). It is seen that the feedback is concisely described by the amplitudes of the normal modes $\{\alpha_i\}$ and the currents in the feedback coils I_c in a compact phase space for the system.

Since resonant field amplification(RFA) is essentially the same as the plasma response of a stable RWM, the above equations can also be applied to describe the response of the plasma during RFA. In this case, the external error field producing current I^e is regarded as imposed through unknown sources. They couple to the RWMs through E_i^e between the error field producing coils and the open loop eigenfunctions. It is easy to get the solution

$$\alpha_i = \frac{E_i^e I_e}{s - \gamma_i} \quad . \tag{E.7}$$

For stable modes, the inverse Laplace transform of equation (E.7) gives a decaying solution in time of the mode amplitude. Usually, the external error field evolves in a much longer time scale than the RWMs, therefore for clarity we give the time domain solution in this case as

$$\alpha_i(t) = \frac{E_i^e I^e}{\gamma_i}[1 - exp(\gamma_i t)] \quad . \tag{E.8}$$

At times long compared with the decay time of the unstable mode, the external error field would have excited the stable modes to the amplitude of

$$\alpha_i(\infty) = \frac{E_i^e}{\gamma_i} I^e \quad . \tag{E.9}$$

Note that equation (E.8) is also the solution for unstable modes. It shows that without being compensated for, the unstable mode will grow to a large amplitude and will lead to an intolerable situation. That is, we need to correct for the resonant error field. Now, consider the situation of using a set of feedback coils for error field correction. In this case, we have two current sources, one is the unknown error field, the other is the known correction coil, the solution of equation (E.4) is given by

$$\alpha_i = \frac{E_i^e I^e + E_i^c I^c}{s - \gamma_i} \quad . \tag{E.10}$$

The long time solution in time for the amplitudes of stable modes is given by

$$\alpha_i(\infty) = \frac{E_i^e I^e + E_i^c I^c}{\gamma_i} \quad . \tag{E.11}$$

Denoting mode 1 as the unstable mode, the requirement that the external error field coupling to mode 1 be completely compensated for is

$$E_1^e I^e + E_1^c I^c = 0 \quad . \tag{E.12}$$

Equation (E.12) represents the best that can be done for this situation. The required current on the feedback coils is given by

$$I_c = -\frac{E_1^e}{E_1^c} I^e \quad . \tag{E.13}$$

At this time all the other modes would then be excited to an amplitude

$$\alpha_i(\infty) = \frac{E_i^e E_1^c - E_i^c E_1^e}{E_1^c} I^e \quad . \tag{E.14}$$

It is seen that the necessary condition of correction of coupling of the error field will necessarily leave a residue deformation to the plasma. The feedback process discussed in section 4 and the non-rigidity of the plasma during feedback is an additional dynamic process in the presence of these error field compensation. These two processes are of a different time scale. Error field correction is usually occurring on a longer time scale than the RWM; the residue deformation is proportional to the "original" external error field before compensation (I^e), whereas the deformation of the RWM is proportional to the instantaneous value of the feedback current (I^c).

We should mention that the 3D code package STARWALL-OPTIM [152] adopted the same approach and separated the problem into the open loop problem treated by STARWALL and the closed loop problem treated by OPTIM. The special feature of the STARWALL-OPTIM package is that it can treat the highly complicated structure of the external wall [162] and other resistive media such as the double wall and blanket modules in ITER [204].

Appendix F. The Valen Model

The Valen code models the induced currents in distributed 3-D structures as a set of R-L circuit equations. The formulation allows analysis in the time domain, and also provides eigenvalue and eigenvector information. This code has been used extensively for the design of hardware configurations for a number of devices. It uses the most unstable mode computed by DCON [72] and has a similar capability as the STARWALL-OPTIM package [152] in treating the full 3D structures of the external resistive wall and blanket modules for feedback studies.

Fields and currents are assumed to be quasi-static, i.e., the circuit approximation is valid. The conducting structures are decomposed into elementary volumes represented as a set of circuit elements with current densities given by

$$J(\vec{r},t) = \sum_k I_k(t) w_k(\vec{r}) \quad . \tag{F.1}$$

The divergence-free shape/weight functions $w_k(\vec{r})$ correspond to macroscopic loops of current. The current amplitudes $I_k(t)$ satisfy

$$[L]\{\dot{I}(t)\} + [R]\{I(t)\} = \{V(t)\} \quad . \tag{F.2}$$

In equation (F.2), $[L]$ is the inductance matrix, $[R]$ is the resistance matrix, $\{I\}$ the current vector and $\{V\}$ the voltage vector. The mutual inductance is given by the free space value between different current elements.

$$L_{ij} = \frac{\mu_0}{4\pi} \int_{vol} \int_{vol'} \frac{w_i(\vec{r}) w_j(\vec{r}')}{|\vec{r} - \vec{r}'|} dv dv' \quad , \tag{F.3}$$

and the resistance R is given by

$$R_{ij} = \int_{vol} \eta w_i(\vec{r}) w_j(\vec{r}') dv \quad . \tag{F.4}$$

The voltage in equation (F.2) represents the induction voltage from all the circuit elements, including the contributions from the plasma. The circuit model for the plasma, unstable to an external unstable mode, is adopted from the formulation given by Boozer [205]. This formulation recognizes that the total plasma potential energy with arbitrary perturbed flux at the plasma boundary may be represented as a set of interacting surface currents on the plasma-vacuum boundary. The change in potential energy of the plasma is given by

$$\delta W = \frac{1}{2} \sum w_i \Phi_i^2 \quad , \tag{F.5}$$

where the $\Phi_i' s$ are the amplitudes of the perturbed normal eigenfunctions which diagonalize the δW, i.e. $\Phi_i = \int f_i(\theta,\phi) \vec{B} \cdot \vec{da}$ where $\int f_i f_j d\theta d\phi = \delta_{ij}$. The (normalized) currents on the plasma surface that produces only the field distribution $f_i(\theta,\phi)$ would be given by a distribution function $g_i(\theta,\phi)$ and magnitude I_i. The proportionality constant

between the flux and the current is the equivalent self-inductance of that particular plasma mode, $\Phi_i = L_i I_i$. The total surface plasma current is then related to the Φ_i through

$$L_i I_i^p = \sum(\delta_{ij} + s_i \lambda_{ij})\Phi_j \quad , \tag{F.6}$$

where $s_i = -\omega_i L_i$ and $\lambda_{ij}^{-1} = \int f_i g_j d\theta d\phi$. For a single mode, the response of the wall is approximated by one circuit, i.e. one current I^w or the associated magnetic flux penetrating the wall, Φ_w. The plasma perturbation is characterized as a single current I^p with flux Φ. Then the full set of equations of the model is

$$L_w I^w + M_{wp} I^d + M_{wp} I^p = \Phi_w \quad , \tag{F.7}$$

$$M_{pw} I^w + L I^d + L I^p = \Phi \quad , \tag{F.8}$$

$$L I^p (1 + s) = \Phi \quad , \tag{F.9}$$

$$\frac{d\Phi_w}{dt} + R_w I^w = V \quad , \tag{F.10}$$

$$\frac{d\Phi}{dt} + R_d I^d = 0 \quad . \tag{F.11}$$

The Valen code implements the equations (F.7), (F.8),(F.9), (F.10), and (F.11) by using their finite element representation for the current elements. Thus, the geometric relationships of the self and mutual-inductances of the current filaments in the plasma, wall and external coils are preserved. The only exception is the self- and mutual-inductances between the plasma current filaments on the surface of the plasma. This is related to the results obtained from ideal MHD codes by the prescription described above and

$$[L_p]\{I^p\} = [S]\{\Phi\} \quad , \tag{F.12}$$

where

$$S_{ij} = (\delta_{ij} + s_i \lambda_{ij}) \quad . \tag{F.13}$$

For feedback, the voltages are given by the time rate of change of the sensor flux $\{V_s\} = -\{\dot{\Phi}_s\}$. The sensor flux matrix is the inner product of the mutual inductance and the current vectors,

$$\{\Phi_s\} = [M_{sw}]\{I^w\} + [M_{sd}]\{I^d\} + [M_{sp}]\{I^p\} \quad . \tag{F.14}$$

Because the Valen code can model the external coils and conducting structures in their geometric detail, it is an important design tool for the sensor and feedback coils used in the feedback stabilization of the RWM.